

GPU-SEARCHES FOR BROADBAND EXTENDED EMISSION IN GRAVITATIONAL WAVES IN NEARBY ENERGETIC CORE-COLLAPSE SUPERNOVAE

MAURICE H.P.M. VAN PUTTEN,¹ AMIR LEVINSON,² FILIPPO FRONTERA,³ CRISTIANO GUIDORZI,⁴
LORENZO AMATI,⁵ AND MASSIMO DELLA VALLE⁶

¹*Sejong University, 98 Gunja-Dong Gwangjin-gu, Seoul 143-747, Korea; E-mail: mvp@sejong.ac.kr*

²*School of Physics and Astronomy, Tel Aviv University, 69978 Tel Aviv, Israel*

³*Department of Physics and Earth Sciences, University of Ferrara, Via Saragat 1, I-44122 Ferrara, Italy, and INAF, IASF, Via Gobetti, 101, I-40129 Bologna, Italy*

⁴*Department of Physics and Earth Sciences, University of Ferrara, Via Saragat 1, I-44122 Ferrara, Italy*

⁵*INAF, IASF, Via Gobetti, 101, I-40129 Bologna, Italy*

⁶*Istituto Nazionale di Astrofisica, Osservatorio Astronomico di Capodimonte, Salita Moiariello 16, I-80131 Napoli, Italy and International Center for Relativistic Astrophysics, Piazzale della Repubblica 2, I-65122, Pescara, Italy*

ABSTRACT

As a parent population to long gamma-ray bursts (LGRBs), energetic core-collapse supernovae (CC-SNe) are leading candidates as multi-messenger sources of electromagnetic and gravitational-wave emission for LIGO-Virgo and KAGRA. While their central engines are currently unknown, this outlook derives from a general association with newly born neutron stars, black holes and high-density accretion disks that may extend down to the Inner Most Stable Circular Orbit (ISCO) of the latter. We here highlight the capability of heterogeneous computing for deep searches for *broadband extended gravitational-wave emission* (BEGE) from non-axisymmetric accretion flows onto rotating black holes with durations of tens of seconds similar to Extended Emission in LGRBs and SGRBEEs. Specific attention is paid to electromagnetic priors derived from BATSE, *BeppoSAX* and *Swift* and data-analysis by GPU-accelerated butterfly filtering with over one million chirp templates per second. In deep searches using banks of up to 8 million chirp templates, the challenge is to identify signals of astrophysical origin in a background of pronounced correlations between the LIGO detectors H1 and L1. As the parent population of normal LGRBs, relatively more frequent supernovae of type Ib/c are of particular interest to blind all-sky searches, in archive LIGO S6 or real-time observation runs concurrently with electromagnetic observations covering the Local Universe up to about 100 Mpc at upcoming Advanced LIGO sensitivity. Detection of their output in gravitational waves is expected to unambiguously determine the nature of their central engines and, by implication, that of GRBs.

Contents

1. Introduction	4
1.1. Quadrupole gravitational radiation	8
1.2. Multi-messenger emission from SN1987A	11
1.3. Roadmap	12
2. Long GRB-supernovae and SGRBEEs	14
2.1. Hyper-energetic GRB-supernovae	14
2.2. Local event rates of energetic CC-SNe	17
2.3. GRBs in the <i>Swift</i> era	18
2.4. Prompt GRB emission	24
2.5. Kolmogorov spectra in <i>BeppoSAX</i>	25
3. Extended emission from rotating black holes	26
3.1. Secular time scale of black hole spin	27
3.2. Observational evidence of black hole spin down	31
3.3. Slow rotating remnants	32
4. Ascending and descending chirps in accretion flows	34
4.1. Alpha-disk model	34
4.2. Fragmentation chirps	36
4.3. Wave patterns in accretion disks	38
4.4. ISCO waves	42
4.4.1. Mass moments about the ISCO	43
4.4.2. Dimensionless strain amplitude	44
4.5. Stochastic background from CC-SNe	47
5. GPU-accelerated searches for broadband extended gravitational-wave emission	49
5.1. LIGO S6 correlations in loudness and pitch	51
6. Summary and future prospects	52
6.1. Deep searches by GPU-accelerated butterfly filtering	54
6.2. Scientific objective and observational strategy	54
Appendix A. Gravitational radiation	57
Hyperbolicity	57
Luminosity in gravitational radiation	59
Radiation from multipole mass moments	60
Appendix B. Relativistic frame dragging	62
Gravitational spin-orbit energy	63
Alfvén waves in a torus magnetosphere	65

LIST OF SYMBOLS

c	velocity of light (3×10^{10} cm s ⁻¹)
c_s	sound speed
D	source distance
E_B	energy in poloidal magnetic field
E_γ	true energy in gamma-rays
E_{iso}	isotropic equivalent energy
E_c	maximal spin energy PNS (3×10^{52} erg)
E_{res}	energy in reservoir
E_{rot}	energy in rotation
η	efficiency
h	dimensionless gravitational strain
ξ	dimensionless mass-inhomogeneity
L_j	luminosity in baryon poor jet (BPJ)
M, M_T	black hole and torus mass
\dot{m}	accretion rate
M_\odot	solar mass (2×10^{33} g)
\dot{N}	event rate
ν	kinematic viscosity
ν_H	black hole rotation frequency in Hz
ω	frame dragging angular velocity
Ω_{ISCO}	angular velocity at ISCO
Ω_H, Ω_T	black hole and torus angular velocity
q	index of rotation in accretion disk
R	branching ratio
R_g	gravitational radius (GM/c^2)
R_S	Schwarzschild radius ($2R_g$)
r_{ISCO}	radius of ISCO
r_c	transition radius to fragmentation by cooling
r_d	Roche radius in accretion flows
r_b	viscosity-to-radiation driven transition radius
T_{spin}	lifetime of black hole spin
τ	coherence time scale
t_{ff}	free fall time scale
z	r_{ISCO}/R_g
θ_H	half-opening angle on horizon

1. INTRODUCTION

The recent LIGO detection GW150914 poses a dramatic opening to a whole new window to the Universe (LIGO-Virgo 2016). Together with the upcoming commissioning of Virgo and KAGRA, we will now be in a position to pursue observations well beyond the limits of electromagnetic radiation, neutrinos and (ultra-)high-energy cosmic rays. As broadband detectors covering 30 - 2000 kHz, LIGO-Virgo and KAGRA offer unprecedented power of discovery relevant to an exceptionally broad class of astrophysical sources (Sathyaprakash & Schutz 2009; Cutler & Thorne 2002). While the black hole merger event GW150914 was unexpected and left no conclusive signature in the electromagnetic spectrum (Kalogera 2017), it nevertheless offered new results of direct astronomical interest with estimates of mass and spin of the black hole progenitor,

$$M_1 = 35.7_{-3.8}^{+5.4} M_\odot, \quad a_1/M_1 = 0.31_{-0.28}^{+0.48}, \quad (1)$$

$$M_2 = 29.1_{-4.4}^{+3.8} M_\odot, \quad a_2/M_2 = 0.46_{-0.42}^{+0.48}, \quad (2)$$

that run counter to familiar observations on stellar mass black holes in X-ray binaries in the Milky Way. The inferred high mass M_i of the black holes may originate from core-collapse of Population III stars (Kinugawa et al. 2014; Inayoshi et al. 2017) and their slow dimensionless spin a_i/M_i may indicate a process of spin down soon after birth such events (van Putten & Della Valle 2017).

Gravitational radiation has long since been known to be important in binary evolution of compact stars, as may be seen by long time observations of binary evolution in the electromagnetic spectrum (Verbunt 1997). Notable examples are Hulse-Taylor pulsar PSR B1913+16 (Taylor & Weissberg 1989; Taylor 1994; Weisberg et al. 2010), the double pulsar PSR J0737-3039 (Lyne et al. 2004), and ultra-short period cataclysmic variables with He mass transfer from a degenerate dwarf directly onto a companion (low mass) white dwarf (Smal 1967; Paczyński 1967; Faulkner 1971; Faulkner et al. 1972; Nelemans 2005; Postnov & Yungelson 2006; Bidsten et al. 2006). For instance, AM CVn ES Cet ($d \simeq 350$ pc) has an orbital period of about 10 min, a mass ratio $q \simeq 0.094$ of the binary with a white dwarf of mass $M \simeq 0.7M_\odot$ and a luminosity $L_{EM} \simeq 10^{34}$ erg s $^{-1}$ (Woudt & Warner 2003; Espaillat et al. 2005). Its gravitational wave-to-electromagnetic luminosity satisfies $L_{GW}/L_{EM} \simeq 0.3$. At an orbital period of about 5 min, current data on RX J0806 (Bidsten et al. 2006) suggest that it conceivably satisfies

$$L_{GW} \simeq L_{EM}. \quad (3)$$

These exceptional cases, therefore, demonstrate genuinely relativistic evolution that ultimately terminates in a binary merger. GW150914 is the most extreme example to-date. In terms of the unit of luminosity

$$L_0 = \frac{c^5}{G} = 3.6 \times 10^{59} \text{ erg s}^{-1}, \quad (4)$$

where G is Newton's constant and c is the velocity of light c , it featured a peak luminosity of about 0.1% L_0 . In this light, PSR B1913+16 is remarkably gentle with $L_{GW} \simeq 10^{-29}L_0$.

Multi-messenger output in electromagnetic and gravitational radiation is expected from neutron star-neutron star (NS-NS) or neutron star-black hole (NS-BH) mergers. These mergers are widely considered to explain the most relativistic transients in the sky: cosmological gamma-ray bursts

(GRBs), discovered serendipitously by nuclear treaty monitoring satellites (Klebesadel et al. 1973). Observationally, we infer their origin in a compact relativistic inner engines from the dimensionless parameter (van Putten 2000)

$$\alpha_E = \frac{GE}{c^5 \delta t} = 2.75 \times 10^{-5} \left(\frac{E_{52}}{\delta t_{-3}} \right) \quad (5)$$

for burst energies $E = E_{52} 10^{52}$ erg and variability times $\delta t = \delta t_{-3}$ ms, where G denotes Newton's constant and c is the velocity of light. The observed isotropic equivalent energies $E_{iso} = 10^{48} - 10^{54}$ erg s⁻¹ and variability times δt down to 0.1 ms show α_E up to 10^{-4} . Such values are extremely large compared to those of other transients, including GRB 980425 associated with SN 1998bw (Galama et al. 1998) and galactic sources such as GRS 1915+105 (Mirabel et al. 1994). It implies inner engines in the form of neutron stars or stellar mass black holes, more likely so than aforementioned white dwarfs in CVs. Neutron star masses tend to cluster around $1.4 M_\odot$ (Thorsett & Chakrabarty 1999), from $1.25 M_\odot$ of PSR J0737-303B (Lyne et al. 2004) to $2.1 M_\odot$ in the NS-WD binary PSR J075+1807 (Nice et al. 2004); masses of black hole candidates in X-ray novae are broadly distributed between about 5-20 M_\odot (Bailyn et al. 1998).

GRBs show anomalous Eddington luminosities of $L_\gamma \simeq 10^8 - 10^{14} L_{Edd}$, given their limited durations of typically less than one minute (Fig. 1). These super-Eddington luminosities defy an origin in electromagnetic interactions in a baryonic energy source. The only physical processes known that might circumvent these limitations are neutrino emissions and gravitational interactions allowed by the theory of general relativity. In anisotropic emission, the true energy in gamma-rays $E_\gamma < E_{iso}$, e.g., when GRBs are produced in jet-like outflows at finite opening angles. Even thus, some events have $E_\gamma \simeq 10^{52}$ erg. Typical values of events that reveal collimation show a relatively narrow distribution around (Frail et al. 2001; Ghirlanda et al. 2006, 2013)

$$E_\gamma \simeq 9 \times 10^{50} \text{ erg.} \quad (6)$$

Normal long GRBs have an accompanying supernova explosion with kinetic energies E_k typically greater than E_γ . In exceptionally energetic events, E_k points to a required energy reservoir E_{res} that exceeds the maximal spin energy E_c of a rapidly rotating neutron star (van Putten et al. 2011b). These events probably mark the birth of a black hole, rather than a neutron star. Following the Burst and Transient Source Experiment (BATSE) classification of short (SGRB) and long GRBs (LGRB) with durations $T_{90} < 2$ s and, respectively, $T_{90} > 2$ s (Fig. 1), *Swift* discovered short GRBs with Extended Emission (SGRBEE) lasting tens of seconds to well over a minute. Their soft EE is very similar to long GRBs with accompanying supernova. In attributing SGRBs to mergers, SGRBEEs defy the dynamical time scale $T_{merger} \simeq 10$ ms of NS-NS or NS-BH mergers by a large factor.

These electromagnetic observations introduce the mystery of the physical nature of GRBs by extreme values of (5) and

$$L_\gamma \gg L_{Edd}, \quad E_{res} > E_c \text{ (in some cases),} \quad T_{90}^{SGRBEE} \gg T_{merger}. \quad (7)$$

GRB inner engines hereby should be ultra-relativistic, conceivably operating by *strong gravitational interactions with high density matter on the scale of their Schwarzschild radius R_S* , defined as twice

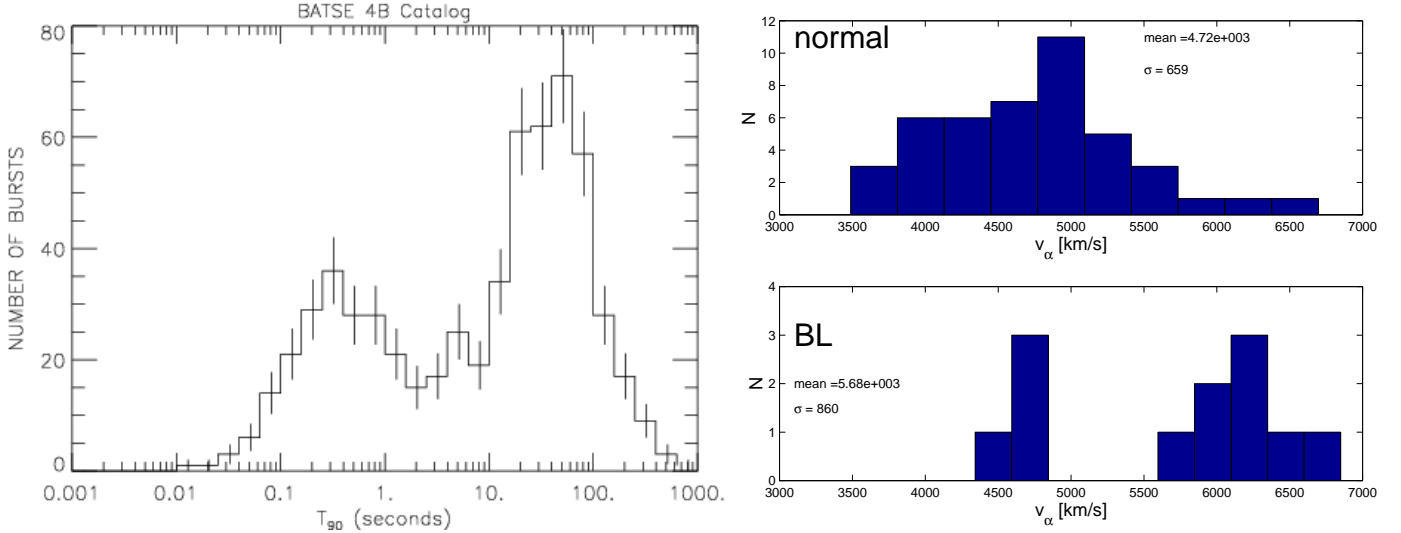


Figure 1. (Left.) The bimodal distribution of durations in the BATSE 4B Catalog, showing a population of short GRBs (less than 2 s) and long GRBs (over 2 s) (Reprinted from (BATSE 2001).) (Right.) Core-collapse supernovae form a heterogeneous class of events, broadly partitioned in normal (narrow line) and relatively more energetic (broad line) events. (Reprinted from (van Putten et al. 2011b), data from (Maurer et al. 2010)).

the gravitational radius

$$R_g = \frac{GM}{c^2} \quad (8)$$

for a mass M . If so, their inner engines may well be luminous in gravitational waves over the lifetime of the inner engine, i.e., up to tens of seconds indicated by long GRBs (van Putten 2001b). Consequently, GRBs are of considerable interest as candidate sources of gravitational radiation that may be probed by upcoming detectors LIGO-Virgo in the US and Europe and KAGRA in Japan. “If gravitational waves are detected from one or more gamma-burst triggers, the waves will almost certainly reveal the physical nature of the trigger” (Cutler & Thorne 2002).

However, GRB triggers within the sensitivity distance of LIGO-Virgo and KAGRA are rare and they are difficult to detect due to beaming. Even corrected for beaming, the true GRB event rate is about one per year within a distance of 100 Mpc. Practically, it is rather similar to the event rate of double neutron star coalescence. To within the distance to Virgo ($D \simeq 20$ Mpc), it implies about one event per century. Beaming is less severe in afterglow emission that follows the prompt phase decreases as the blast wave slows down and, at late times, the emission is ultimately roughly isotropic. In such cases, an observer might detect an orphan afterglow emission at radio wavelengths (Levinson et al. 2002), a few months after the explosion. Identifying GRBs by afterglow emissions leaves uncertain the true time-of-onset of the trigger, however, hampering efficient search for an accompany gravitational wave burst. For SGRBs from mergers, considerable improvement in sensitivity will be realised in the upcoming advanced generation of LIGO-Virgo and KAGRA at frequencies up to a few hundred Hz by advanced seismic suspension. However, at higher frequencies expected to be relevant to LGRBs from CC-SNe, improvement in sensitivity requires high laser power expected in next generation detectors. For instance, a sensitivity distance out to 35 Mpc by advanced VIRGO-LIGO and KAGRA may

include the LLGRB event GRB 980425/SN1998bw (Galama et al. 1998). Our perspectives hereby improve but not substantially with an anticipated rate of one detectable GRB-SN every few years.

To circumvent the above mentioned observational limitations to detect long GRBs, we propose a focus on type Ib/c supernovae (Maeda et al. 2002, 2008; Fruchter et al. 2006), that are far more numerous given their relatively small branching ratio of about 1% into long GRBs. Core-collapse supernovae (CC-SNe) form a remarkably heterogenous class of events (Fig. 1), and the most energetic events of type Ib/c stand out as the parent population of normal LGRBs.

The small branching ratio of CC-SNe into successful GRBs is commonly attributed to the challenge of creating an energetic inner engine sufficiently long lived, perhaps intermittently, for its ultra-relativistic outflows to successfully break out of the progenitor remnant envelope. Unsuccessful jet breakout from the stellar envelope in a CC-SN event (Mazzali et al. 2008; Couch et al. 2011; Bromberg et al. 2012) will lead to so called “choked GRB.” Such supernovae may appear as a low-luminosity long GRB or, more broadly, as a class of X-ray transients (Soderberg et al. 2008). Conceivably, therefore, the formation of energetic inner engines is more frequent than successful GRB-SNe. In this review, we shall therefore focus on the outlook on gravitational wave emissions from such energetic inner engines with or without a successful long GRB. Similar considerations might apply to their emission in neutrinos (Mészáros & Waxman 2001).

For energetic type Ib/c supernovae, we set out to develop an outlook and search for *broadband extended gravitational-wave emission* (BEGE) by the nature of black hole formation and evolution in CC-SNe.

Our outlook is modelled based on current phenomenology of GRBs and accompanying hyper-energetic supernovae. Detailed spectral and temporal analysis of GRBs from BATSE, *BeppoSAX* and *Swift* combined points to long-lived inner engines comprising rotating black holes, that appear common endpoints to energetic core-collapse events and mergers of neutron stars with neutron stars or stellar mass black holes alike. They hereby define a leading candidate as a universal inner engine to LGRBs and the *Swift* class of SGRBEE and LGRBNs (van Putten et al. 2014b). In interaction with high density accretion flows, potentially powerful gravitational wave emission may ensue, powered by accretion or the angular momentum of the black hole mediated by relativistic frame-dragging. The existence of frame dragging is not in doubt: recent measurements of non-relativistic frame dragging around the Earth are in excellent agreement with general relativity (Ciufolini et al. 2004, 2007; Ciufolini et al. 2009; Everitt et al. 2011). (Gravity Probe-B measurement is equivalent to that at 5 million Schwarzschild radii of a black hole at extremal spin with the same angular momentum as the Earth.) Specifically, accretion flows onto rotating black holes offer a window to broadband extended gravitational-wave emission, from non-axisymmetric accretion flows and high density matter accumulated at the Inner Most Stable Circular Orbit (ISCO), contemporaneously with two-component relativistic outflows that may drive an accompanying supernova explosion and GRB. Some of these model considerations can be confronted with data from GRB catalogues of BATSE, *BeppoSAX* and *Swift*. The resulting outlook on long duration ascending and descending chirps from accretion flows onto rotating black holes suggests searches for BEGE, accelerated by recent developments in high performance computing.

The prospect for *long duration* gravitational-wave bursts from accretion flows onto rotating black holes core-collapse of massive stars highlighted here is aimed at broadening our outlook beyond various existing discussions on gravitational waves from CC-SNe, much of which focused on complex

short duration bursts from core-collapse and core-bounce in the first one or two seconds producing neutron stars (Ott 2009) with a LIGO sensitivity distance limited to a few Mpc (Röver et al. 2009). Their connection to GRB-supernovae and extremely energetic supernovae, however, is not obvious (Burrows et al. 2007; Dessart et al. 2008). In contrast, the universal appearance of Extended Emission in LGRBs and SGRBs indicates central engine lifetimes of tens of seconds that may be at work in the more frequent group of energetic type Ib/c supernovae. It therefore appears opportune to search for gravitational-wave bursts with extended emission of potentially similar durations from, broadly speaking, nearby energetic core-collapse supernovae and to develop the required near-optimal search algorithms to achieve maximal sensitivity distance.

The energetic output in BEGE may be large by the ample energy reservoir in angular momentum of rotating black holes, exceeding that of rotating neutron stars by some two orders of magnitude opens a radically new window to energetic bursts in gravitational waves with durations up to minutes. If detected, LIGO-Virgo and KAGRA probes may reveal rotating black holes by calorimetry on their output in gravitational waves (van Putten & Levinson 2002). In general terms, gravitational radiation from non-axisymmetries associated with core-collapse of high angular momentum progenitors and non-axisymmetric collapse has been well appreciated (Bekenstein 1973; Thuan & Ostriker 1974; Novikov 1975; Epstein 1976; Detweiler & Lindblom 1981), see further (e.g. Detweiler & Lindblom 1981; Kotake et al. 2006; Ott 2009; Fryer & New 2011). Here, we emphasise potentially extreme luminosities from non-axisymmetric accretion flows down to ISCO powered by the angular momentum of the central black hole (van Putten 2001b), and hence the need for a general search method for both ascending chirps and descending chirps from accretion flows onto rotating black holes (Levinson et al. 2015).

Energetic type Ib/c supernova have an event rate of about 100 per year within a distance of 100 Mpc, and they are readily found in optical surveys using moderately sized telescopes. As targets of opportunity for gravitational wave bursts, they are hereby competitive with mergers, whenever the fraction successfully producing a gravitational wave burst exceeds 1% (Heo et al. 2015). Additionally, nearby galaxies such as M51 ($D \simeq 8$ Mpc) and M82 ($D \simeq 4$ Mpc) each with an event rate of over one core-collapse supernova per decade. By their proximity, these events appear of interest as well, independently of any association with type Ib/c supernovae or GRBs (Ando et al. 2013; Aasi et al. 2014). While CC-SNe define the most energetic transients in the Universe, the dimensionless strain amplitude of any accompanying gravitational waves will be small by the time it reaches the detector *and* by a possibly prolonged duration of emission. To extract signals deeply within the detector noise, it is desirable to take full advantage of high performance computing on *Graphics Processor Units* (GPUs), to search for essentially un-modelled emission with near-optimal detection sensitivity by matched filtering against a large bank of chirp templates.

Given the current quest for a multi-messenger source of gravitational radiation, we believe it to be opportune to highlight prospects and search for gravitational radiation from energetic type Ib/c supernovae as a parent population of long GRBs, of interest to LIGO-Virgo and KAGRA up to distances of about 100 Mpc at advanced detector sensitivity.

1.1. *Quadrupole gravitational radiation*

Normal long GRBs, SGRBs with Extended Emission, energetic core-collapse SNe and possibly superluminous SNe are all likely powered by neutrons stars or stellar mass black holes. From their generally aspherical output in electromagnetic radiation, it may be inferred that their putative inner

engine should be rich in angular momentum. Angular momentum serves as a reservoir of energy that, in collapse, points to the formation of an accretion disk. In the present context, the density of any such disk will be high. Any non-axisymmetry introduces a multipole mass moment, that will inevitably luminous in gravitational waves.

Non-axisymmetries in mass-flow may result from instabilities (van Putten 2002; Kobayashi & Meszaros 2003; van Putten & Levinson 2003; Piro & Pfahl 2007) due to cooling in self-gravitating disks (e.g. (Gamma 2001; Rice et al. 2005; Mejia et al. 2005; Lovelace et al. 2014; Hadley et al. 2014)), magnetic stresses (Tagger et al. 1990; Tagger & Pellat 1999; Tagger 2001; Lovelace et al. 2014), that may account for high frequency QPOs in micro-quasars (Tagger & Verriere 2006) or flaring in SgrA* (Tagger & Mella 2006), or enhanced pressure by heating or magnetic fields due to feedback by a rotating black hole (van Putten & Levinson 2003; Bromberg et al. 2006). In addition, intermittent accretion onto the black hole may lead once more to aforementioned excitation of QNM ringing.

Gravitational radiation is essentially *inevitable* from extreme transient events forming neutron stars and black holes, arising from non-axisymmetric mass-motion on the Schwarzschild radius R_S of the system, e.g., a wobbling neutron star or a non-axisymmetric accretion flow onto the black holes. Its basic premises derive from dimensional analysis and, with no small parameters, the gravitational wave luminosity L_{GW} will be a fraction of L_0 in (13).

Gravitational radiation is a key prediction of general relativity as a mixed elliptic-hyperbolic theory of gravitation described by a metric with associated Riemann tensor (Pirani 1957, 2009; Trautman 2009) coupled to matter. In what follows, we shall change to geometrical units and denote the gravitational radius (8) by M . Equivalently, we put $G = c = 1$ in (8). Thus, M parametrizes perturbations in space-time at a distance D in terms of a *dimensionless strain*

$$h = \frac{M}{D} + h_{GW}, \quad (9)$$

where h_{GW} is the strain amplitude in gravitational radiation. At large distances, h_{GW} satisfies the linearized Einstein equations in vacuo, given by a second order wave equation for small amplitude perturbations that satisfies the same dispersion relation as electromagnetic waves (Appendix A).

At the lowest frequency, gravitational radiation is described by the quadruple gravitational-wave formula, that may be derived from the rotating tidal field in a binary system. This time harmonic excitation acts as a source terms to gravitational wave emission. More generally, tidal fields arise from multipole mass moments I_{lm} , where l and m refer to the poloidal and azimuthal quantum numbers of spherical harmonics. Thorne (Thorne 1980) gives a comprehensive overview of gravitational wave luminosity in h_{GW} above from multipole mass moments defined by projections on the spherical harmonics Y_{lm} ($l \geq m \geq 2$),

$$L_{lm} = \frac{1}{32\pi} \frac{G}{c^{2l+1}} \left(\frac{d^{l+1}}{dt^{l+1}} I_{lm} \right)^2 \quad (10)$$

by

$$I_{lm} = \frac{16\pi}{(2l+1)!!} \left[\frac{(l+1)(l+2)}{2(l-1)l} \right]^{\frac{1}{2}} \int_V Y_{lm}^* r^l dm, \quad (11)$$

where $dm = \rho d^3x$ over the source region V expressed in spherical coordinates (r, θ, φ) as before.

In contrast, radial motion introduces time-dependence with $m = 0$ which, by (10-11), does not tap into the angular momentum of the source. Gravitational wave emission from axisymmetric sources tends to be remarkably inefficient. Illustrative is the gravitational wave output of about 0.2% from head-on collisions of two black holes (Anninos et al. 1993) (cf. (Gibbons 1972)). This low efficiency reflects the effective regularization by black hole event horizons of the singular behavior of Newton's law between point particles (van Putten 2012b). In contrast, the $m \neq 0$ tidal fields in binary mergers shows appreciable efficiency up to about 2% (e.g. Kyutoku (2013); Szilágyi et al. (2015)) and slightly more in neutron star-neutron star coalescence (Bernuzzi et al. 2015b).

In a binary with binary separation a much larger than the Schwarzschild radius of the system, the gravitational potential at the root of the metric is the Newtonian potential $U = M/a$ along with an orbital frequency ω , $\omega^2 = M/a^3$. The total luminosity L_{GW} in gravitational radiation, dimensionless in geometrical units, hereby satisfies $L_{GW} \sim U^n \times (M\omega)^2 = (M/a)^{3+n}$ for some n , taking into account scaling with dimensionless orbital frequency $M\omega$. In the distant radiation field, $L_{GW} = 4\pi D^2 w$ in terms of the radiation intensity $w = k\dot{h}^2$ for some constant k . In geometrical units, w is of dimension cm^{-2} . The angular frequency of a tidal field is twice the angular velocity ω of the binary motion, i.e., $\dot{h} = 2\omega h$. Since h_{GW} and $L_{GW} = 4\pi D^2 w$ are both dimensionless, h_{GW} factors over the Newtonian scale factor M/D and U (9), i.e., $L_{GW} = 4\pi D^2 (2\omega(M/D)U)^2$. Hence $n = 2$ with the familiar result (e.g. Wald 1984)

$$L_{GW} \propto M^2 a^4 \omega^6 \propto (M\omega)^{\frac{10}{3}}. \quad (12)$$

L_{GW} in cgs units obtains by multiplying (12) with the unit of gravitational wave luminosity (13).

For a binary of two masses M_i ($i = 1, 2$) in circular motion, a detailed derivation obtains the quadrupole formula of gravitational radiation (Appendix A)

$$L_{GW} = \frac{32}{5} (\mu\Omega)^{\frac{10}{3}}, \quad (13)$$

further replacing M with the *chirp mass* $\mu = M_1^{\frac{3}{5}} M_2^{\frac{3}{5}} (M_1 + M_2)^{-\frac{1}{5}}$. An extension to non-circular orbits by incorporating enhanced emission at higher frequency harmonics obtains by including a factor $F(e) = (1 + (73/24)e^2 + (37/96)e^4)/(1 - e^2)^{7/2}$ as a function of ellipticity (Peters & Mathews 1963; Postnov & Yungelson 2006). It has been verified experimentally in long-term radio observations of the orbital decay of the Hulse-Taylor binary PSR 1913+16 to better than 0.1% (Taylor 1994) by the additional factor of $F(e) = 11.8568$ for the observed ellipticity $e = 0.6171334$. At the distance of 6.4 kpc, its $L_{GW} \simeq 8 \times 10^{31} \text{ erg s}^{-1}$ produces an instantaneous dimensionless strain at the Earth that, as such, may be evaluated directly in geometrical units as

$$h \simeq \frac{L_{GW}^{1/2}}{\Omega D} \simeq 1.38 \times 10^{-22}, \quad (14)$$

based on previous arguments with $k = 1/16\pi$ (Appendix A). As a relatively compact binary, the Hulse-Taylor binary coalesces in about 310 Myr (Postnov & Yungelson 2006).

Coincidentally, (14) is very similar to the scale for the maximal strain produced in the final merger of a circular binary of two neutron stars of total mass $M = M_1 + M_2$ in the Local Universe. In this event, $L_{GW} = (2/5) (M/a)^5$ defines the observed strain amplitude for an equal mass binary.

Following averaging over the orientation of the source (e.g., (Postnov & Yungelson 2006) for a more general discussion)

$$h = \sqrt{\frac{2}{5}} \frac{M^2}{aD} = \sqrt{\frac{2}{5}} \frac{M}{D} (\pi M f_{GW})^{\frac{2}{3}}, \quad (15)$$

where we dropped the subscript GW . It explicitly shows that h is the product of the Newtonian specific binding energy $U = M/a$ and the scale factor M/D (see also (Sathyaprakash & Schutz 2009)). Here, we expand the result to the gravitational wave frequency $f = 2f_{orb}$ in terms of the orbital frequency f_{orb} . That is (e.g. (Thorne 1992; Ju et al. 2000; Postnov & Yungelson 2006)),

$$h = 6.3 \times 10^{-23} \left(\frac{M}{3M_{\odot}} \right)^2 \left(\frac{D}{100 \text{ Mpc}} \right)^{-1} \left(\frac{f}{1000 \text{ Hz}} \right)^{\frac{2}{3}}. \quad (16)$$

In NS-NS coalescence, the chirp (16) holds true up to the instant when h peaks at $f \simeq 800$ Hz (Baiotti et al. 2008). Numerical simulations show that the neutron stars subsequently break up, and merge into a hyper massive object (e.g. (Bernuzzi et al. 2015a)) followed by collapse into a stellar mass black hole accompanied by a burst of quasi-normal mode (QNM) ringing. The result is a rapidly rotating low-mass black hole of close to mass M with an accretion disk of about 0.01-0.1 M_{\odot} (Baiotti et al. 2008). It may give rise to a short GRB, but perhaps also a SGRB with Extended Emission (SGRBEE) (van Putten et al. 2014b).

1.2. Multi-messenger emission from SN1987A

SN1987A in the Large Magellanic Cloud (LMC, $D \simeq 50$ kpc (Figs. 2-1) stands out as the first genuine multi-messenger event by a luminous output in electromagnetic radiation and MeV neutrinos. Characteristic for a core-collapse supernova, SN 1987A was radio-loud (Turtle 1987) and aspherical (Papalios et al. 1989). It also featuring relativistic jets (Nisenson & Papaliosios 1999) with possible black hole remnant, based on a lack of detection of a neutron star and on evidence for a black hole in the rather similar type IIL event SN1979C (Mattei et al. 1979; Pagnaud et al. 2011). Collectively, core-collapse supernova form a rather heterogeneous group (Filippenko 1997), that may be broadly partitioned in narrow line and broad line events (Fig. 1), where the latter tend to be relatively more energetic featuring relativistic ejection velocities. SN1987A belongs to a class with a relatively massive progenitor (Gilmuzzi et al. 1987; Kirshner et al. 1987) powered by a probably angular momentum rich inner engine based on the dramatically aspherical supernova remnant (Fig. 1).

Its output $E_{\nu} \simeq 10^{53}$ erg in > 10 MeV neutrinos offered our most direct view yet on the innermost workings of a CC-SN. It may, in fact, have produced a stellar mass rotating black hole, as may be inferred from the aspherical remnant seen today. Spectroscopic observations of SNe-Ibc (Mazzali et al. 2005; Tauberger et al. 2009; Modjaz et al. 2014) reveal that the geometry of ejecta of stripped envelope supernovae is, in about 50% of the observed events, is strongly asymmetric. Any non-axisymmetric angular momentum rich explosion mechanism inevitably produce gravitational waves, which may be generic to energetic supernovae.

E_{ν} is particularly relevant as evidence of the formation of high density matter that, combined with ample angular momentum in the progenitor as may be inferred from the aspherical supernova remnant, are just the kind of conditions leading up to an additional output in gravitational radiation, provided this collapse event developed canonical non-axisymmetric mass-motion at its core. Such

output will be especially luminous, whenever such mass motion takes place on the Schwarzschild scale of the system, e.g., the Inner Most Stable Circular Orbit (ISCO) around a newly formed black hole. By virtue of the large value of L_0 in (4), the quadrupole formula (12) predicts an appreciable luminosity even when L_{GW} in (13) is small, e.g.,

$$L_{GW} \simeq 10^{50} - 10^{53} \text{ erg s}^{-1} \quad (17)$$

by $10^{-9} - 10^{-6}$ in (13) is on par with the observed luminosities in the electromagnetic radiation and neutrino emissions of SN1987A. This outlook opens a broad window to observationally relevant gravitational wave luminosities, even in the face of considerable model uncertainties and chirp masses small relative to the central object.

To be specific, consider a mass-inhomogeneity with gravitation radius δm about a mass M with the aforementioned chirp mass in the limit of $M_2 = \delta m$ much smaller than $M_1 = M$. By virtue of (4), L_{GW} reaches luminosities on par with SN1987A's neutrino luminosity already for $\delta m/M \simeq 0.1\%$ orbiting at a few times the Schwarzschild radius $R_S = 2R_g$. As a mass perturbation in a torus or inner disk of mass $M_T \simeq 0.01M$, the gravitational wave luminosity (13) of δm satisfies $L_{GW} = \frac{32}{5} (\delta m/M)^2 (M/a)^5 L_0$ in the limit of a small chirp mass. Expressed in terms of the dimensionless inhomogeneity $\xi = \delta m/M_T$ and mass $\sigma = M_T/M$, we have

$$L_{GW} = 2 \times 10^{51} \left(\frac{\xi}{0.1} \right)^2 \left(\frac{\sigma}{0.01} \right)^2 \left(\frac{4M}{a} \right)^5 \text{ erg s}^{-1}, \quad (18)$$

where a denotes the orbital separation. The observed dimensionless strain at a source distance D satisfies

$$h = \frac{L_{GW}^{\frac{1}{2}}}{\Omega D} = 4 \sqrt{\frac{2}{5}} \xi \sigma \frac{M}{D} (\pi M f)^{\frac{2}{3}}. \quad (19)$$

Generalized to a similar event in the Local Universe, e.g., SN1979C (Pagnaud et al. 2011), scaled to a distance of 20 Mpc, we have

$$h = 3.4 \times 10^{-23} M_1 \frac{\xi}{0.1} \frac{\sigma}{0.01} \left(\frac{D}{20 \text{ Mpc}} \right)^{-1} \left(\frac{f}{600 \text{ Hz}} \right)^{\frac{2}{3}}, \quad (20)$$

where $f = 2f_{orb}$ in the Newtonian approximation $2\pi f_{orb} = M^{-1}(M/a)^{3/2}$ and $M = M_1 10M_\odot$.

1.3. Roadmap

With a focus on multi-messenger emission from energetic type Ib/c supernovae powered by black hole inner engines, our roadmap is as follows.

§2 discusses evidence for black holes as a common inner engine to LGRBs and SGRBEEs from detailed analysis of BATSE data of long GRBs. In particular, LGRBs and SGRBEEs may share a common central engine in the form of a rotating black hole, and normal LGRBs may be associated with the formation of near-extremal black holes.

§3 highlights the likely complex process of birth and evolution of rotating black holes in core-collapse supernovae, various stages of accretion therein each with their own outlook on gravitational radiation with extended emission in the form of ascending and descending chirps.

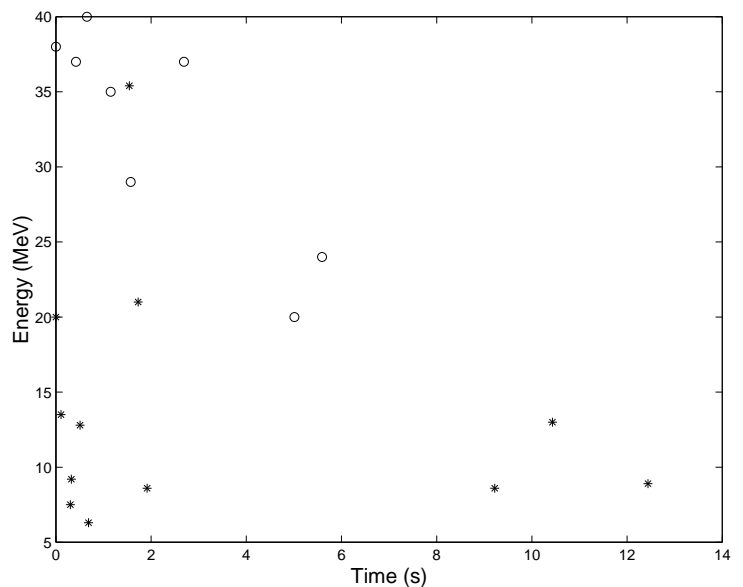
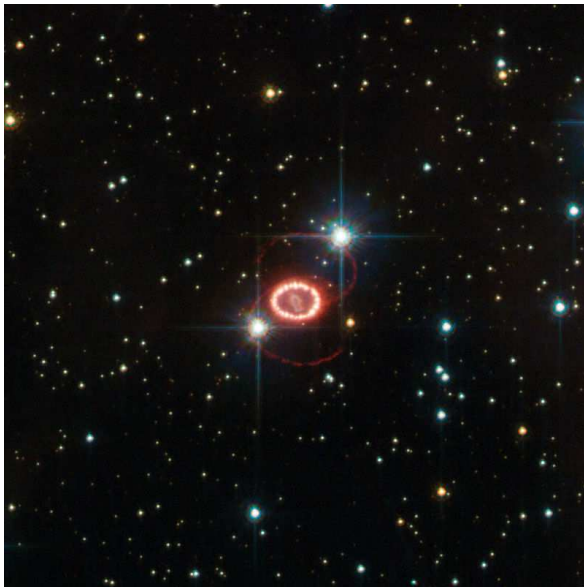


Figure 2. (Left.) SN 1987A is a Type II supernovae produced by core-collapse of the supergiant Sanduleak -69° 202 in the Large Magellanic Cloud at a distance of about 50 kpc (Gilmozzi et al. 1987; Kirshner et al. 1987). Shown is the neutrino light curve compiled from Kamiokande (stars) and IMB (circles) listed in (Burrows & Lattimer 1987) associated with the optical identification of SN 1987A (Garrison et al. 1987; Herald et al. 1987; Kunkel et al. 1987). (Right.) The SN1987A neutrino light curve, showing an initial energy of >10 MeV representative for the formation of high density matter, possibly through continuing collapse of a protoneutron star. The final remnant is conceivably a stellar mass black hole, though undetected at present. (Reprinted from van Putten (2005a)).

§4 gives a general framework for BEGE from non-axisymmetric accretion onto rotating black holes. Specifically, we identify extended emission currently observed in GRBs with the lifetime of black hole spin, T_{spin} , as a secular time scale extending to tens of seconds relevant to normal long GRBs and SRBEEs. We identify ascending and descending chirps with non-axisymmetric waves in accretion flows. In the Kerr metric (Kerr 1963), we model the latter by ISCO waves, extended by feedback over an inner torus magnetosphere with an expanding ISCO during black hole spin-down. Thus, a central engine conceivably emits simultaneously descending and ascending chirps from accretion onto rotating black holes (van Putten 2003; Levinson et al. 2015).

§5 Given the outlook on extended emission in gravitational waves, we introduce a new GPU-accelerated pipeline of butterfly filtering enabling deep searches for BEGE by matched filtering against over banks of millions of chirp templates in real-time, the results of which would appear as tracks in a chirp-based spectrograms. This approach differs from Fourier-based spectrograms (Sutton et al. 2010; Prestegard & Thrane 2012; Thrane & Coughlin 2013, 2014; Coughlin et al. 2015; Abbott et al. 2015; Gossan et al. 2015) by bandpass filtering signals with finite slope $|df(t)/dt| \geq \delta > 0$ for some $\delta > 0$ (van Putten et al. 2014a) (Fig. 8, Fig. 13).

§6 summarises our proposed search strategy to probe nearby energetic core-collapse supernovae for BEGE, by LIGO-Virgo and KAGRA in blind all-sky searches or by follow-up of triggers from optical-radio transients surveys. The latter may be obtained from any of the existing (Drout et al. 2011; Li et al. 2011a) or upcoming all sky optical surveys such as Pan-STARRs (Scolnic et al. 2011) or the planned Caltech Zwicky Transient Facility (Kulkarni et al. 2014; Belkin 2015). Searches for

their contribution to the stochastic background in gravitational waves may be pursued by multi-year correlations between two or more gravitational wave detectors (e.g. (Sathyaprakash & Schutz 2009)). Existing observations of LGRBs and SGRBEEs justify a vigorous probe of the inner most workings of energetic CC-SNe which, if successful, may identify rotating black holes by true calorimetry on their evolution over times scales of tens of seconds.

2. LONG GRB-SUPERNOVAE AND SGRBEEs

The association of normal LGRBs with supernovae and shared spectral properties in prompt GRB-emission with Extended Emission to SGRBEEs discovered by *Swift*, poses novel questions on a common inner engine to both, even as the latter derives from mergers. In what follows, we review some of the observational highlights on these two classes of GRBs.

2.1. Hyper-energetic GRB-supernovae

Aspherical CC-SNe (Papaliosis et al. 1989; Höfflich et al. 1999; Maeda et al. 2008) such as SN1987A derive from relatively massive progenitors that are unlikely produced by their associated MeV neutrino burst. Instead, they may be powered by an internal magnetic wind (Bisnovatyi-Kogan 1970) or an internal relativistic jet (MacFadyen & Woosley 1999) derived from a central engine. In core-collapse following a drop in thermal pressure at the end of nuclear burning or associated with pair-instability if the mass of the star is exceptionally large (Bisnovatyi-Kogan et al. 1966; Barkat et al. 1967; Gal-Yam et al. 2009; Chardonnet et al. 2010), the central object thus produced is either a (rotating) neutron star or black hole.

The energy E_k in a supernova explosion powered by angular momentum is constrained by the maximal rotational energy of the engine, i.e., a (proto-)neutron star or black hole, and the efficiency in expulsion of the remnant stellar envelope by a putative internal wind or jet. The maximal rotational energy E_c of a neutron star is attained at its break up frequency whereas the same of a black hole of mass M is attained when its angular momentum reaches GM^2/c . Canonical bounds for the rotational energy of the inner engine of a CC-SN are

$$E_{rot}^{NS} \leq E_c = 3 \times 10^{52} \text{ erg}, \quad E_{rot}^H \leq 6 \times 10^{54} \left(\frac{M}{10M_\odot} \right) \text{ erg} \quad (21)$$

for a rotating neutron star, respectively, black hole. Here, there is some uncertainty in the bound E_c due to the equation of state of neutron stars. The efficiency $\eta = E_k/E_w$ in the expulsion of the envelope with kinetic energy E_k by a wind or jet with energy E_w depends on the baryon loading of the wind, i.e., (van Putten et al. 2011b)

$$\frac{1}{2}\beta_{ej} < \eta < 1, \quad (22)$$

where $\beta_{ej} = v_{ej}/c$ denotes the observed velocity of the ejected envelope relative to the velocity of light c . The efficiency increases with baryon loading, as the outflow velocity becomes moderately relativistic. The efficiency reduces to $(1/2)\beta_{ej}$ in the limit of baryon-poor jets, whose velocity approaches c . By the above, E_k is bounded by ηE_c or ηE_{rot}^H .

Jet powered supernovae are of particular interest to the diversity in CC-SNe in long GRBs (Fig. 1) as well as a diversity in their associated GRBs. Certain types of supernova explosions may lead to a

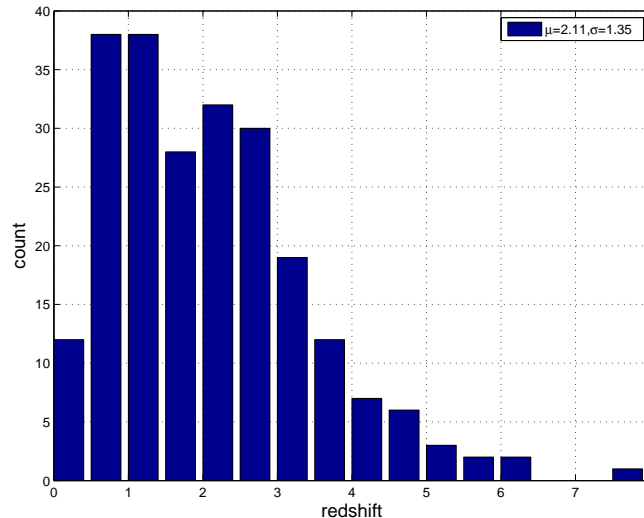


Figure 3. The distribution of observed redshifts of 230 LGRBs in the *Swift* catalogue shows a mean redshift $\mu = 2.11$ with standard deviation $\sigma = 1.35$. This distribution is significantly biased towards low redshifts. (Reprinted from (van Putten 2012a).)

relativistic shock breakout that may explain (nearby) low-luminosity GRBs (LLGRBs) but not the prompt GRB emission of normal long GRBs (Nakar & Sari 2012). The latter class is thought to be produced by collimated ultra-relativistic baryon-poor jets (BPJ) that penetrate through the stellar envelope. Failure to breakout the stellar envelope leads to a “choked GRB,” which is considered the leading candidate for LLGRBs (Nakar & Sari 2012).

For long GRBs, the association with massive stars is now supported by four pieces of evidence:

- supernovae (SNe) accompanying a few nearby events (Hjörth et al. 2011);
- detection of SN features in the spectra of “rebrightenings” during GRB afterglow decay, at intermediate redshifts, most recently GRB 130427A ($z=0.34$, (Melandri et al. 2013)) up to $z \simeq 1$ (Della Valle et al. 2003);
- the host galaxies are spiral and irregular with active star formation typical for environments hosting core-collapse SN-Ic’s (Kelly et al. 2008; Raskin et al. 2008); and
- a cosmological distribution of redshifts of long GRBs, consistent with the cosmic star formation rate (Wanderman & Piran 2010; Grieco et al. 2012) (Fig. 3).

The fact that E_{rot}^H is about two orders of magnitude larger than E_c in (21) allows for E_k to be considerably larger than ηE_c even at modest efficiency. Additionally, black hole-disk systems can produce two-component outflows comprising an ultra-relativistic jet along their spin axis surrounding by a baryon-rich and possibly collimating disk wind. The first offers the potential for high energy emissions upon breakout from the stellar envelope, whereas the second offers the potential for an efficient explosion. In contrast, neutron stars may produce a one-component magnetic outflow, that may facilitate either one but not both.

Exceptional E_k ’s are observed in GRB 031203/SN2003lw and 030329/SN2003dh with $E_{SN} \simeq 6 \times 10^{52}$ erg and $E_{SN} \simeq 4 \times 10^{52}$ erg, respectively (Table 1). Like SN1987A, supernovae accompanying LGRBs are aspherical and radio-loud. Hyper-energetic events with $E_k > E_c$ (see (21)) are no

Table 1.[†] References refer to SNe except for GRB 070125. E_* in units of 10^{51} erg.

GRB	Supernova	z	E_γ	E_{tot}	E_{SN}	η	E_{rot}/E_c	Ref.
	SN2005ap	0.283			> 10	1	> 0.3	1
	SN2007bi	0.1279			> 10	1	> 0.3	1
980425	Sn1998bw	0.008	< 0.001		50	1	1.7	2
031203	SN2003lw	0.1055	< 0.17		60	0.25	10	3
060218	SN2006aj	0.033	< 0.04		2	0.25	0.25	4
100316D	SN2006aj	0.0591	0.037-0.06		10	0.25	1.3	5
030329	SN2003dh	0.1685	0.07-0.46		40	0.25	5.3	6
050820A		2.607		42			1.4	7
050904		6.295		12.9			0.43	7
070125		1.55		25.3			0.84	7
080319B		0.937		30			1.0	7
080916C		4.25		10.2			0.34	7
090926A		2.1062		14.5			0.48	8
070125		1.55		25.3			0.84	9

[†] (van Putten et al. 2011b); 1. (Gal-Yam et al. 2009; Quinby et al. 2009); 2. (Galama et al. 1998); 3. (Malesani et al. 2004); 4. (Masetti et al. 2006; Modjaz et al. 2006; Campana et al. 2006; Sollerman et al. 2006; Mirabal et al. 2006; Pian et al. 2006; Cobb et al. 2006b); 5. (Chornock et al. 2010; Bufeno et al. 2011); 6. (Stanek et al. 2003; Hjörth et al. 2003; Matheson et al. 2003); 7. (Cenko et al. 2010); 8. (de Ugarte Postigo et al. 2011); 9. (Chandra et al. 2008).

exception. In the model of (Bisnovaty-Kogan 1970), these explosive events are attributed to magnetic winds powered by angular momentum extraction of a compact object, i.e., a PNS or magnetar (e.g. (Woosley 2010; Kasen & Bildsten 2010) in SN2007bi (Nicholl et al. 2013)) or a rotating black hole-disk system (BHS, (van Putten & Levinson 2003)). Taking into account a finite efficiency for the conversion of angular momentum to a (largely radial) explosion, $\eta < 1$, we determined that aforementioned two events require a central energy E_{rot} in angular momentum exceeding the maximal spin energy of a rapidly rotating neutron star by a factor of 10 and, respectively, 5.3 (Table 1). With a total output of about 10^{52} erg in optical emission alone, SN2015L (Dong et al. 2015) likewise defies the limit ηE_c in the face of reasonable efficiencies η and finite efficiency in dissipating kinetic energy to electromagnetic radiation.

Given uncertainties in the observed explosion energy by a factor of no more than a few, it appears that, in light of (21), these two events cannot be attributed to spin down of PNS, unless the efficiency is at least 100 %. For this reason, the central engine of these two events stand out as candidate BHS, powering the explosion by the spin energy of a black hole. If so, the required explosion efficiency is brought back to a reasonable few %. In particular, we have a wind energy E_w that may derive from disk winds or black hole spin energy E_{rot}^H satisfying

$$E_w = 6 \times 10^{52} \left(\frac{\Omega_T}{0.1\Omega_H} \right)^2 \left(\frac{M}{10M_\odot} \right) \text{ erg} \quad (23)$$

for rapidly spinning black hole of mass M parameterized by the ratio of the angular velocity Ω_T of a torus about the ISCO to the angular velocity Ω_H of the black hole. The fiducial scale of 0.1 in (23) is rather conservative.

2.2. Local event rates of energetic CC-SNe

As a parent population of long GRBs, nearby energetic core-collapse supernovae define targets of opportunity (TOOs) to LIGO-Virgo (Abramovici et al. 1992; Acernese et al. 2006, 2007) and KAGRA (Somiya 2012; KAGRA 2014). Current GRB and SN rates measurements point to a branching ratio

$$R = \frac{N(\text{GRB-SNe})}{N(\text{Type Ib/c})} \simeq 0.2 - 3\%, \quad (24)$$

covering a conservative (van Putten 2004; Ghirlanda et al. 2013) to a more optimistic estimate (Guetta & Della Valle 2007). As targets of opportunity for LIGO-Virgo and KAGRA, the event rate of SN Ib/c is larger than GRB-SNe by R^{-1} .

The origin of the small value of R in (24) is not well understood. Evidently, an observable GRB event requires the formation of an inner engine sufficiently powerful for its energetic outflows to overcome various adverse conditions out of which it emerged, namely a high density environment formed in core-collapse of a massive progenitor star, perhaps in a short period binary (Paczynski 1998). A possible additional factor is the time of residence of the newly formed black hole in the center of the star, that may be sufficiently long only when the kick velocity is low. The latter may be rare. Alternatively, it may reflect the small probability of forming nearly extreme Kerr black holes, i.e., about the Thorne limit reached along a modified Bardeen trajectory as the initial condition for long GRBs (van Putten 2015c).

We estimate the event rate of Type Ib/c supernovae within a distance D_S in the Local Universe to be

$$\dot{N}(\text{Type Ib/c}, D < D_S) = 109 \text{ yr}^{-1} \left(\frac{D_S}{100 \text{ Mpc}} \right)^3, \quad (25)$$

based on a weighted average of the volumetric rates derived from Asiago (Capellaro et al. 1999; Barbon et al. 1999) and Lick surveys (Li et al. 2011a,b). In a 5 year observational window, we expect about 4, 15 and 35 asymmetric Type Ib/c explosions in within a distance of 20, 30 and 40 Mpc respectively. These numbers offer a realistic perspective on simultaneous detections of GWBs and electromagnetic radiation.

The event rate (25) refers to regular Type Ib/c supernovae. Broad line events (cf. Fig. 1) associated with normal LGRBs are more rare by an order of magnitude. Even so, the event rate of these energetic events is a few per year within 100 Mpc, and hence more numerous than the true event rate of LGRBs (corrected for beaming) by up to one order of magnitude.

The relatively high event rate (25) should be viewed in light of the anticipated high frequency in gravitational waves, where LIGO-Virgo and KAGRA sensitivity is limited by photon shot-noise. The shot-noise dominated output of these detectors is above the frequency around 100-200 Hz of minimal (thermal) noise, below which sensitivity is limited by seismic noise. By frequency alone, GWBs from Type Ib/c supernovae are less suitable as gravitational wave sources for these detectors than mergers

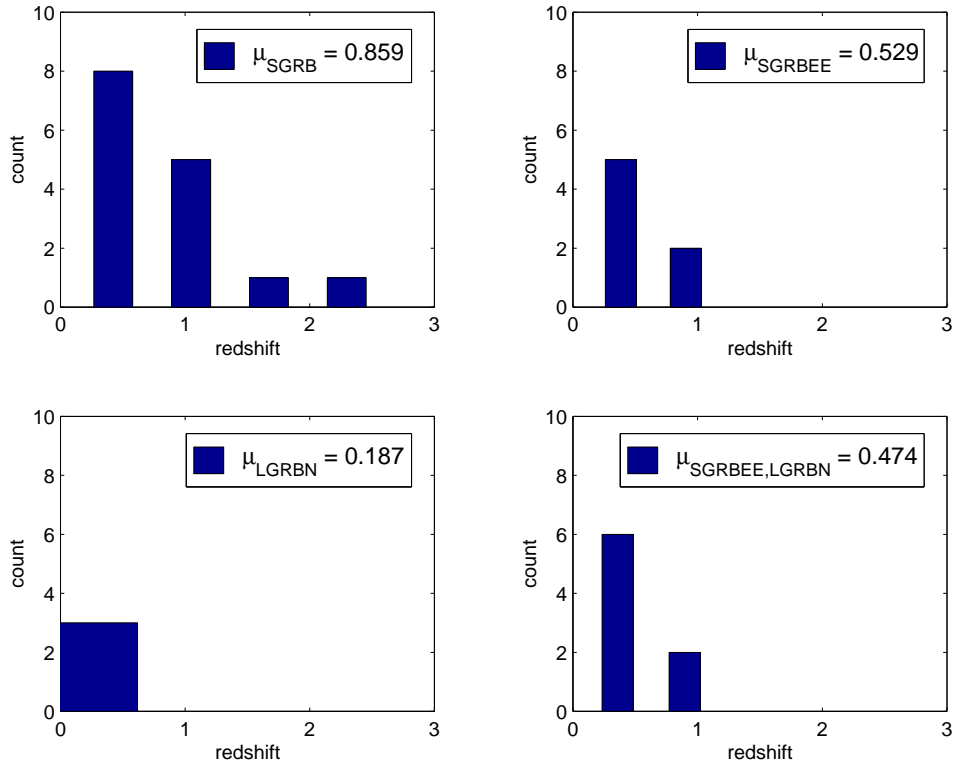


Figure 4. Shown are the distributions of observed redshifts of SGRB, SRGBEE, LGRBN and SGRBEE+LGRBN combined and the associated mean redshifts μ . (Reprinted from (van Putten et al. 2014b).)

of double neutron star binaries (§2). This drawback is considerably ameliorated by the relatively high event rate (25), that brings Type Ib/c supernovae statistically more nearby by a factor of about 4.8.

Detecting energetic supernovae such as Type Ib/c events is very easy, especially in the Local Universe within 100 Mpc. In contrast, electromagnetic counterparts to mergers of double neutron star binaries appear to be quite challenging (kasen et al. 2013; Barnes & Kasen 2013; Tanaka & Hotokezaka 2013) and may be seen only in the most fortuitous of cases (Tanvir et al. 2013).

2.3. GRBs in the Swift era

Calorimetry on the kinetic energy in supernovae and the prompt GRB emission offers our most prominent views yet on the inner engine of GRB-SNe, in addition to the MeV neutrino burst from SN1987A. We next review the present classification, spectral and temporal properties of GRBs relevant to the question whether their inner engine is a black hole or neutron star. Particularly relevant are the catalogues of BATSE, *BeppoSAX* and *Swift* of long and short GRBs.

Immediately following the serendipitous discovery of GRBs, Stirling Colgate suggested an association to supernovae - gamma-ray flashes from type II supernova shocks (Colgate 1968, 1970, 1974) - now seen by the association of normal long GRBs with core-collapse of massive stars (Woosley & Bloom 2006). Indeed, shock breakout in regular CC-SNe is likely to produce high energy

Table 2.[†] *Swift* SGRB, SGRBEE^a and LGRBNs. E_{iso} in 10^{52} erg, E_p in keV.

	T_{90}	z	host ^b	E_{iso} ^c	E_p ^c
SGRB					
061201	0.760	0.111	galaxy cluster ¹	0.013	969
050509B	0.073	0.225	elliptical galaxy ²	0.00027 ³	-
060502B	0.131	0.287	massive red galaxy ⁴	0.022	193
130603B	0.18	0.356	SFR ⁵	0.2 ⁶	90 ⁶
070724A	0.4	0.457	moderate SF galaxy ⁷	-	
051221A	1.400	0.547	SF, late type galaxy ⁸	0.25 ⁹	
131004A	1.54	0.717	low mass galaxy ¹⁰	-	
101219A	0.6	0.718	faint object ¹¹	0.48	842
061217	0.210	0.827	faint galaxy ¹²	0.008 ¹²	
090510	0.3	0.903	field galaxy ¹³	3.8 ¹³	
070429B	0.47	0.904	SFR ¹⁴ $1.1M_{\odot} \text{ yr}^{-1}$	-	-
060801	0.49	1.131	-	0.027 ¹⁵	
100724A	1.4	1.288	probably LGRB ¹⁶	-	-
050813	0.45	1.8	galaxy cluster ^{17,18}	0.017 ¹⁸	-
090426	1.2	2.609	irreg. SF galaxy ¹⁹	-	-
SGRBEE					
060614 ^{d e f g}	108.7	0.125	faint SFR ^{20,21}	0.21 ²⁰	55 ²⁰
050724 ^{d e f g}	69	0.258	elliptical, weak S ²²	0.0099 ²³	-
071227A ^{e f}	1.8	0.384	edge-on S ²⁴	0.008 ²⁵	-
061210 ^{d e f g}	85.3	0.41	bulge dominated ²⁶	0.046 ²⁶	-
061006 ^{d e f g}	129.9	0.438	exp. disk profile ²⁷	0.18	955
070714B ^{d e f g}	64	0.92	SF galaxy ²⁸	0.16 ^{28,29}	-
050911 ^{d e}	16.2	1.165	EDCC493 cluster ³⁰	0.0019 ³⁰	-
LGRBN					
060505	4	0.089	spiral, H ⁺ , no SN ³¹	0.0012 ²¹	120
060614 ^{d e f g}	108.7	0.125	faint SFR, no SN ²⁰	0.21 ²¹	-
061021	46	0.3462	no SN ³²	0.68	630

[†] (van Putten et al. 2014b); ^a From HEASARC (2016); ^b galaxy type, SN association; ^c Isotropic-equivalent energy and peak energy for events with reliable estimates of the bolometric E_{iso} across a large enough energy band, under the assumption $\Omega_m = 0.3$ and a Hubble constant $H_0 = 70 \text{ km s}^{-1} \text{ Mpc}^{-1}$; ^d (Perley et al. 2009); ^e (Norris et al. 2010); ^f (Coward et al. 2012); ^g (Gompertz et al. 2014); 1. (Berger et al. 2007c); 2. (Fong et al. 2010; Page et al. 2006; Perley et al. 2009); 3. (Bloom et al. 2006, 2007); 4. (Bloom et al. 2007); 5. (Cucciara et al. 2013); 6. (Frederiks 2013); 7. (Kocevski et al. 2010); 8. (Berger & Soderberg 2005; Berger et al. 2007); 9. (Golenetskii et al. 2005); 10. (Perley et al. 2013); 11. (Perley et al. 2010); 12. (Berger et al. 2006; de Ugarte Postigo et al. 2006); 13. (Rau et al. 2009; Nicuesa Guelbenzu et al. 2012); 14. (Cenko et al. 2008); 15. (Cucciara et al. 2006; Berger et al. 2007a); 16. (Ukwatta et al. 2010); 17. (Bloom et al. 2007; Prochaska et al. 2006; Berger 2006; Ferraro et al. 2007); 18. (Berger 2005b); 19. (Antonelli et al. 2009); 20. (Della Valle et al. 2006); 21. (Fynbo et al. 2006; Cobb et al. 2006a); 22. (Berger et al. 2005; Page et al. 2006; Berger et al. 2007a; Fong et al. 2010); 23. (Prochaska et al. 2005); 24. (Berger et al. 2007b); 25. (Berger et al. 2007d); 26. (Cenko et al. 2006); 27. (Fong et al. 2010; Berger et al. 2007a); 28. (Graham et al. 2009); 29. (Graham et al. 2007); 30. (Berger et al. 2007); 31. (Jakobsson & Fynbo 2007); 32. (Moretti et al. 2006)

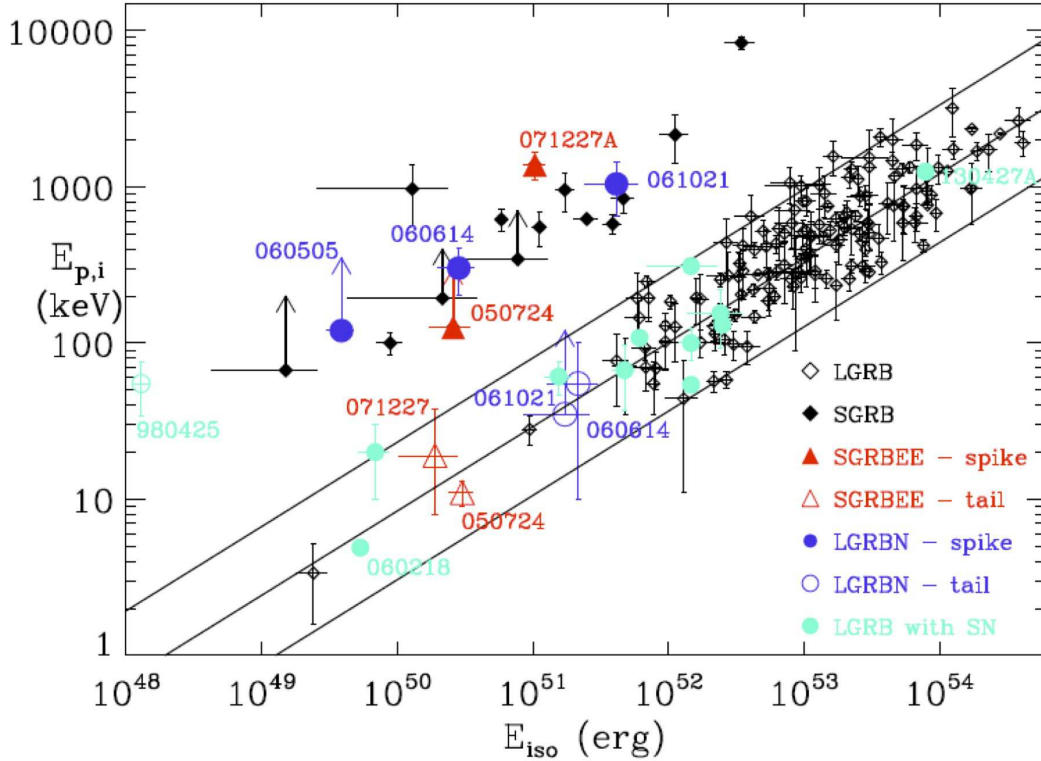


Figure 5. Shown is the location of short GRBs with Extended Emission (SGRBEE) and long GRBs with no apparent association with supernovae (LGRBN) in the $E_{p,i} - E_{iso}$ plane (Amati et al. 2002, 2006) including GRB-SNe 030329, 050525A, 081007,091127,100316D,101219B. The lines are the best-fit of the $E_{p,i} - E_{iso}$ correlation for normal long GRBs and its $\pm 2\sigma$ confidence region. As a sub-energetic GRB, GRB980425/SN1998bw has a distinguished symbol. Highlighted are GRBEEs 050724 and (also a LGRBN). The tail of these two SGRBEEs (open triangles, red) and that of their more luminous counterparts listed in Table 1 falls well within the group of the tails of LGRB with SNe indicated by medium sized filled circles (green). In contrast, the initial pulse of SGRBEEs (solid triangles, red) falls into the separate group of SGRBs, in common with the initial pulse of LGRBNs (large size filled circle, blue). Limits shown are 90% confidence levels. Data mostly from (Amati et al. 2008, 2009; Cano et al. 2014; Swift 2016). (Reprinted from (van Putten et al. 2014b).)

emission in UV light (Gezari 2008), X-rays (Campana et al. 2006) up to gamma-rays (Weaver 1976; Höfflich et al. 2009; Katz et al. 2010; Nakar & Sari 2010; Svirski et al. 2012). While conceivably relevant to low luminosity (long) GRBs (LLGRBs), the prompt GRB emission from normal long GRBs is now understood to derive, instead, from dissipation in ultra-relativistic BPs (below).

BATSE identified short and long GRBs by the observed bimodal distribution in durations T_{90} in a large number of events (Fig. 1). They are now associated with, respectively, mergers of the NS-NS (Eichler et al. 1989) or NS-BH (Paczynski 1991) variety, albeit with a large overlap between these two populations (Bromberg et al. 2012, 2013). T_{90} is defined by the time interval covering a 90 percentile

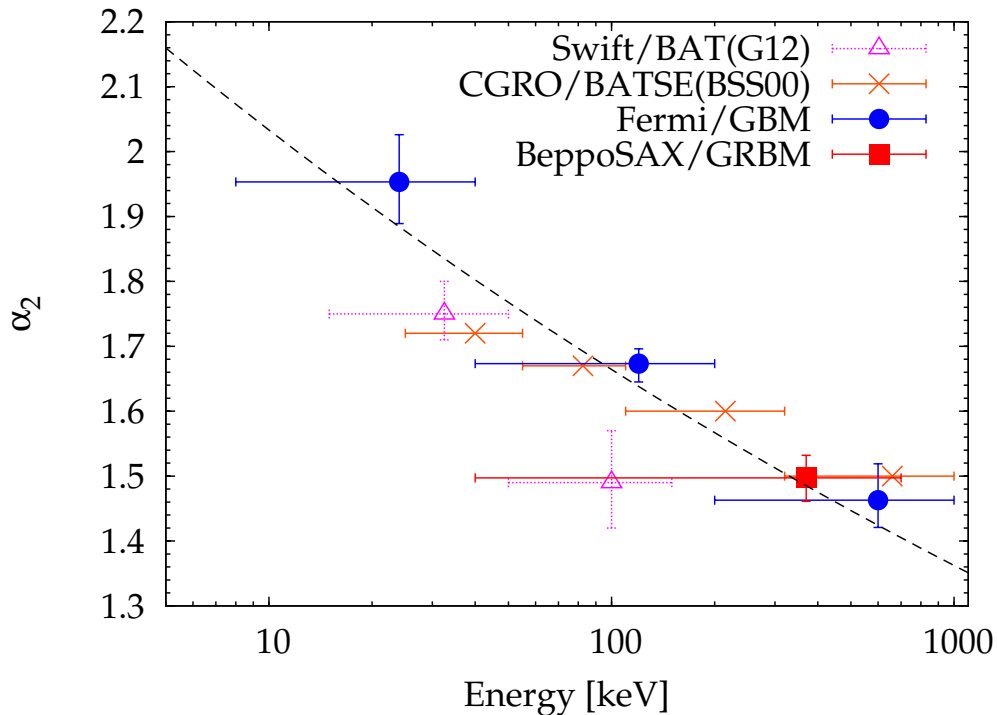


Figure 6. The power law index of the average PDS in the frequency range $10^{-2} < f/\text{Hz} < 1$ obtained by Fourier analysis from different data sets as a function of the observed energy. Dashed line ($\alpha_2 \propto E^{-0.09}$) illustrates the α_2 dependence on energy as estimated from Fermi data. (Reprinted from (Dichiara et al. 2013a).)

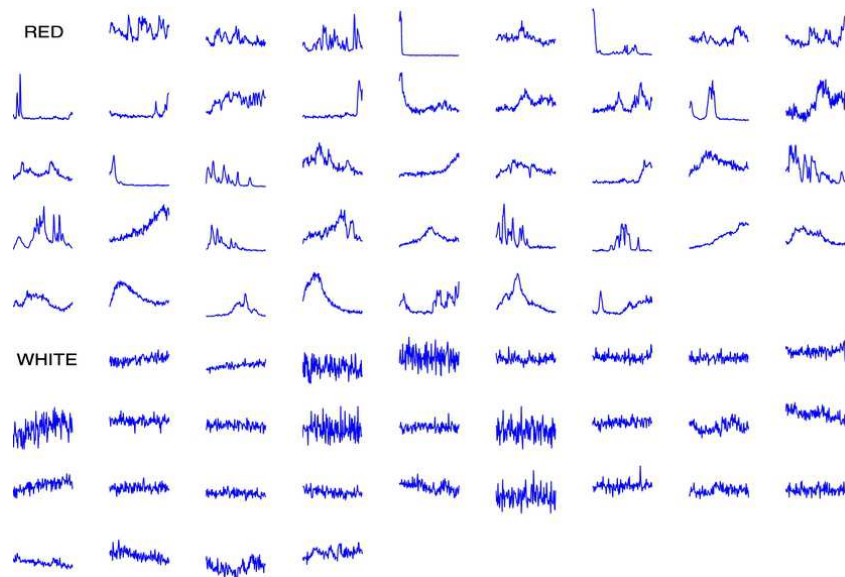


Figure 7. Shown are the smoothed light curves of 72 bright long GRBs in the BeppoSAX catalog sampled at 2 kHz for the first 8-10 seconds. 42 have a pronounced autocorrelation (“red”) with mean photon counts of 1.26 per 500 μ s bin, while 30 have essentially no autocorrelation (“white”) with mean photon counts of 0.59 per 500 μ s bin. (Reprinted from (van Putten et al. 2014a).)

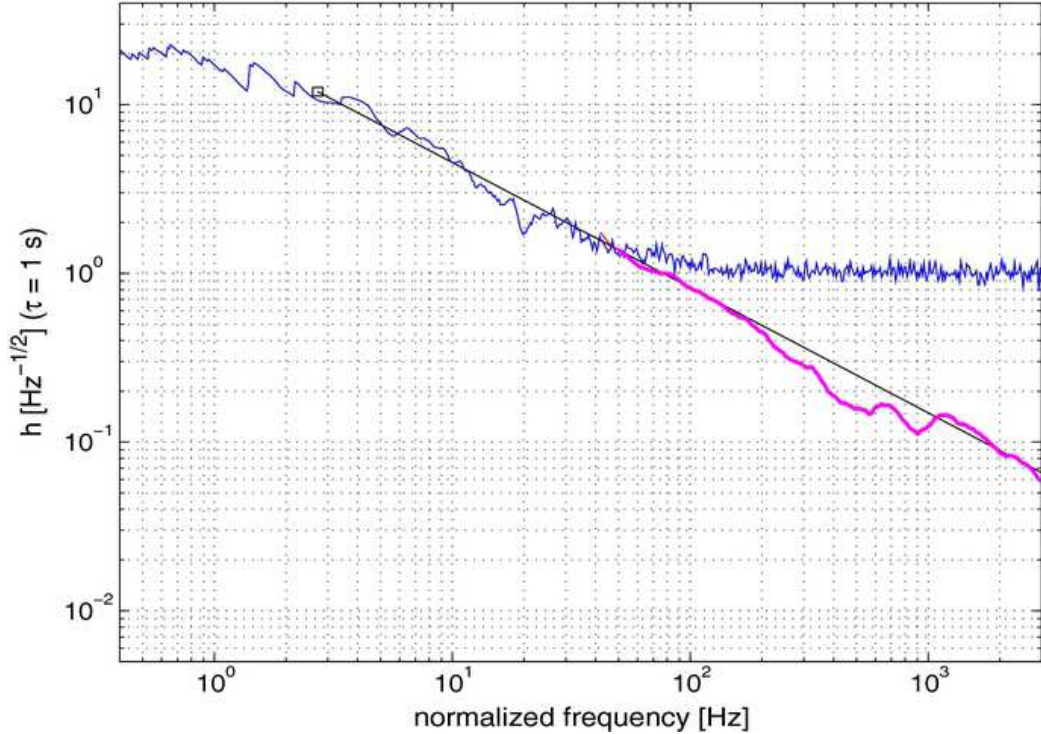


Figure 8. Broadband Kolmogorov spectrum averaged over 42 spectra of “red” bursts with non-trivial autocorrelation functions, extracted by matched filtering using a bank of 8.64 million chirp templates. The results shown in the source frame show a continuation (black line) to a few kHz (purple, in the source frame of the GRBs) of the Kolmogorov spectrum identified by low-frequency Fourier analysis (blue). (Reprinted from (van Putten et al. 2014a).)

in total photon count (Kouveliotou et al. 1993). BATSE identified a mostly non-thermal spectrum, which is typically well described by a smoothly broken power-law (Band spectrum (Band et al. 1993)).

BeppoSAX seminal discovery of X-ray afterglow emission to GRB 970228 by (Costa et al. 1997) allowed rapid follow-up by optical observations (van Paradijs et al. 1997), providing a first cosmological redshift ($z = 0.835$ of GRB 970508) in optical absorption lines of FeII and MgII (Metzger et al. 1997; Amati et al. 1998). When detected, afterglow emission of short GRBs tends to be very weak compared to those of LGRBs, consistent with less energy output and burst locations outside star forming regions. Weak X-ray afterglow emission discovered by *Swift* in the High Energy Transient Explorer-2 (HETE II) event GRB 050507 (Fox et al. 2005) and the *Swift* event GRB 050509B (Gehrels et al. 2005) were anticipated for GRBs from rotating black holes (van Putten & Ostriker 2001). Following GRB 970508, *BeppoSAX*, HETE II and *Swift* provided a growing list of GRBs with measured redshifts. Presently, the total number of redshifts identified is about 350 with 287 due to *Swift* alone. Fig. 3 shows the distribution of the latter.

Swift identified the new class of short GRBs with Extended Emission (SGRBEEs). GRB060614 ($T_{90}=102$ s) has no detectable supernova (Della Valle et al. 2006; Fynbo et al. 2006; Gal-Yam et al. 2006) and GRB 050724 is a SGRB with Extended Emission (SGRBEE) with an overall emission time $T_{90}=69$ s in an elliptical host galaxy (Berger et al. 2005, 2007). Neither is readily associated with a massive star. Since then, the list of SGRBEEs has grown considerably (Table 2). Table 2 further shows a few long GRBs with no apparent association to SNe (LGRBNs). SGRBEE and

LGRBNs challenge the BATSE classification into short and long events. Though both show an initial hard pulse, characteristic of short GRBs, a subsequent long duration soft tail features a spectral peak energy ($E_{p,i}$)-radiated energy (E_{iso}) correlation that satisfies the Amati-correlation holding for normal long GRBs. This “hybrid” structure of observational properties of SGRBEE and LGRBNs suggests that they share the *same astronomical origin as short GRBs with the same physics in the central engine as normal long GRBs*, albeit with somewhat smaller values of E_{iso} .

The prompt GRB emission has a characteristic peak energy $E_{p,i}$ at which the νF_ν photon spectrum peaks in the cosmological rest-frame. It typically ranges from tens of keV to thousands of keV. If the isotropic-equivalent energy E_{iso} is the radiation output by a GRB during its whole duration (assuming spherical symmetry), it is found that E_{iso} , commonly used in the absence of reliable information on the degree of collimation in individual GRB events, correlates with $E_{p,i}$ (see Fig. 5). This correlation, now known as the Amati relation, is well established for long GRBs, while short GRBs do not appear to satisfy this Amati-correlation ((Amati et al. 2006) and references therein).

To quantify our level of confidence in the merger origin of SGRBEE and LGRBNs, we recently considered the mean values μ of the observed redshifts (Fig. 4), i.e., μ_L^N of LGRBNs, μ_{EE} of SGRBEEs, μ_S of SGRBs and μ_L of LGRBs, and concluded that they satisfy

$$\mu_L^N < \mu_{EE} < \mu_S < \mu_L, \quad (26)$$

where $\mu_S^{EE} = 0.5286$, $\mu_S = 0.8587$, $\mu_L^N = 0.1870$, and $\mu_L = 2.1069$ based on the redshifts shown in Table 2.

By a Monte Carlo test, we determined the probability that, from the mean redshift, the *Swift* samples of SGRBEE ($n_1 = 7$), SGRB ($n_2 = 15$) and LGRBNs ($n_3 = 3$) are drawn from the observed distribution of LGRBs ($n = 230$). Because of the small n samples and the broad distribution of redshifts of LGRBs (with an observational bias towards low z), we proceed with Monte Carlo test by drawing samples of size n_i ($i = 1, 2, 3$) from the distribution of the $n = 230$ redshifts of the latter. Doing so N times for large N obtains distributions of averages μ_i of the redshifts in these small n samples under the Bayesian null-hypothesis of coming from the distribution of redshifts of LGRBs. We find (van Putten et al. 2014b)

$$\begin{aligned} \text{SGRBEE} \not\subset \text{LGRB}: \quad \sigma &= 4.6700 \\ \text{SGRB} \not\subset \text{LGRB}: \quad \sigma &= 4.7520 \\ \text{LGRBN} \not\subset \text{LGRB}: \quad \sigma &= 4.3140 \end{aligned} \quad (27)$$

For SGRBs, (27) is consistent with a relatively low redshift origin inferred from identification of host galaxies in the local Universe (Tanvir et al. 2005). At a level of confidence exceeding 4σ , SGRBEE and LGRBNs have inner engines originating in mergers in common with normal long GRBs originating in CC-SNe, given that both share the Amati-correlation in the long/soft tail.

Our results (27) show with relatively high confidence that the enigmatic LGRBN GRB060614 is a merger event, suggested earlier based on other arguments (van Putten 2008; Caito et al. 2010b), whose long durations in soft extended emission can be identified with the lifetime of spin of a rotating black hole (§2); see (Zhang 2006; Zhang et al. 2007) for various other explanations of extended emissions from mergers. Baryon-rich jets such as shown in Fig. ?? from accretion disks produced in naked inner engines formed in mergers may dissipate into lower energy emissions, perhaps including a radio burst (van Putten 2009).

2.4. Prompt GRB emission

Three main stages are involved in the generation of the prompt GRB emission: (i) extraction of energy and formation of outflows, (ii) dissipation of the outflow bulk energy, and (iii) conversion by dissipation into electromagnetic radiation. These processes are most likely interrelated. Successful breakout of the jet from the stellar envelope is a necessary condition for producing a GRB. Due to the compactness of the energy source, the largely non-thermal electromagnetic emission originates from large radii and, therefore, does not provide a direct probe of the central engine. Nevertheless, *some* of the temporal properties of the activity of the engine may be imprinted in the light curve of the prompt emission (Kumar et al. 2008a; van Putten & Gupta 2009).

The conventional wisdom has been that GRB jets are powered by magnetic extraction of the rotational energy of a magnetar (Usov 1994; Metzger et al. 2011) or a hyper-accreting black hole, where the latter is a particularly attractive alternative to account for low baryon-loading (Levinson & Eichler 1993; Eichler 2011). In some cases (van Putten et al. 2011b), evidence is tilting towards an association to black holes rather than neutron stars. At sufficiently high accretion rates, annihilation of neutrinos that originate from the hot matter surrounding a Kerr black hole can also power a GRB outflow (Zalamea & Beloborodov 2011; Levinson & Glubus 2013), although magnetic extraction seems favorable. In the latter case, it is believed to form an outgoing Poynting flux which, on large enough scales, is converted somehow into kinetic energy in baryonic contaminants. This conversion process has not been identified yet, but it is generally believed to involve gradual acceleration of the flow (e.g., (Bogovalov 1995; Chiueh et al. 1991; Heyvaerts & Norman 1989; Lyubarsky 2009)), impulsive acceleration (Granot et al. 2011; Lyutikov 2011), magnetic reconnection (Giannios & Spruit 2007; Levinson & van Putten 1997; Lyubarsky 2010; Lyutikov & Blandford 2003; Zhang & Yahn 2011; McKinney et al. 2012), and/or current driven instabilities (Levinson & Begelman 2013).

The production of high energy emission requires substantial dissipation above, or just below the photosphere. It most likely results from the formation of internal (Mészáros & Rees 1993; Rees & Mészáros 1992) and/or collimation (Bromberg & Levinson 2007; Lazzati et al. 2009) shocks in cases where the flow is hydrodynamic in the vicinity of the photosphere, or magnetic reconnection (Giannios & Spruit 2007; McKinney et al. 2012) if the flow remains highly magnetized at large radii. Dissipation at very large optical depths will merely lead to re-acceleration of the flow, or in case of magnetic extraction to a transition to kinetic energy dominated outflows (Granot et al. 2011; Levinson & Begelman 2013). It can, nonetheless, help increasing the specific entropy, which seems to be required by the observed SED peaks.

The nature of the prompt emission mechanism is yet an open issue. The emitted spectrum, although exhibiting notable variations from source to source, can generally be described by a broken power law (Band function (Band et al. 1993)), with some exceptions, e.g., GRB 090902B. It has been originally proposed that the observed spectrum is produced by synchrotron emission of non-thermal electrons accelerated at internal collisionless shocks (for reviews see (Piran 1999, 2004)). However, subsequent analysis (e.g., (Beloborodov 2013; Crider et al. 1997; Eichler & Levinson 2000; Preece et al. 1998)) indicated that the synchrotron model has difficulties accounting for some common properties exhibited by the GRB population, specifically, the clustering of peak energies around 1MeV, the hardness of the spectrum below the peak, and the high efficiencies inferred from the observations. At the same time, it has been argued (Ryde 2004, 2005) that a thermal component appears to be present in

some bursts, which may be transient as in the BeppoSAX event GRB 990712 (Frontera et al. 2001). These developments, and the recent detection of some GRBs with a prominent thermal component (e.g., GRB 090902B) or multiple peaks (e.g., GRB 110721A, GRB 120323A) have motivated a re-consideration of photospheric emission (Beloborodov 2013; Eichler & Levinson 2000; Giannios 2012; Peer et al. 2006; Ryde & Peer 2009; Vurm et al. 2013).

On theoretical grounds, one naively anticipates a significant dissipation of the bulk energy of a GRB outflow just below the photosphere, either by internal (Eichler 1994; Bromberg et al. 2011b; Morsony et al. 2010) or collimation shocks (Bromberg & Levinson 2007; Lazzati et al. 2009). They are mediated by radiation and their typical size is on the order of a few Thomson depths (Budnik et al. 2010; Katz et al. 2010; Levinson & Bromberg 2008; Levinson 2012), larger than any kinetic scale by many orders of magnitudes. Their structure and emission are, therefore, vastly different than those of collisionless shocks that can only form above the photosphere, where the Thomson optical depth is well below unity. The large shock width strongly suppresses particle acceleration (Levinson & Bromberg 2008; Katz et al. 2010), yet a non-thermal spectrum can be produced inside the shock via bulk Comptonization (Budnik et al. 2010) and formation of a Band-like spectrum is conceivable (Keren & Levinson 2014). Alternatively, sub-photospheric dissipation may be accomplished through magnetic reconnection if the flow remains highly magnetized at mild optical depths, in which case particle acceleration may ensue. Under such conditions, formation of a Band spectrum is also plausible (Beloborodov 2013; Giannios 2012; Vurm et al. 2013).

Observationally, a photospheric model (black body plus power law) or a Band function provides a satisfactory fit to most BATSE GRB light curves. However, extending spectra to the low energy range of 2-28 keV (of the BeppoSAX Wide Field Cameras) poses challenges in a number of cases. For the extended energy range of 2-2000 keV, a Comptonization model appears more robust in producing satisfactory fits (Frontera et al. 2013). The low energy window is consistent with Comptonization of black body background photons by an initially non-relativistic expanding outflow, perhaps representative of the initial launch at stellar breakout of the outflow creating the GRB. A particular example, the breakout of a striped MHD jet, computed using numerical simulations, is here presented in §5.2.

The prompt GRB emission is often followed by afterglow emissions at lower energies, especially in X-rays down to radio in some cases. Afterglow emission was anticipated based on the GRB association with ultra-relativistic outflows, further enabling identifying host properties and, in some cases, calorimetry on the total energy output. We refer the reader to existing reviews on this subject (Piran 1999, 2004). *Swift* made a key discovery with the identification of long duration X-ray tails, that appear to represent latent activity of the remnant inner engine (e.g. (Chincarini et al. 2010; Bernardini et al. 2011)). Remarkably, these X-ray tails, when observed, are very similar to short and long GRBs, lending some support for a common engine remnant.

2.5. Kolmogorov spectra in BeppoSAX

To probe for high frequency signatures in the prompt GRB emission and, possibly, any intermittency or quasi-periodic behavior in the inner engine, the *BeppoSAX* catalogue of 2 kHz light curves offers a unique window to broadband spectral analysis. As mentioned above, prompt GRB emission probably originates from ultra-relativistic, baryon poor jets, launched from a compact stellar mass object (Sari & Piran 1997; Piran & Sari 1997) (see also (Kobayashi et al. 1997; Nakar & Piran 2002)), commonly believed to be black holes or neutron stars (Thompson 1994; Metzger et al. 2011).

Shock induced emission predicts a spectrum that is a power law in energy (e.g. (Sari et al. 1998; Thompson et al. 2007)) and turbulent in temporal behavior. Indeed, a Fourier analysis reveals a Kolmogorov spectrum in the BATSE and BeppoSAX catalogs of light curves of long GRBs (Beloborodov et al. 1998, 2000; Guidorzi et al. 2012; Dichiara et al. 2013a,b). The index of power law behavior in the observed PSD spectra is broadly distributed about the Kolmogorov value of $5/3$ with a negative gradient as a function of energy (Fig. 6). Conceivably, this spectral-energy gradient might be due to scale dependent dissipation in turbulent flows, which is only beginning to be explored by high resolution numerical simulations in the approximation of relativistic hydrodynamics (Zrake & MacFadyen 2013) (see also (Calafut & Wiita 2014)).

However, Fourier spectra are limited to tens of Hz due to strong Poisson noise in high frequency sampled gamma-ray light curves. The Kolmogorov spectrum is expected to continue to higher frequencies. This has recently been identified in broadband spectra obtained by a chirp search method. The method uses matched filtering using chirp templates with frequencies slowly moving up or down of 1 second duration (Appendix D). Applied to 2 kHz sampled *BeppoSAX* light curves of long GRBs (7), an approximately Kolmogorov spectrum is found to extend to 1 kHz in the observer’s frame or, equivalently, a few kHz in the source frame (Fig. 8).

The above gives considerable evidence for LGRBs produced by successful breakout of ultra-relativistic jets emerging from an energetic CC-SNe (and LLGRBs as their failed-to-breakout counterparts). While the latter may be powered by an associated baryon-rich collimating wind, the GRB is attributed to dissipation in internal and/or collimation shocks in the former, that may be the result of intermittency at the source.

The preceding data point to a common origin in mergers of SGRBEE, LGRBNs and normal LGRBs: their soft/long tail sharing the same Amati-relation (Fig. 5) and the Kolmogorov spectrum of gamma-ray fluctuations is smooth with no evidence for a bump that might indicate the formation of proto-pulsars. These hints point to a *common engine producing soft extended emission*, and probably so from black holes in mergers and CC-SNe alike. Additionally, rotating black holes have ample energy to account for the most energetic GRB-SNe (Table 1). Apart from the low number counts, the only reservation would be extremely sub-luminous CC-SNe (cf. (Pastorello et al. 2007)), that would be undetectable in our sample LGRBNs (Fig. 4).

On the premise of black holes unifying the soft extended emission in normal LGRBs (in core-collapse of massive stars) and SGRBEEs (from mergers), we next turn to a model for extended emission from rotating black holes, parameterised largely by black hole mass, defined by a secular time scale of spin down against surrounding high density matter rather than any time scale of accretion or free fall.

3. EXTENDED EMISSION FROM ROTATING BLACK HOLES

The exact Kerr (1963) solution of rotating black holes is parameterised by mass M , angular momentum J and electric charge Q . Rotation is commonly expressed by the dimensionless parameter a/J , where $a = J/M$ denotes the specific angular momentum. According to the Kerr solution, $-1 \leq a/M \leq 1$, allowing $\sin \lambda = a/M$ in terms of $|\lambda| \leq \pi/2$ (van Putten 1999). Spacetime about a rotating black holes is dragged into rotation at an angular velocity ω , that may be observed as the angular velocity of test particles (at constant radial distance and poloidal angle) with vanishing angular momentum as measured at infinity. The angular velocity Ω_H of the black hole is defined as the limit of ω as one approaches the black hole that, by the no-hair theorem, reduces to a constant

$\Omega_H = \tan(\lambda/2)/2M$ on the event horizon. At a corresponding spin frequency $\nu_H = \Omega_H/2\pi$,

$$\nu_H = 1.6 \text{ kHz} \tan(\lambda/2) \left(\frac{10M_\odot}{M} \right), \quad (28)$$

the total energy in angular momentum satisfies $E_{rot} = 2M \sin^2(\lambda/4)$, i.e.,

$$E_{rot}^H \simeq 6 \times 10^{54} \text{ erg} \left(\frac{M}{10M_\odot} \right) \left(\frac{\sin(\lambda/4)}{\sin(\pi/8)} \right)^2. \quad (29)$$

In an astrophysical environment, rotating black holes can naturally account for extended emission with characteristic features (5-7) upon identifying durations with the lifetime of their spin.

3.1. Secular time scale of black hole spin

To be specific, we propose that BATSE durations T_{90} of their prompt emission (Fig. 1) represents a proxy for the lifetime of the engine (van Putten 1999; van Putten & Ostriker 2001; van Putten & Levinson 2003), i.e.,

$$T_{engine} \simeq T_{90} \quad (30)$$

while $\Omega_H > \Omega_{ISCO}$, where $\Omega_{ISCO} = (M(z^{3/2} \pm \sin \lambda))^{-1}$ is the angular velocity of matter at the ISCO for prograde (+) and retrograde (-) orbital motion (e.g. Shapiro & Teukolsy 1983). The inequality $\Omega_H > \Omega_{ISCO}$ is readily satisfied. According to the Kerr metric, it holds whenever their rotational energy exceeds about 5.3% of their maximal spin energy (for a given black hole mass-at-infinity M).

In the proposed identification (30), T_{90} provides a unique signature of the inner engine of LGRBs and SGRBEEs, where the latter derives from the merger of a neutron star with another neutron star or rotating companion black hole. We herein identify SGRBs (without EE) with hyper-accretion onto slowly rotating black holes, produced in mergers of neutron stars with a slowly spinning black hole companion (van Putten & Ostriker 2001) (Fig. 9).

In (30), black holes are envision to be losing angular momentum primarily to surrounding matter about the ISCO, leaving a minor release about the spin axis in open outflows powering the baryon-poor ultra-relativistic jets (BPJ) seen in gamma-rays with luminosity (van Putten & Levinson 2003; van Putten 2009)

$$L_j \simeq 1.4 \times 10^{51} \text{ erg s}^{-1} \left(\frac{M}{7M_\odot} \right) \left(\frac{T}{20 \text{ s}} \right) \left(\frac{\theta_H}{0.5} \right)^4. \quad (31)$$

For rapidly rotating black holes, L_j along open magnetic flux tubes is supported by Carter's magnetic moment μ_e^H of the black hole (Carter 1968; Cohen et al. 1973; Wald 1974), in equilibrium with the external magnetic field supported by the surrounding inner disk or torus in a state of suspended accretion (van Putten & Ostriker 2001; van Putten & Levinson 2003).

Fig. 10 illustrates in poloidal cross-section the structure of open outflows in a suspended accretion state, allowing the black hole to lose angular momentum J to surrounding matter. Like their supermassive counter parts (e.g. Macchetto et al. 1997; Walsh et al. 2013) or galactic stellar mass black holes in micro-quasars such as GRS 1915+105 (Mirabel et al. 1994; Greiner et al. 2001), accretion flows in catastrophic events are believed to be likewise magnetised, exposing the central black

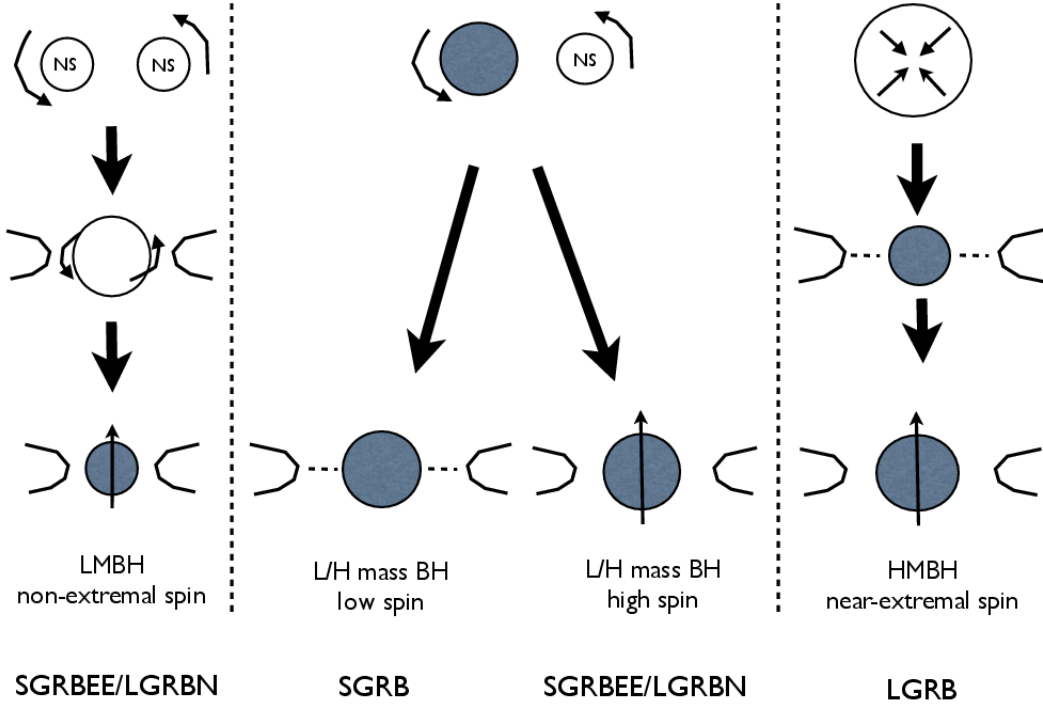


Figure 9. GRBs from rotating black holes may originate in mergers of neutron stars with another neutron star (NS-NS, left) or stellar mass black hole (NS-BH, middle) as well as core-collapse of a massive star (CC-SN, right). The black hole-disk or torus system will be of relatively low (LMBH) or high mass (HMBH). NS-NS produces a LMBH with high but non-extremal spin after passing through a super-massive near-extremal neutron star phase (e.g. [Baiotti et al. 2008](#)). The spin of the HMBH following NS-BH mergers depends largely on the spin of the BH in the progenitor binary, unless its mass and spin are extremely low. Black hole formation in core-collapse passes through Bondi and modified Bardeen accretion, causing the black hole to surge to high mass and near-extremal spin. We identify soft Extended Emission (EE) with the spin down phase of rapidly rotating black holes, producing SGRBEEs or LGRBs with no supernovae (LGRBN) from mergers (involving rapidly rotating black holes) and normal LGRBs from core-collapse of massive stars. This common physical origin is supported by a common Amati-correlation. (Reprinted from ([van Putten 2015c](#)).

hole to a finite magnetic flux by accretion ([Ruffini & Wilson 1975](#); [Bisnovatyi-Kogan et al. 1976](#); [Blandford & Znajek 1977](#)) or the formation of a torus magnetosphere ([van Putten 1999](#)). Strong magnetic fields may derive from the magneto-rotational instability (MRI, [Balbus & Hawley \(1991\)](#); [Lubow et al. \(1994\)](#); [Globus & Levinson \(2014\)](#)), whose $m = 0$ component of the infrared spectrum of MHD turbulence represent a net poloidal flux. In turbulent accretion ([Bisnovatyi-Kogan et al. 1976](#)) or by forcing ([van Putten 1999](#)), μ_H will follow changes in sign in the $m = 0$ part of the infrared MHD spectrum on an Alfvén crossing time scale. Exposed to a finite variance in poloidal magnetic flux, a rapidly rotating black hole develops a finite magnetic moment that preserves maximal magnetic flux through the event horizon at all spin rates. This holds true especially at maximal spin ([Wald 1974](#); [Dokuchaev 1986](#); [van Putten 2001a](#)). In the absence of a small angular parameter in the connection of magnetic flux from the latter to the former, the result is an Alfvén wave over an inner

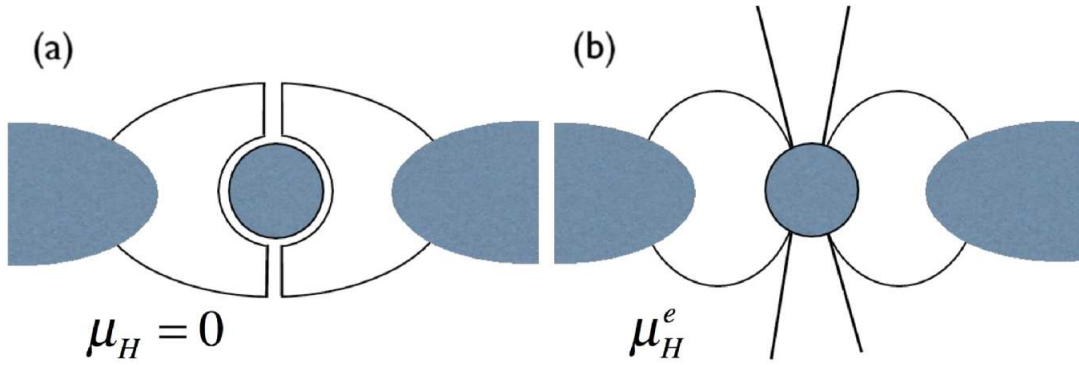


Figure 10. An extremal black hole with vanishing Carter’s magnetic moment is out-of-equilibrium with vanishing horizon flux (a), which rapidly settles down to an equilibrium state with essentially maximal horizon flux. An open magnetic flux tube forms supported by the equilibrium value μ_H^e (b). In (a), the black hole does not evolve. At sub-critical accretion rates, frame dragging may produce BPJs while accretion from the ISCO is suspended by feedback from the black hole by Alfvén waves via an inner torus magnetosphere (b). Major dissipation ($E_D > 0$) by forced MHD turbulence about the ISCO implies $R_{jD} = E_j/E_D \ll 1$. By slip and no-slip boundary conditions on the event horizon and, respectively, matter at the ISCO, the black hole gradually loses angular momentum, giving rise to a finite lifetime T_s of rapid spin. (Reprinted from van Putten (2015c).)

torus magnetosphere, allowing black holes losing angular momentum to a torus about the ISCO. In this process, the latter is heated and expected to be driven non-axisymmetric instabilities balanced by cooling in gravitational radiation (van Putten 2012a). The strength in poloidal magnetic flux may be derived from a magnetic stability limit $E_B/E_k \simeq 1/15$ of energy E_B of the poloidal magnetic field to the kinetic energy E_k in the inner disk or torus (van Putten & Levinson 2003). Conceivably, this bound may be circumvented by strongly intermittent inner engines (van Putten 2015b), see also (McKinney et al. 2012). As a result, a key parameter setting the lifetime of rapid spin of the black hole is the mass M_T in the torus.

The output (31) is robust in being a consequence of differential frame-dragging. (ω decays to zero at infinity from Ω_H on the black hole.) Locally, the effect is manifest in Papapetrou forces (Papapetrou 1951; Pirani 1956) acting on the canonical angular momentum of charged particles supporting a Poynting flux-dominated outflow. The line-integral thereof is a potential energy (van Putten & Gupta 2009) $E = \omega J_p$. For charged particles, J_p is defined by total magnetic flux on the flux-surface at hand (which is an adiabatic invariant). In super-strong magnetic fields typically considered in models of GRB inner engines, E assumes energies on the scale of Ultra-High Energy Cosmic Rays (UHECRs). This may be processed downstream to gamma-ray emission in relativistic shocks or, for intermittent sources, into UHECRs by acceleration of ionic contaminants ahead of outgoing Alfvén fronts (van Putten & Gupta 2009).

The jet luminosity (31) differs from the open model of force-free flux surfaces rotating at one-half the angular velocity of the black hole envisioned in (with $\theta_H = \pi/2$ in Blandford & Znajek 1977), in that only a minor fraction of the black hole luminosity channeled in an open outflow whenever $\theta_H \ll \pi/2$. In van Putten (2015c), we consider $\theta_H = \theta_H(t)$ positively correlated to the ISCO: $L_j \propto \Omega_H^2$ and, since L_j is dimensionless in geometrical units, $L_j \propto (r_{ISCO}\Omega_H)^2$ for a correlation to the ISCO. Consequently, $L_j \propto z^2\Omega_H^2$ in a Taylor series expansion in $z = r_{ISCO}/M$, where r_{ISCO} denotes the ISCO radius around the black hole with angular velocity Ω_H . Numerical integration of

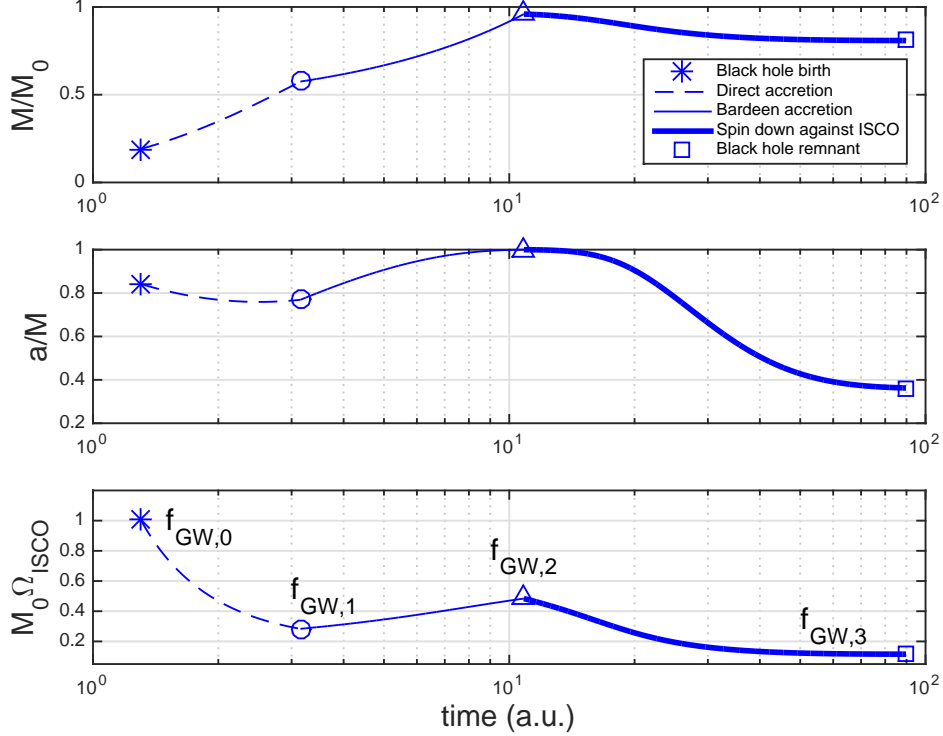


Figure 11. Evolution of a rotating black hole following birth in a progenitor of mass M_0 in three phases of accretion: surge in direct accretion (*dashed*), growth by Bardeen accretion (*continuous*) followed by spin down against matter at the ISCO when accretion becomes subcritical (top and middle panels). Shown is further the associated evolution of any quadrupole gravitational wave signature from matter at the ISCO, marked by frequencies f_{GW_0} at birth, f_{GW_1} at the onset of Bardeen accretion, f_{GW_2} at the onset of spin down and f_{GW_3} at late times, when the black hole is slowly rotating in approximate corotation with matter at the ISCO (lower panel.)

the equations of suspended accretion (with fixed points at extremal and slow spin) obtains a light curve $L_j(t)$ from (31), providing a template suitable for normalising light curves by matched filtering (van Putten 2012a; van Putten & Della Valle 2017). If L_j represents an opening outflow supported by horizon flux over the *full hemisphere* of the black hole event horizon, E_j will be a substantial fraction of E_r . For GRBs, however, this runs counter to a generically small fraction of true energy in prompt GRB outflows relative to E_{rot}^H of a black hole (van Putten & Levinson 2003; van Putten 2015c).

Immediately after birth, a black hole in core-collapse grows by Bondi accretion (Bondi 1952; Shapiro & Teukolsky 1983), up to the moment that an accretion disk first forms by angular momentum hang-up about the ISCO of the newly formed rotating black hole. Subsequently, Bardeen (1970) accretion is expected to ensue (McKinney 2005; Kumar et al. 2008b; King & Pringle 2006) - modified by open outflows (van Putten 2015c) - driving the black hole to a near-extremal state, provided there is sufficient mass infall to reach this state. As accretion rates become sub-critical in the sense of Globus & Levinson (2014), such near-extremal black hole may experience angular momentum loss to surrounding matter at the ISCO through Alfvén waves in an inner torus magnetosphere, until its angular velocity Ω_H drops to Ω_{ISCO} of matter orbiting at the ISCO - a stable fixed point in the equations of suspended accretion (van Putten 2008).

Fig. 11 illustrates the complex sequence of different types of accretion, over the course of which the black grows in mass and spins down (Bondi accretion), grows in mass and spins up (Bardeen accretion), and loses mass-energy and spins down (suspended accretion). The latter introduces a radically new secular time-scale (van Putten & Levinson 2003; van Putten & Della Valle 2017)

$$T_s \simeq 30 \left(\frac{\sigma}{10^{-2}} \right)^{-1} \left(\frac{M}{7M_\odot} \right) \left(\frac{z}{6} \right)^4 \text{ s}, \quad (32)$$

defined by the ratio $\sigma = M_T/M$ of the mass M_T of a torus at the ISCO to M and its normalised radius $z = R/M$. According to (32), the process of losing angular momentum to matter at the ISCO can extend to ultra-long durations when σ is small, e.g.,

$$T_s \simeq 100 \left(\frac{\sigma}{10^{-7}} \right)^{-1} \text{ d}, \quad (33)$$

which time scale can be found in superluminous supernovae such as SN2015L (van Putten & Della Valle 2017).

The process of black holes losing angular momentum to matter at the ISCO is expected especially from a fully developed turbulent disk. Exposed to a finite variance in poloidal magnetic flux, a rapidly rotating black hole develops a finite magnetic moment that preserves maximal magnetic flux through the event horizon at all spin rates. This holds true especially at maximal spin (Wald 1974; Dokuchaev 1986; van Putten 2001a). Fig. 12 shows the overall efficiency of radiation thus catalytically converted from black hole spin.

3.2. Observational evidence of black hole spin down

Normalized light curves (nLC) extracted from the BATSE catalogue of LGRBs allow a confrontation with model templates of spindown, of black holes against high density matter at the ISCO and (proto-)neutron stars by magnetic winds. In making the connection to the observed GRB emission, we consider a linear correlation between ultra-relativistic baryon-poor outflows and the observed prompt GRB emission. Fig. 13 shows match between nLC and model templates. The results favour the first, especially so for very long duration events with T_{90} exceeding tens of seconds. Similar results obtain for nLC extract from *Swift* (Gupta & van Putten 2012). Noticeable also is an improvement in the fit for relatively long duration events with $T_{90} > 20$ s (van Putten 2009). We attribute this to the time scale of jet breakout in a remnant stellar envelope for the majority of long GRBs originating in CC-SNe (van Putten 2012a), possibly further in association with the most rapidly spinning black holes (van Putten 2009). Based on different observations related to the relatively flat distribution of T_{90} below 20 s, a similar conclusion obtains (Bromberg et al. 2013).

Eq.(30) may be contrasted with various time scales of accretion, generally associated with growth and spin-up of the central black hole. In Kumar et al. (2008b), a distinction is outlined between fall-back at high and low (down to zero) accretion rates. The first implies an initial $\dot{m} \propto t^{-1/2}$ for the first ten seconds or so in transition to $\dot{m} \propto t^{-3}$ on the time scale of one hundred seconds. The second implies $\dot{m} \propto t^{-n}$ with $4/3 \leq n \leq 2$, depending on the detailed radial profile of mass-loss in winds. Assuming a linear correlation between black hole luminosity L_H powering the prompt GRB emission and accretion rate (Kumar et al. 2008b), the same procedure applied to these accretion models shows matches vastly sub-par to those shown in Fig. 13 (van Putten & Della Valle 2017). For power law

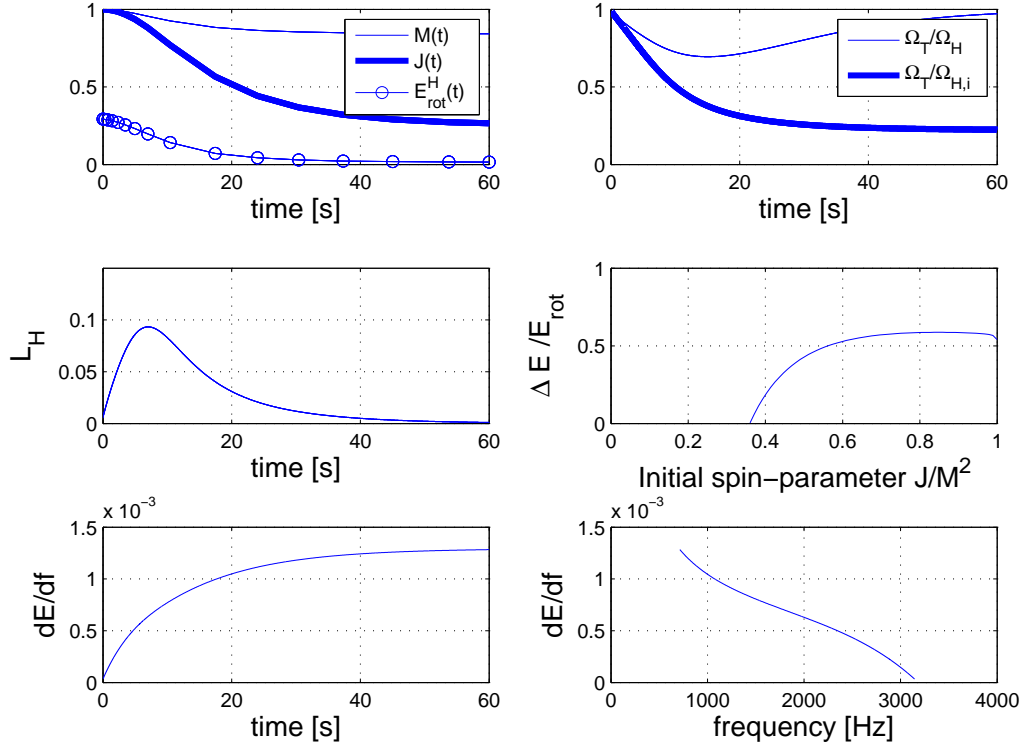


Figure 12. (Top panels.) An initially extremal Kerr black hole may lose mass M and angular momentum J (normalized to initial values $M(0)$ and $J(0)$, respectively) to a surrounding matter at the angular velocity $\Omega_T \simeq \Omega_{ISCO}$. M , J and the rotational energy E_{rot} hereby decrease by 15.8%, 74.4% and, respectively, 94.7% during evolution to the fixed point, at $\Omega_H = \Omega_{ISCO}$ of an initially extremal black hole, and Ω_{ISCO} decreases to that of a slowly spinning black hole from its initial value $\Omega_{H,i} = 1/2M$. (Middle panels.) For an initial $M = 10M_\odot$, the black hole luminosity L_H onto matter at the ISCO peaks at about $0.1M_\odot \text{ s}^{-1}$, neglecting a minor output in ultra-relativistic baryon-poor jets along the spin axis. (Bottom panels.) The spectral energy density satisfies $dE/df \simeq E/f$ (in units of $M_\odot \text{ Hz}^{-1}$) for $E = M_\odot$ and $f = 1000 \text{ Hz}$.

accretion profiles, discrepant behavior appears notably in a spike between the nLC and the model light curves, characterized by a prompt switch-on (cf. short GRBs). In contrast, Fig. 13, shows a satisfactory match the nLC with the model light curve of black holes losing angular momentum against matter at the ISCO across the full duration of the bursts. The results for $T_{90} > 20 \text{ s}$ provide some support for very long GRBs commencing from near-extremal rotating black holes, perhaps in the Thorne limit of the Bardeen trajectory of evolution (van Putten 2015c). Furthermore, extreme luminosities in GRBs can derive from a nonlinear response to intermittent accretion about the ISCO (van Putten 2015b), perhaps stimulated by feedback from the black hole starting from aforementioned nearly extremal spin.

3.3. Slow rotating remnants

A principle outcome of black hole evolution shown in Fig. 11 is a slowly rotating remnant, whose angular velocity has reached the fixed point $\Omega_H = \Omega_{ISCO}$ in the equations of suspended accretion, satisfying

$$a/M \simeq 0.36 \quad (34)$$

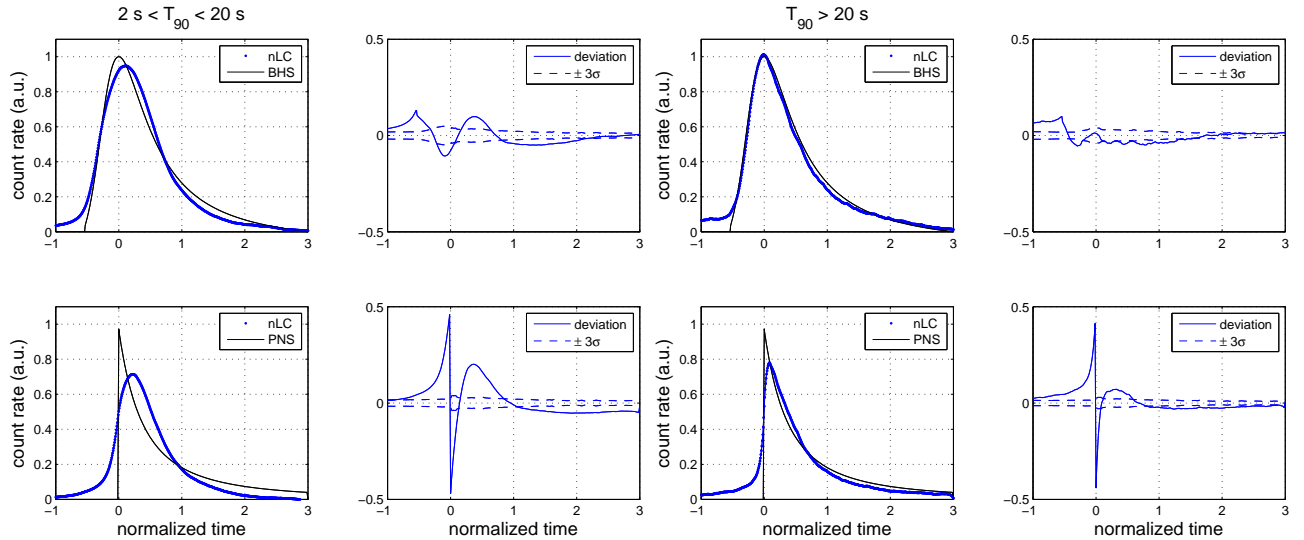


Figure 13. Normalized GRB light curves (nLC, thick lines) extracted from the BATSE catalog, by matched filtering on model templates (thin lines) for outflows from spindown of rotating black holes (BHS, A) and proto-neutron stars (PNS, C). Consistency is relatively better for the former, especially so for durations greater than 20 s. We attribute this time scale to that of jet breakout of a stellar remnant envelope. (Adapted from (van Putten 2012a).)

as a black hole gradually lost most of its angular momentum, and the surrounding Kerr space time relaxed to the space time of a slowly spinning black hole. Just such slow spin appears to be present in the progenitor binary estimates (2) of GW150914.

As a stable fixed point, the black hole luminosity will reach a plateau with finite luminosity in open outflows, provided there is a continuing (latent) accretion. In attributing SN2015L to black hole spin down following (33), just such plateau is seen at late times in the optical light curve. Following (32), it may signal X-ray tails (XRT) over time scales of thousands of seconds, discovered by *Swift*, that are remarkably universal to LGRBs and SGRBs alike, pointing to a common remnant (Eichler et al. 2009). We here identify this remnant with slowly rotating black holes about the stable fixed point (34), as a sure outcome regardless of prior formation and evolution history and progenitor (Fig. 14). In the present context, XRT’s may possibly be accompanied by long lasting low luminosity gravitational wave emission. As a common endpoint, this may appear both to normal LGRBs and SGRBs originating in mergers, following messy break-up of neutron stars in the tidal field of a companion black hole (Lee & Kluzniak 1998; Lee & Kluznian 1999) or in the merger of two neutron stars (Rosswog 2007).

We estimate the resulting release in X-rays to have a luminosity $L_X \simeq 0.25 \dot{m}$ for an accretion rate \dot{m} . Accompanying gravitational wave emissions should be very weak with negligible increase in black hole mass and angular momentum in view of the observed X-ray luminosities, e.g., $L_X \simeq 10^{41}$ erg s⁻¹ in GRB060614 (Mangano et al. 2007). If unsteady, large amplitude flaring may occur in, e.g., GRB050502B (Gehrels et al. 2009) by fluctuations between feedback of the black hole ($\Omega_H > \Omega_T$) or accretion ($\Omega_H < \Omega_T$). See also (Lei et al. 2008).

In this broad outlook on “multi-phase multi-messenger” emissions in core-collapse events, we shall focus on a general framework for BEGE from accretion onto rotating black holes and a specific

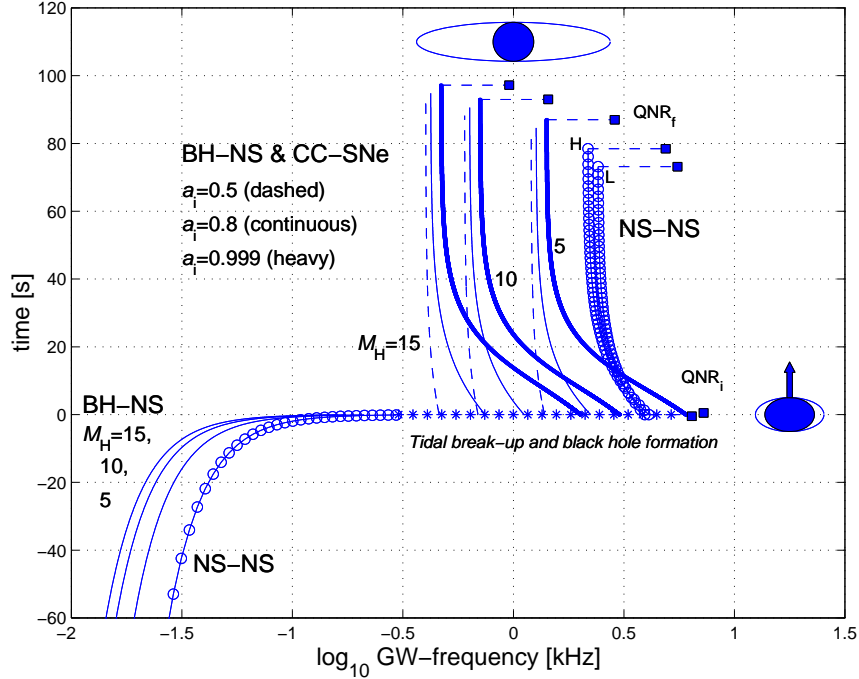


Figure 14. Rotating black holes surrounded by a high density disk are a common outcome of the coalescence of neutron stars with another neutron star or black hole and core-collapse of relatively massive stars. If the black hole spins rapidly, it may lose angular momentum to the surrounding matter leading to catalytic conversion of its spin energy into gravitational waves (van Putten 2001b). The result is a descending chirp for the lifetime of rapid spin. In the relaxation of spacetime to that of a slowly rotating black hole, the ISCO expands the frequency asymptotes to (80). For the merger of two neutron stars, this asymptotic result is tightly constrained by the narrow distribution of their masses and spin (Baiotti et al. 2008), here emphasized by H and L for high- and low-mass neutron stars. Absent a remnant stellar envelope, such binary merger creates a naked inner engine, whose magnetic winds may produce an observable radioburst. (Reprinted from (van Putten 2009).)

connection to the ample energy in angular momentum of rapidly spinning black holes following Fig. 11.

4. ASCENDING AND DESCENDING CHIRPS IN ACCRETION FLOWS

The relatively high densities anticipated in accretion flows in catastrophic events such as mergers and core-collapse of massive stars forms a promising starting point for broadband extended gravitational-wave emission. In essence, we expect gravitational radiation derived from accretion flows and, possibly, ISCO waves excited by input from the black hole, converting angular momentum in orbital motion and, respectively, spin of the central black hole. A key pre-requisite for this outlook is the onset of non-axisymmetric waves.

4.1. *Alpha-disk model*

The *alpha-disk* model allows us to give a general frame work for mass-inhomogeneities in accretion flows. We consider a disk with the following properties:

1. A kinematic viscosity ν expressed in terms of a dimensionless α parameter given by

$$\nu = \alpha c_s H = \frac{\alpha \Omega H^2}{\sqrt{2}} = \frac{\alpha H^2}{\sqrt{2} M} \left(\frac{M}{r} \right)^{3/2}, \quad (35)$$

using $c_s = \Omega H / \sqrt{2}$ for the sound speed in terms of orbital angular velocity Ω . Here, r is the radial distance to the black hole of mass M and, typically, $0.001 < \alpha < 0.1$. Where accretion flows are governed by viscous torques, the surface density of the disk satisfies $\Sigma(r) = \dot{m} / (3\pi\nu)$ (Pringle 1981) for an accretion rate \dot{m} with asymptotic radial migration velocity v_r^ν , i.e.,

$$\Sigma = \frac{M \dot{m} \sqrt{2}}{3\pi \alpha H^2} \left(\frac{r}{M} \right)^{3/2}, \quad v_r^\nu = \frac{3\nu}{2r} = \frac{3\alpha H^2}{2\sqrt{2} M} \left(\frac{M}{r} \right)^{5/2}. \quad (36)$$

As shown below, under certain conditions, there exists a critical radius r_ν in (55) within which angular momentum loss is dominated by gravitational radiation;

2. A Lagrangian disk partition, given by annular rings of radius r , radial width $l(r)$ and mass $\Delta m(r) \equiv \sigma(r)M$, here in the approximation that $l(r)$ is similar to the vertical scale height $H(r)$ of the disk. A ring is parametrised by its mass inhomogeneity, total energy and gravitational wave luminosity

$$\delta m = \xi \Delta m, \quad \Delta E = \frac{\sigma M}{2} \left(\frac{M}{r} \right), \quad \Delta L_{GW} = \frac{32}{5} \xi^2 \sigma^2 \left(\frac{M}{r} \right)^5. \quad (37)$$

in terms of the dimensionless parameter $0 \leq \xi < 1$ (Appendix A), where ξ is not necessarily small, in a local Keplerian approximation $q = 3/2$ in the angular velocity distribution

$$\Omega(r) = M^{-1} \left(\frac{M}{r} \right)^q. \quad (38)$$

We shall cover gravitational radiation from mass-inhomogeneities in accretion flows down to the ISCO. By self-gravity, these may appear as instabilities driven by cooling, wave-like or as fragments, when cooling times are on the order of the orbital period (Gamma 2001; Rice et al. 2005). In accretion flows onto rotating black holes, a crucial condition is that such instabilities set in at a radius outside the ISCO. In this event, accretion may be driven by angular momentum loss in gravitational radiation rather than viscous torques across some critical radius greater than r_{ISCO} . Although the detailed origin and structure of mass-inhomogeneities formed is uncertain, we shall, for illustrative purposes, discuss these in the quadrupole approximation. In this approximation, migration of mass-inhomogeneities is described by (29-31) of Appendix A.

Spiral in of inhomogeneities by gravitational radiation dominated angular momentum loss may commence at radii large compared to r_{ISCO} . In this event, the luminosity in gravitational waves at a given mass accretion rate

$$\dot{M} = \dot{m} \dot{m}_0, \quad \dot{m}_0 = \frac{c^3}{G} = 4 \times 10^{38} \text{ g s}^{-1}, \quad (39)$$

satisfies

$$\frac{L_{GW}}{\dot{m}} \simeq \frac{M}{2r_{ISCO}}. \quad (40)$$

For illustrative purposes, we express (40) in a Newtonian approximation of the gravitational binding energy at the ISCO to the central black hole. A more precise estimate for the latter is given by $1 - e$, where e denotes the specific energy of orbiting matter in the Kerr metric given. Our aim here is to develop leading order estimates within a factor of a few. Accretion onto the ISCO may be followed by a plunge into the black hole or mass ejection in the form of a disk wind.

The scale (40) points to a potentially substantial energy output E_{GW} in gravitational waves, provided that a window $r_c > r_{ISCO}$ or $r_b > r_{ISCO}$ for gravitational radiation dominated angular momentum transport exists. As the following two sections show, this depends on cooling, viscous transport by random walks of large scale eddies describes by the alpha disk model (2) above and mass-inhomogeneities parameterized by ξ . The α and ξ are probably inversely correlated, although a detailed description thereof is not known. For instance, small α disks have relatively high density and/or low temperature, by which they are prone to a variety of self-gravity and wave-like instabilities that may produce ξ .

We introduce

$$P = \frac{\xi}{\alpha} \quad (41)$$

to reflect the ratio of gravitational radiation-to-viscous mediated angular momentum transport. P effectively acts as an efficiency parameter in the gravitational wave output from the extended disk $r > r_b$ in the alpha model, assumed to hold for $r \geq r_b > r_{ISCO}$. In this region, the efficiency in gravitational radiation is relatively low and the approximation $l \simeq H$ in (36) gives the mass density profile

$$\sigma = 2\pi r l \Sigma = \frac{2\sqrt{2} M}{3\alpha H} \left(\frac{r}{M}\right)^{\frac{5}{2}} \dot{m} \quad (r > r_b). \quad (42)$$

Accordingly, (37) implies

$$\Delta L_{GW} = \frac{256}{45h^2} P^2 \left(\frac{M}{r}\right)^2 \dot{m} \quad (r > r_b). \quad (43)$$

Adopting a scaling $H = h_0 r$, the total disk luminosity $L_{GW} = \int_{r_b}^{\infty} \Delta L_{GW} dn$, $dn = dr/l$, satisfies

$$\frac{L_{GW}}{\dot{m}} = \frac{256}{90h^3} \frac{P^2}{z_b^2} \dot{m} \simeq 1.4 \frac{P_1^2}{z_\nu^2} \left(\frac{h_0}{0.1}\right)^{-3} \left(\frac{\dot{M}}{M_\odot \text{ s}^{-1}}\right), \quad (44)$$

where $z_b = r_b/M$ and $P = 10 P_1$ associated with a fiducial value $\alpha = 0.1$.

Based on these preliminaries, we next turn to some specific estimates of r_c and r_b .

4.2. Fragmentation chirps

In self-gravitating accretion flows, a possible origin of mass inhomogeneities is fragmentation when the cooling time of the accreted matter in the instability zone is on the order of or shorter than the orbital time (e.g., (Gamma 2001; Rice et al. 2005; Mejia et al. 2005)). The disk is unstable to axisymmetric perturbations if (Toomre 1964; Goldreich & Lynden-Bell 1965)

$$Q = \frac{c_s \Omega}{\pi G \Sigma} < 1, \quad (45)$$

and to non-axisymmetric perturbations at slightly larger values, $Q \lesssim 2$ (e.g. (Griv 2011)).

For our α -disk model, (45) yields a characteristic radius beyond which the instability may be generated (Piro & Pfahl 2007):

$$\frac{r_c}{M} > \left(\frac{3\alpha h_1^3}{\sqrt{2}\dot{m}} \right)^{2/3} \simeq 300\alpha_{-1}^{2/3} \left(\frac{h_1}{0.5} \right)^2 \left(\frac{\dot{M}}{M_\odot \text{ s}^{-1}} \right)^{-2/3} \quad (46)$$

adopting $H = h_1 r$ at this radius (Popham et al. 1999; Chen & Beloborodov 2007) with the fiducial scale $h_1 = 0.5$ for the relatively colder disk flow further out. The characteristic wavelength of the fastest growing mode is of the order of QH , and its mass is $(QH)^2 \Sigma$.

Cooling may derive from several channels. Among electron-positron pair annihilation to neutrinos, URCA process, and photo-disintegration of ${}^4\text{He}$, it has been argued that the latter may be most effective one in the instability zone (Piro & Pfahl 2007). Rapid cooling may thus lead to fragmentation into a gravitationally bound clumps of mass m_f up to a few percent of the mass of the black hole, i.e. (Piro & Pfahl 2007):

$$m_f = M\sigma_f \simeq M\Sigma(QH)^2 \simeq \frac{M}{\pi} h_1^3 \simeq 0.04 M. \quad (47)$$

It is unclear how many fragments are produced in this process. In (Piro & Pfahl 2007), it is suggested that if multiple fragments form, they may merge into a mass of $0.1 - 1 M_\odot$. Fragments thus produced will subsequently migrate inwards, initially so by viscous stresses. Any gravitational wave emission hereby derives its energy from the accretion flow. The characteristic strain amplitude hereby scales with the instantaneous strain amplitude, i.e., $h_{char}(f) \propto f^{2/3}$ (cf. 20). When it reaches small enough radius with associated transition frequency f_e in gravitational waves, angular momentum loss may be overtaken by gravitational wave emission. In this event, the gravitational wave luminosity effectively derives from gravitational binding energy of the inhomogeneities to the central object, as opposed to the accretion flow, until complete disruption by tidal forces.

At the fragment's Roche radius $r_d \simeq 1.26\eta M(m_f/M)^{1/3}$ for a black hole size ηM , where $1 \leq \eta \leq 2$ parametrizes uncertainty in black hole spin (Fishbone 1972; Lattimer & Schramm 1974, 1976), the orbital frequency is roughly $\Omega_d \simeq 1/M(M/r_d)^{3/2}$. With (47) adopted for m_f , the corresponding gravitational wave frequency window is

$$W_c : f_c < f < \min\{f_d, 2f_{ISCO}\}, \quad (48)$$

where where f_{ISCO} denotes the orbital frequency at the ISCO and

$$f_c \simeq 1.2 M_1^{-1} \frac{1}{\alpha_{-1}} \left(\frac{h_1}{0.5} \right)^{-3} \left(\frac{\dot{M}}{M_\odot \text{ s}^{-1}} \right) \text{ Hz}, \quad f_d \simeq 300 - 900 M_1^{-1} \left(\frac{h_1}{0.5} \right)^{3/2} \text{ Hz}, \quad (49)$$

where $M = M_1 10M_\odot$ and the range in f_d refers to the uncertainty in η . The broad bandwidth in W_c essentially covers the full operational bandwidth of sensitivity of LIGO-Virgo and KAGRA. The associated characteristic strain amplitude satisfies the canonical scaling of binary coalescence. For a mass fragment (47), we have, adapted from (31) of Appendix A:

$$h_{char}(f > f_e) = 1.7 \times 10^{-22} D_{100}^{-1} M_1^{1/3} \left(\frac{\sigma_f}{0.04} \right)^{1/2} \left(\frac{f}{100 \text{ Hz}} \right)^{-1/6} (f \in W_c) \quad (50)$$

with $\sigma_f = m_f/M$, $D = D_{100} 100$ Mpc and $W_c = [f_e, \min\{f_d, 2f_{ISCO}\}]$. A plot of the fragmentation chirps is exhibited in Fig. 15.

4.3. Wave patterns in accretion disks

We shall consider continuous accretion in a non-fragmented disk with deformations $\xi > 0$ originate at large radii in wave motion, such as spiral waves by self-gravity in Lin-Shu type wave instabilities (Griv 2011). These deformations may evolve as matter accretes inwards, though this is poorly understood at present.

In what follows, we consider a general framework of steady-state accretion and assume, for simplicity, that ξ is a constant. Given the definition of δm in (37), this means that δm varies in proportion to $\sigma = \sigma(r)$. This model approach is hereby distinct from ordinary constant mass inhomogeneities.

Once more we focus on quadrupole emission, although any Jeans type self-gravitating instability, as in fragmentation, is inherently local and need not couple to the large scale structure of the disk to ensure that the lowest order modes are the most unstable. For illustrative purposes, we nevertheless focus on the $l = m = 2$ instabilities.

Fig. 15 illustrates our identification of quadrupole mass-moments in a spiral wave, in rings following discretization in polar coordinates. Each ring is has finite annular width. By the underlying spiral wave, each ring has a quadrupole mass-moment of over-dense regions, here represented by a pair of mass-inhomogeneities δm . Due to rotation, each pair of δm emits quadrupole gravitational wave emission at twice the Keplerian frequency, defined by the radius of each ring. In accretion flows, the spiral wave gradually tightens. As δm migrates inwards, their gravitational radiation broadens in frequency, each imprinting their own stamp in the gravitational wave spectrum. The total luminosity is the sum of the luminosity in each ring by Parseval's theorem.

Our focus on quadrupole wave emissions gives a leading order approximation, that ignores possibly further emissions by higher order mass moments. The full spectrum of gravitational wave emission from all multiple mass moments can be calculated, but likely so the total luminosity is dominant in $m = 2$ (van Putten 2002; Bromberg et al. 2006).

We consider a transition radius r_b , beyond which accretion is by viscous angular momentum transport following standard thin disk accretion theory. Within r_b , accretion is driven by gravitational radiation losses in the inspiral in region

$$r_{ISCO} < r < r_b. \quad (51)$$

Provided that r_b is sufficiently larger than r_{ISCO} , (51) implies maximal efficiency in gravitational radiation with a luminosity satisfying (40). We now show that $r_b > r_{ISCO}$ is satisfied at hyper-accretion rates.

By ΔL_{GW} in (37), the ring shrinks, thereby reducing its total energy by $d\Delta E = M^2\sigma/2r^2 dr = -\Delta L_{GW} dt_{GW}$ ($dr < 0$), that is

$$dt_{GW} = \frac{5}{64} \left(\frac{M}{r}\right)^{-3} \xi^{-2} \sigma^{-1} dr. \quad (52)$$

The time for a radial drift dr by viscous torques alone is

$$dt_b = \frac{2r}{3\nu} dr = \frac{\sqrt{8}M^2}{3\alpha H^2} \left(\frac{M}{r}\right)^{-\frac{5}{2}} dr. \quad (53)$$

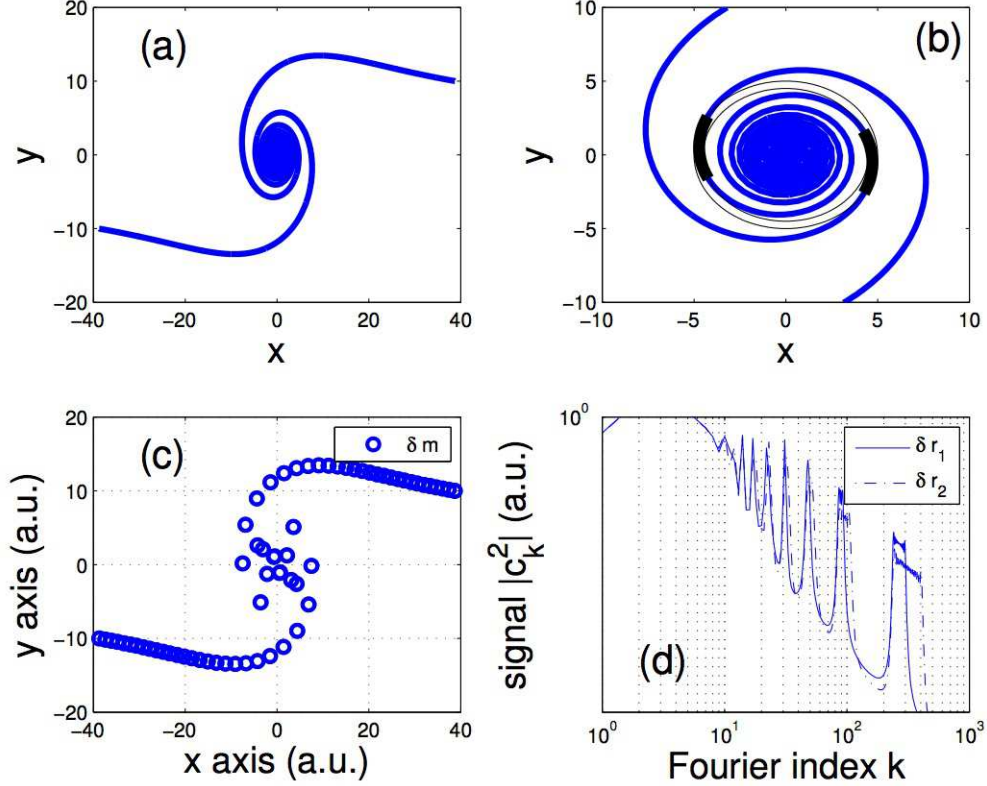


Figure 15. (a) A spiral density wave pattern in a disk. (b) Over-dense regions (thick black) in an annular region $4.5 < r < 5$ (thin black circles) of finite angular extend $\delta\varphi/2\pi \ll 1$. (a) Approximation of the over-dense regions in (b) by local mass-inhomogeneities δm , here 2×32 on a grid with 32 annular rings. (d) Keplerian rotation implies distinct quadrupole emission spectra of each δm in (c) that are non-overlapping in frequencies. The Fourier coefficients $|c_k|^2$ show broadening due to accretion, shown in (d) for two accretion rates, corresponding to radial migrations $\delta r_2 < \delta r_1 < 0$. (Reprinted from (Levinson et al. 2015).)

We define the transition radius r_b below which gravitational driven migration dominates over viscous transport by equating (52) and (53), i.e., $dt_{GW} = dt_b$ at the transition radius

$$\frac{r_b}{M} = \left(\frac{128\sqrt{2}\xi^2\sigma M^2}{15\alpha H^2} \right)^2. \quad (54)$$

To be specific, consider a vertical scale height $H(r)/r$ slowly increasing with r from about 0.1 within a few gravitational radii to about 0.5 at about $100 M$, based on numerical results for neutrino cooled disk models (Popham et al. 1999; Chen & Beloborodov 2007). These numerical results show that H/r depends relatively weakly on α . For illustrative purposes, we shall therefore adopt $H(r) = h_0 r$, $h_0 \simeq 0.1$, in the inner region. Our (α, ξ) model (35-37) thus obtains

$$\frac{r_b}{M} = \frac{512\xi^2}{45\alpha^2 h_0^3} \dot{m} \simeq 5.7 P_1^2 \left(\frac{h_0}{0.1} \right)^{-3} \left(\frac{\dot{M}}{M_\odot \text{ s}^{-1}} \right), \quad (55)$$

where $P = 10 P_1$, $P_1 = \xi/\alpha_{-1}$, $\alpha = 0.1\alpha_{-1}$. Integration of (43) then yields

$$L_{GW}(r) = \frac{\dot{m} M r_\nu}{4r^2} \quad (r > r_b), \quad L_{GW}(r_b) = 2.2 \times 10^{-7} P_1^{-2} \left(\frac{h_0}{0.1} \right)^3. \quad (56)$$

In the region $r_{ISCO} < r < r_b$ the accretion flow is driven by gravitational radiation losses, where the mass profile of the enclosed number of $dn = dr/l$ rings is determined from the relation $(\sigma M)dn = \Delta m dn = \dot{m} dt_{GW}$. Using (52) with $l = H$, $H = h_0 r$, we obtain

$$\sigma = \frac{1}{5.7\xi} \sqrt{5h_0\dot{m}} \left(\frac{r}{M}\right)^2. \quad (57)$$

Note the relatively steep radial dependence compared to (42) due to a modified surface density Σ . Following substitution of (57) into (37), it is seen that $\Delta L_{GW} \propto \dot{m} r^{-1}$ is strongest at the smallest radii. The total luminosity is roughly the sum over the inner rings, $L_{GW} \simeq (r_{ISCO}/l)\Delta L_{GW}(r_{ISCO}) \simeq h_0^{-1}\Delta L_{GW}(r_{ISCO})$. In the high efficiency regime $r_b > r_{ISCO}$, we thus obtain the total disk luminosity (40). It shows that a major fraction of the accretion flow is converted to gravitational radiation, *independent of P* .

According to (55), $r_b > r_{ISCO}$ holds at hyper-accretion rates

$$\frac{\dot{M}}{M_\odot \text{ s}^{-1}} > \frac{1}{5.7} z P_1^{-2} \quad (58)$$

with luminosity (40) provided that mass inhomogeneities originating at $r > r_b > r_{ISCO}$ survive all the way to $r_{ISCO} = zM$. If they dissipate at $r_{ISCO} < r_{diss} < r_b$, then r_{ISCO} should be replaced by r_{diss} in (40), and the net result is a relatively lower L_{GW} emitted at lower frequencies. It will also be appreciated that for (58) to proceed on a long duration time scale of tens of seconds, a large progenitor remnant stellar envelope mass is required or α is small.

We express the outlook above in terms of the frequency window associated with quadrupole emissions at r_b and r_{ISCO} :

$$W_b : f_b < f < \max\{f_{diss}, 2f_{ISCO}\}, \quad (59)$$

where

$$f_b \simeq 468 M_1^{-1} P_1^{-3} \left(\frac{h_0}{0.1}\right)^{\frac{9}{2}} \left(\frac{\dot{M}}{M_\odot \text{ s}^{-1}}\right)^{-\frac{3}{2}} \text{ Hz}. \quad (60)$$

The observable relevant to W_b is the associated characteristic strain amplitude. Over a time period τ , an accretion rate \dot{m} implies a mass migration $\dot{m}\tau$ in the annular region down to r from r_b by the associated energy $\Delta E_{rad} = (1/2)(M/r)\dot{m}\tau$ in gravitational radiation. For $r_{ISCO} \leq r \ll r_b$, it is emitted over a bandwidth given by the difference between the gravitational wave frequency at r and f_b ,

$$\Delta f = f(r) - f_b \simeq f(r) = (\pi M)^{-1} \left(\frac{M}{r}\right)^{\frac{3}{2}} \quad (61)$$

in the present Keplerian approximation. Consequently,

$$\frac{\Delta E_{rad}}{\Delta f} = \frac{\pi \dot{M} \tau M}{2} \left(\frac{M}{r}\right)^{-\frac{1}{2}}, \quad (62)$$

and hence the characteristic strain for a source at a distance D is

$$h_{char}(f) = \frac{\sqrt{2}}{\pi D} \sqrt{\frac{\Delta E_{rad}}{\Delta f}} \simeq \frac{M}{\sqrt{\pi} D} \sqrt{\frac{\dot{M} \tau}{M}} (\pi M f)^{-1/6} = \sqrt{2} \kappa (f/f_b)^{-\frac{1}{6}} \quad (63)$$

for $f \in W_b$ with

$$\kappa = \kappa_0 \left(\frac{f_b}{f_0} \right)^{-\frac{1}{6}}, \quad \kappa_0 = \frac{M}{\sqrt{2\pi D}} \sqrt{\frac{\dot{M}\tau}{M}} (\pi M f_0)^{-1/6}. \quad (64)$$

Numerically, we have

$$\kappa_0 = 8.3 \times 10^{-22} \frac{M_1^{\frac{1}{3}}}{D_{100}} \sqrt{\frac{M_{acc}}{M_\odot}} \left(\frac{f_0}{1000 \text{ Hz}} \right)^{-\frac{1}{6}}, \quad (65)$$

where we put $M_{acc} = \dot{M}\tau$. It shows that $h_{char}(f)$ is maximal in W_b at $f \simeq f_b$. Observationally, f_b is the most relevant frequency in W_ν provided that it falls in the thermal or shot noise dominated region of the LIGO-Virgo and KAGRA detectors.

By the strong dependence of f_b on \dot{M} in (60), it will be appreciated that W_b opens up a window $f_b < 2f_{ISCO}$ only at large hyper-accretion rates, when

$$\frac{\dot{M}}{M_\odot \text{ s}^{-1}} > \left(\frac{M_1 f_{ISCO}}{216 \text{ Hz}} \right)^{-\frac{2}{3}} \alpha_{-1}^2 \simeq \frac{1}{6} \left(z^{\frac{3}{2}} + \hat{a} \right)^{\frac{2}{3}} \alpha_{-1}^2 \geq 0.26 \alpha_{-1}^2, \quad (66)$$

where $z = r_{ISCO}/M$, $\hat{a} = a/M$ denotes the dimensionless spin rate of the black hole and the lower bound on the right hand side refers to an extremal Kerr black hole ($z = \hat{a} = 1$). The inequality on the right hand side of (66) provides a necessary but not sufficient condition. Around non-extremal black holes, the required \dot{M} is larger. Furthermore, the frequency windows W_c and W_b satisfy different scalings with accretion rate \dot{M} . Around a nearly extremal Kerr black hole, we note that $f_c = f_b$ only when

$$\dot{m} \simeq 10 \left(\frac{h_1}{0.5} \right)^{\frac{5}{6}} \alpha_{-1}^{\frac{5}{6}}. \quad (67)$$

Unless α_{-1} is small, i.e., $0.001 < \alpha < 0.01$, we expect

$$W_b \subset W_c. \quad (68)$$

In the external region $r > r_b$, the emission in gravitational waves is at frequencies $f < f_b$. In this region, the emission is relatively inefficient and satisfies (56). We can estimate the effective strain $h_{eff} = h(f)\sqrt{f\tau}$ from the instantaneous strain $h = L_{GW}^{1/2}/\Omega D$, $\Omega = \pi f$, and the number of wave periods $n = f\tau$. By $h_{char}\sqrt{f^{-1}\Delta f} = \sqrt{2}h_{eff}$, we thus estimate the characteristic strain associated with a one-sided frequency spectrum as

$$h_{char}(f) = \frac{M}{\sqrt{2\pi D}} \sqrt{\frac{M_{acc}}{M}} (\pi M f_b)^{-\frac{1}{6}} (f/f_b)^{\frac{1}{6}} (f < f_b). \quad (69)$$

A matching of the expressions (63) and (56) obtains by noting that the luminosity in the inner radiatively efficient region $[r, r_b]$, $r_{ISCO} \leq r \ll r_b$, satisfies

$$L_{GW}^i([r, r_\nu]) = \frac{M\dot{m}}{2r} - \frac{M\dot{m}}{4r_b} = \frac{M\dot{m}}{4r} \left[2 - (f_b/f)^{\frac{2}{3}} \right]. \quad (70)$$

With (65), we therefore have (Levinson et al. 2015)

$$h_{char}(f) = \kappa \begin{cases} (f/f_b)^{\frac{1}{6}} & (f < f_b) \\ (f/f_b)^{-\frac{1}{6}} \left[2 - (f_b/f)^{\frac{2}{3}} \right]^{\frac{1}{2}} & (f \geq f_b). \end{cases} \quad (71)$$

This broadband spectrum increases with \dot{m} . Due to (56), the increase in $f < f_b$ is entirely due a shrinking of the bandwidth, as r_ν increases and f_b decreases with \dot{M} . In contrast, the increase in $f > f_b$ is due to an increase in the luminosity (70). A plot of the proposed broadband emission (71) is exhibited in Fig. 18 for various choices of $M_{acc} = \dot{m}\tau$ and f_b .

4.4. ISCO waves

Following (30), we consider sub-critical accretion allowing for the formation of a torus in suspended accretion, which catalytically converts most of the input from the black hole into gravitational radiation at frequencies about

$$f_{GW} \simeq \pi^{-1} \Omega_{ISCO} \quad (72)$$

with lesser emission at higher frequencies (Bromberg et al. 2006), accompanied by a minor output (31) in BPJs. The former features a distinctive descending chirp, due to expansion of the ISCO as the black hole spins down (van Putten 2008). This emission is subsequent to any gravitational burst associated with the initial formation of the black hole and continuing accretion (Rees et al. 1974; Duez et al. 2004; Lipunov 1983; Leung et al. 1997; Font & Papadopoulos 2001; Nagar et al. 2007; Lipunova et al. 2009; Fryer et al. 2002) and separate from any quasi-mode ringing (QNR) of the event horizon (Thorne et al. 1986; Kokkotas & Schmidt 1999) with relatively high frequencies ($l = m = 2$) (Echeverria 1998)

$$f_{QNM} = 3200 \text{ Hz} \left[1 - 0.63 \left(1 - \frac{a}{M_H} \right) \right]^{\frac{3}{10}} \left(\frac{M_H}{10M_\odot} \right)^{-1}. \quad (73)$$

Quite generally, gravitational radiation from ISCO waves is described by mass moments I_{lm} in the quantum numbers l and m of spherical harmonics has a luminosity (Appendix A)

$$L_{GW} \propto \Omega_T^{2l+2} I_{lm}^2. \quad (74)$$

In practice, it appears that most of the emission comes from $m = l$ (Bromberg et al. 2006). To leading order $\Omega_T^2 \propto r^{-3}$, whereby (74) satisfies

$$L_{GW} \propto \frac{1}{r^{m+3}}. \quad (75)$$

Consequently, gravitational wave luminosity tends to be maximal at the ISCO, such as exemplified in the previous section.

Susceptibility to non-axisymmetric instabilities at the ISCO is due to a variety of processes. In particular, energetic feedback by black hole sets in at E_{rot}^H in excess of 5.3% of E_{rot}^{max} , when $\Omega_H > \Omega_{ISCO}$. Black holes losing angular momentum to surrounding matter enforce turbulence with associated heating and enhanced (thermal and magnetic) pressure van Putten (2002, 2012a). An improved criterion

for the black hole to be rapidly spinning, is when its forcing onto the surrounding matter exceeds the luminosity in magnetic winds from the latter, taking advantage of $\Omega_H/\Omega_{ISCO} > 1$ (the ratio extends up to 1.4396 in the Kerr metric) and the substantial surface area of the event horizon. Using the Shakura-Sunyaev solution (Shakura & Sunyaev 1973) as a leading order approximation of the inner disk, the time integrated luminosity of the black hole E_H onto the inner disk exceeds the energy loss E_w^* of the latter in magnetic winds whenever $a/M \geq 0.4433$ (van Putten 2012a). Equivalently, E_{rot}^H initially exceeds E_{rot}^{max} by about 9%, which is still small. The excess $E_H - E_w^*$ can be radiated off in gravitational waves and MeV neutrinos. Here, we attribute the excitation of non-axisymmetric wave instabilities to enhanced thermal and magnetic pressures induced by such feedback.

4.4.1. Mass moments about the ISCO

Papaloizou-Pringle (Papaloizou & Pringle 1984) considered (38) with non-Keplerian rotation index $q > 3/2$. Applied to a torus, the associated surface gravity allows surface waves to be excited at the inner and outer surface. In the approximation of an incompressible fluid, a detailed analysis shows that the coupling between waves on these two opposite faces allows for angular momentum transport outwards on a dynamical time scale. In the singular limit of an infinitesimally slender torus considered in (Papaloizou & Pringle 1984), these surface waves become unstable to all of $m \geq 1$ modes at the same critical rotation index $q_c = \sqrt{3}$.

Here, we envision $q > 3/2$ induced by feedback from the central rotating black hole. Extending the Papaloizou-Pringle instability to tori of arbitrary width (van Putten 2002), non-axisymmetric instabilities are found to set in consecutively, starting at $m = 1$, as a function of the rotation index of a torus (Appendix B). When $q > q_{cm}(\delta) \geq \sqrt{3}$ exceeds a critical value, its azimuthal modes $m = 1, 2, \dots$ become successively unstable (as a function of q), where (van Putten 2002)

$$q_{c1}(\delta) = \sqrt{3} + 0.27 \left(\frac{\delta}{0.7506} \right)^2, \quad q_{c2} = \sqrt{3} + 0.27 \left(\frac{\delta}{0.3260} \right)^2, \dots \quad (76)$$

as a function of the ratio $\delta = b/R$ of minor-to-major radius of the torus. Here, $\sqrt{3}$ refers to the singular limit $\delta = 0$ of infinitesimally slender tori in (Papaloizou & Pringle 1984). The curves (76) are analytic approximations to semi-analytical results shown in Fig. 16. This instability has also been observed in recent numerical simulations (Kiuchi et al. 2011).

From heating alone, a minimum value of q can be associated with the temperature $T = T_{10}10^{10}$ K (van Putten & Levinson 2003)

$$T_{10} \simeq 2L_{\nu,52} \left(\frac{M_T}{0.1M_{\odot}} \right)^{-\frac{1}{6}}. \quad (77)$$

For a torus of minor-to-major radius $\delta = b/R$, the resulting thermal pressure enhances q according to

$$q = 1.5 + 0.15 \left(\frac{R}{M} \right) \left(\frac{\delta}{0.2} \right)^2 T_{10}. \quad (78)$$

Thermal pressures and magnetic pressures will be similar at temperatures of about 2 MeV (van Putten & Gupta 2009). When $q > q_{cm}(\delta) \geq \sqrt{3}$ exceeds a critical value, its azimuthal modes $m = 1, 2, \dots$ become unstable as shown in Fig. 16.

A mode that becomes unstable is generally strengthened by gravitational radiation back reaction (van Putten 2002). As a result, inducing gravitational wave emissions by (76) is reminiscent of a Hopf bifurcation (van Putten 2012a). The result is a characteristic descending chirp during black hole spin down (Fig. 16).

Ultimately, the luminosity is determined by a nonlinear saturation amplitude, balancing *heating* in dissipation and *cooling* in gravitational waves, MeV neutrino emission and magnetic winds (van Putten 2012a), unless aforementioned feedback is intermittent or the torus as a whole is unstable. The first allows for an analytic estimate in case of a flat infrared spectrum of MHD turbulence (van Putten 2001b). The latter is possibly of interest to the most luminous sources, perhaps resulting from hyper-accretion onto the ISCO in core-collapse supernovae (van Putten 2015b).

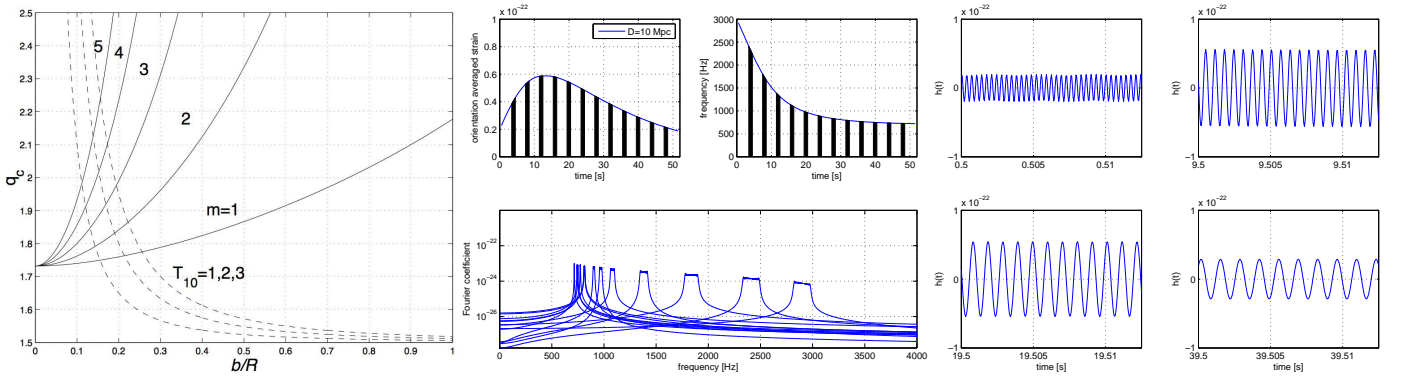


Figure 16. (Left panel.) The neutral stability curves for buckling modes expressed in terms of the critical rotating index q_c as a function of minor-to-major radius $\delta = b/a$. Labels refer to azimuthal quantum numbers $m = 1, 2, \dots$, where instability sets in above and stability sets in below. Of particular interest is the range $q \leq 2$, where $m = 0$ is Rayleigh-stable. For $q = 2$, instability sets in for $b/a < 0.7385$ ($m = 1$), 0.3225 ($m = 2$) and, asymptotically, for $b/a < 0.56/m$ ($m \geq 3$). Included are the curves of q_c as a function of δ at various temperatures $T = T_{10} 10^{10}$ K. (Reprinted from (van Putten 2002, 2012a).) (Middle and right panels.) Theoretical wave form of ISCO waves induced around an initially extremal black hole obtained by integration of the equations of suspended accretion in the strong interaction limit $L_{GW} \simeq L_H \simeq -\dot{M}$. Shown is the orientation averaged strain amplitude $h(t)/\sqrt{5}$. Due to a turbulent background accretion flow, phase-incoherence is anticipated to be limited intermediate time scales. The wave form is sliced into chirp templates of intermediate duration $\tau = 1$ s for use in matched filtering. (Reprinted from (van Putten 2008).)

4.4.2. Dimensionless strain amplitude

The wave instability (76) has the desirable property that the associated mass-moments are predominantly at the lowest quantum numbers, which ensures that most of the gravitational wave output is at the lowest quadrupole emission frequency. Around a stellar mass black hole of $10M_{\odot}$, the resulting frequency is broadly in the range of 500-3000 Hz for emissions from quadrupole mass moments, which falls within the sensitivity wave band of the upcoming advanced ground based detectors. Emissions from $m = 3$ and higher are unlikely to be detectable by these detectors. (Emissions from $m = 1, 2$ in a disk or torus produce quadrupole emissions at the same frequency from the combined black hole plus disk or torus system). Even so, their output may be of interest to future, next generation detectors. The same conclusion holds for gravitational wave spectra produced by magnetic pressure induced multipole mass moments based on a numerical simulation (Bromberg et al. 2006). Accordingly, the

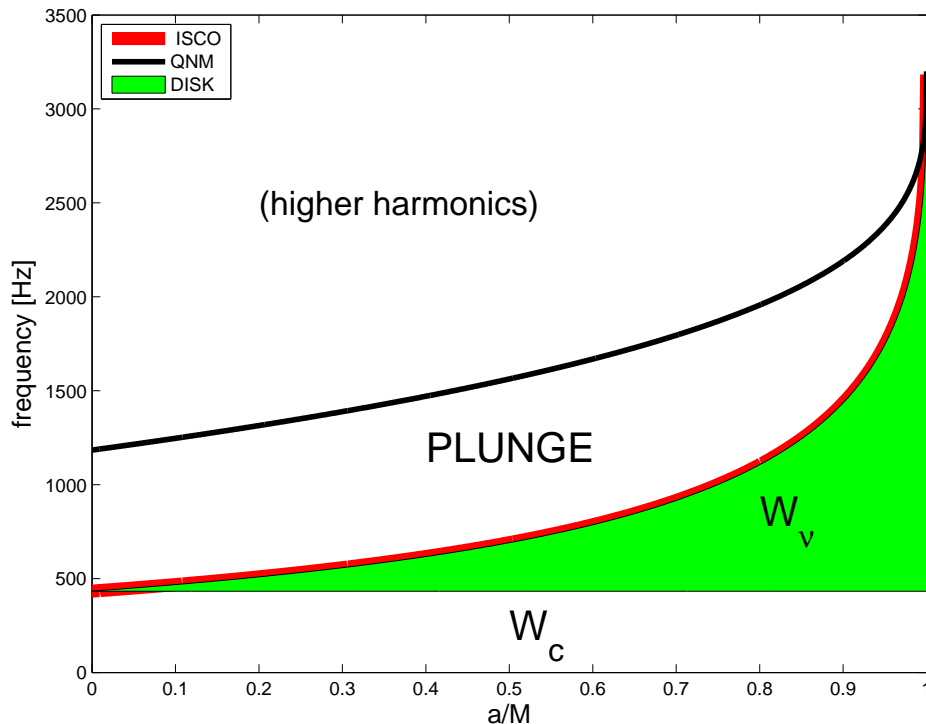


Figure 17. Schematic overview of quadrupole gravitational radiation derived from accretion flows onto rotating black holes in non-axisymmetric wave patterns (W_b) or spiral in of fragments (W_c), or ISCO waves (red curve). The first produces one or more ascending chirps at sufficiently high accretion rates, the second descending chirps. Fragmentation may occur at sufficient cooling in the extended accretion disk. Wave instabilities from a torus about the ISCO arise from heating and magnetic pressure by feedback from the central black hole if $\Omega_H > \Omega_{ISCO}$. High frequency radiation can be produced by Quasi-Normal Mode ringing of the event horizon that may be exciting by matter plunging in (black curve). The spectrum may contain additional radiation from higher order modes (not shown), e.g., by high m multipole mass moments in the disk or torus, as well as fragments in elliptical orbits (not shown).

frequency of gravitational wave emissions is fixed by the Kerr metric for a given mass and angular momentum of the black hole with those of quadrupole emission satisfying

$$f_{GW} = 2f_{ISCO}, \quad (79)$$

where $f_{ISCO} = \Omega_T/2\pi$, where Ω_T denotes the angular velocity of the torus formed at the ISCO. For stellar mass black hole systems, this ensures that frequencies are within the LIGO-Virgo and KAGRA bandwidth of sensitivity. At late times, when the angular velocity of the black hole approaches that of the ISCO, we have for an initial black hole mass M the frequency range (van Putten et al. 2011a)

$$f_{GW} = 595 - 704 \text{ Hz} \left(\frac{M}{10M_\odot} \right)^{-1}, \quad (80)$$

where the 15% frequency range 595-704 Hz refers to different choices of black hole initial spin. (The minimum value of 595 Hz corresponds to an initially maximally spinning black hole.)

The instantaneous strain implies an *effective* strain $h_{eff} = \sqrt{nh}$, where $n \simeq fT$ at a characteristic frequency f for a burst duration T . Thus, $h_{eff} \simeq \pi^{-1}D^{-1}\sqrt{E/f}$ represents the strain that can

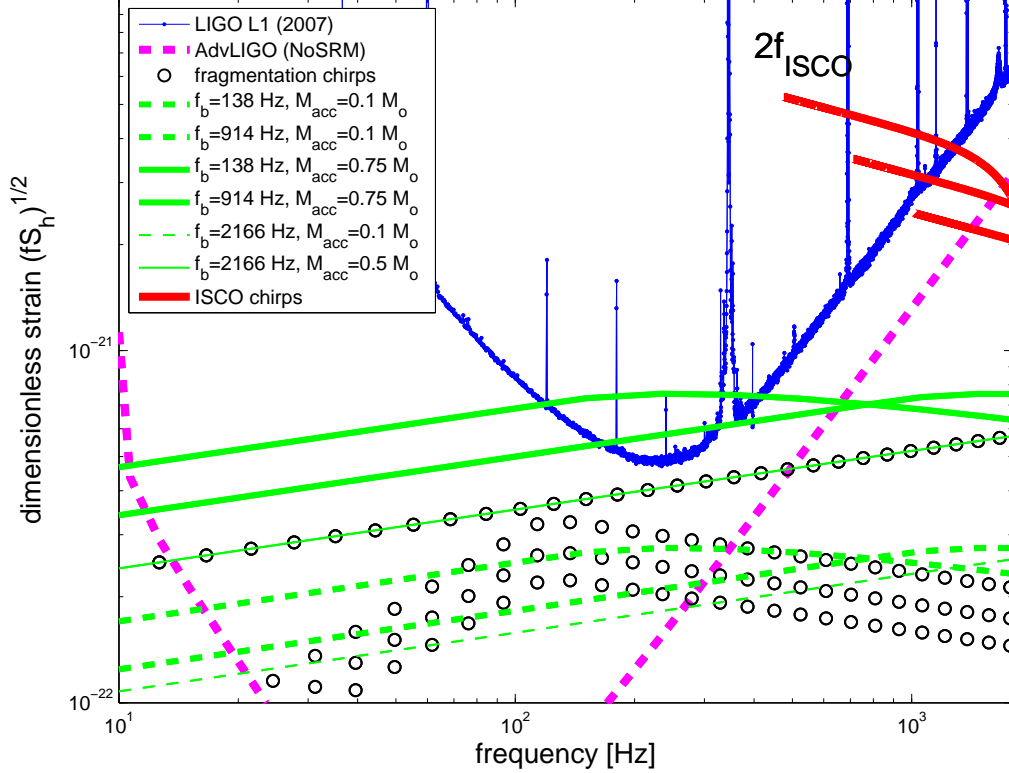


Figure 18. Overview of the characteristic strain $h_{char}(f)$ of quadrupole gravitational radiation from accretion flows around rotating black holes formed in core-collapse of massive stars at $D = 100$ Mpc. The vertical distance to the dimensionless strain $h_n = \sqrt{fS_h}$ in LIGO S5 represents the maximal attainable S/N ratio obtainable by filtering. The model curves shown are broadband emission from non-axisymmetric accretion flows (green), fragmentation chirps of (Piro & Pfahl 2007) (circles, $\sigma_f = 0.1$, $f_e = 120$ Hz) and ISCO waves induced by feedback from a central black hole (red). The curves shown refer to a black hole mass $M = 10M_\odot$ (black), $M = 7, 10$ and $15M_\odot$ (green, red). (Reprinted from van Putten (2016).)

be recovered by matched filtering in the ideal limit of matching the entire signal with a model. Similar to the derivation of (69), we have, in the frequency domain (Flanagan & Hughes 1998a,b), the corresponding characteristic amplitude satisfies

$$h_{char}(f) \simeq \frac{\sqrt{2}}{\pi D} \sqrt{\frac{dE}{df}} \simeq 3.5 \times 10^{-21} D_{100}^{-1} M_1 \quad (81)$$

based on $dE/df \simeq 4.5 \times 10^{12} M_1^2 \text{ cm}^2$ across a frequency range of about 600 - 1500 Hz ($10M_\odot/M$) calculated in the next section.

Fig. 14 summarizes our perspective on gravitational wave chirps associated with mergers and black holes losing angular momentum following Fig. 9. For the suspended accretion state, the chirps shown have a characteristic late time frequency around 600-700 Hz for a $M = 10M_\odot$ black hole following (80). It should be mentioned that Fig. 14 represents trajectories when matter about the ISCO orbits in the equatorial plane. This assumption need not hold. Any misalignment between its angular momentum and that of the black hole would lead to Lense-Thirring precession and hence line-broadening of the trajectories shown (van Putten 2004).

For a low mass black hole formed in a double neutron star merger producing a SGRBEE, the late frequency (80) of about 2.3 kHz is particularly well defined, given the narrow range of neutron star masses around $1.5M_\odot$. The latter outlook may be of interest to future narrow band detector modes (Cutler & Thorne 2002).

Figs. 17-18 summarize the frequencies and strain amplitude of quadrupole emissions from accretion flows and a torus about the ISCO. Concluding this section, we anticipate, further to (30), that for the gravitational wave emissions most likely observable by LIGO-Virgo and KAGRA with durations $T_{GW} \simeq T_{engine}$, where T_{GW} represents either the time scale of hyper-accretion or the lifetime of spin of the central black hole.

4.5. Stochastic background from CC-SNe

In a homogeneous isotropic universe, the contribution to the stochastic background in gravitational waves from a source population locked to the cosmic star formation rate (SFR) can be expressed in terms of the spectral energy density ϵ'_B per unit volume per unit frequency. It is common to express the same per unit logarithmic frequency relative to the closure density, i.e., $f\epsilon'_B$ relative to ρ_c , where f denotes the observed frequency in gravitational waves and $\rho_c = 3H_0^2/8\pi$ in geometrical units for a present-day Hubble constant H_0 . It can be calculated (van Putten 2005b) based on (a) Einstein's adiabatic relationship $E = hf$ for the energy E of a graviton of frequency f , where h is Planck's constant; (b) conservation of radiation energy within a co-moving volume during cosmological evolution; and (c) a scaling of the SFR over the cosmic evolution described by the Hubble constant $H(z) = H_0h(z)$ (e.g. Porciani & Madau 2001). In three-flat Λ CDM at late times, $h(z) = \sqrt{1 - \omega_m + \omega_m(1+z)^3}$ with present-day matter (dark and baryonic) density ω_m expressed relative to aforementioned ρ_c .

The event number density per unit redshift $N(z)$ and the event rate volume density $R(z)$ satisfy $N(z)dz = R(z)dt_e$ where dz refers to the redshift interval with a corresponding locally measured time interval dt_e (measured in the source frame). Consequently,

$$N(z) = R(z) \frac{dt_e}{dz} dz = R(z) \frac{dt_e}{dt} \frac{dt}{dr} \frac{dr}{dz} = \frac{R(z)dz}{(1+z)H_0h(z)}, \quad (82)$$

where $dt_e/dt = 1/(1+z)$ is the cosmological dilation in time, $dr/dt = 1$ is the velocity of light measured at $z = 0$ and $dr/dz = (H_0h(z))^{-1}$ denotes the change in proper distance with respect to redshift. According to (c) derived in Porciani & Madau (2001), the cosmic SFR expressed in terms of a rate per unit volume $R_{SF2}(z, \Omega_\Lambda)$ in a three-flat cosmology parametrized by Ω_Λ satisfies

$$R_{SF2}(z, \Omega_\Lambda) = R_{SF2}(z, 0) \frac{h(z)}{h_0(z)}, \quad h_0 = (1+z)^{\frac{3}{2}}. \quad (83)$$

By Einstein's adiabatic relationship (a), dE/df is redshift invariant as a function of $(1+z)f$ for a given f . Hence, by conservation of radiation (b), we have (cf. (Phinney 2001) for a closely related expression)

$$\epsilon'_B(f) = \int_0^\infty \frac{dE}{df} ((1+z)f) N(z) dz, \quad (84)$$

where z_{max} denotes the maximal redshift in the cosmic SFR model rate (83). For a gravitational wave source locked to the cosmic SFR,

$$N(z) = N_0 \frac{R_{SF2}(z, \Omega_\Lambda)}{R_{SF2}(0, \Omega_\Lambda)}, \quad (85)$$

where N_0 denotes the the observed rate volume density at $z = 0$. By (83), it follows that

$$\epsilon'_B(f) = n_0 \int_0^\infty \frac{dE}{df} [(1+z)f] \frac{\hat{R}_{SF2}(z)}{(1+z)^{\frac{3}{2}}} dz, n_0 = \frac{R_0}{H_0}, \quad (86)$$

where $\hat{R}_{SF2}(z) = R_{SR2}(z, 0)/R_{SF2}(0, 0)$ denotes the normalized cosmic SFR satisfying $\hat{R}_{SF2}(0, 0) = 1$.

A concrete example of a cosmic SFR model rate is (Porciani & Madau 2001)

$$R_{SF2}(z, 0) = \frac{0.16h_{73}}{1 + 660e^{-3.4(1+z)}} M_\odot \text{ yr}^{-1} \text{ Mpc}^{-3}, \quad (87)$$

where $H_0 = h_{73} \times 73 \text{ km s}^{-1} \text{ Mpc}^{-1}$, whereby

$$\hat{R}_{SF2}(z) = \frac{23}{1+660e^{-3.4(1+z)}}, \quad N(z) = \frac{23N_0}{(1+660e^{-3.4(1+z)})(1+z)^{\frac{3}{2}}} \quad (88)$$

is an approximation to the observed cosmic SFR over the redshift range $0 \leq z \leq 5$. For a given observational parameter N_0 and source model dE/df , $\epsilon'_B(f)$ can thus be evaluated by numerical integration. In what follows, we shall write $E_f = dE/df$. Thus, Schwarz' inequality provides an a priori bound on $\epsilon'_B(f)$, given by

$$\epsilon'_B(f) \leq n_0 A_2 E_2, \quad E_2 = \sqrt{\int_0^\infty E_f^2(x) \frac{dx}{x}}, \quad A_2 = \sqrt{\int_0^\infty \frac{\hat{R}_{SF2}^2(z)}{(1+z)^2} dz} \quad (89)$$

with $A_2 = 12.72$.

For a source effectively described by a constant $E_f = E_f^0$ over a finite bandwidth $B = f_2 - f_1$ between two cut-off frequencies $f_{1,2}$, i.e., we have

$$\epsilon'_B(f) = n_0 E_f^0 \int_{1+z=f_1/f}^{1+z=f_2/f} \frac{\hat{R}(z)}{(1+z)^{\frac{3}{2}}} dz \leq n_0 E_f^0 A_{\frac{3}{2}}, \quad A_{\frac{3}{2}} = \int_0^\infty \frac{\hat{R}(z)}{(1+z)^{\frac{3}{2}}} dz, \quad (90)$$

where $A_{\frac{3}{2}} = 5.8$. The maximum of $\epsilon'_B(f)$ attains at $\epsilon''_B(f) = 0$, i.e.,

$$\hat{R} \left(\frac{f_1}{f} - 1 \right) = \sqrt{\frac{f_1}{f_2}} \hat{R} \left(\frac{f_2}{f} - 1 \right). \quad (91)$$

For a cosmic SFR that is asymptotically constant, i.e., $\hat{R}(z) \simeq \hat{R}_*$ at large z , e.g., $\hat{R}_* = 23$ in (87), (91) reduces to the implicit equation

$$\hat{R} \left(\frac{f_1}{f} - 1 \right) = \sqrt{\frac{f_1}{f_2}} \hat{R}_* \quad (92)$$

whenever $f_2 \gg f_1$. To exemplify, $f_1 = 600 \text{ Hz}$ and $f_2 = 3000 \text{ Hz}$ associated with a black hole mass $M = 10 M_\odot$ imply a maximum at

$$f_{B,peak} = 272 \text{ Hz} \quad (93)$$

as the root of (92) for the model rate (87) (with a corresponding $z_c = 0.84$). Note that $f_2/f_c = 11.0$, which is still within the redshift range of star formation. At this frequency, (90) gives the maximum

$$\epsilon'_B(f) = n_0 E_f^0 A_*, \quad (94)$$

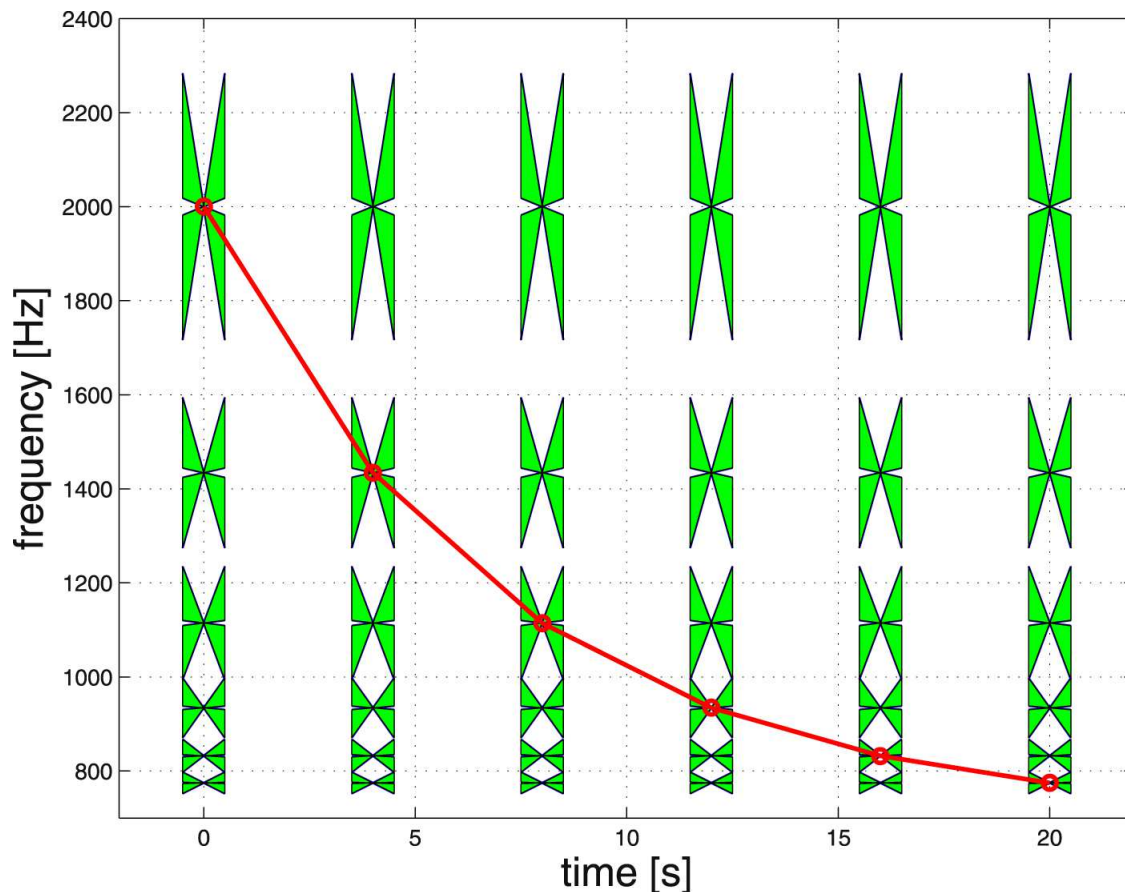


Figure 19. Butterfly filtering is a bandpass filter of trajectories of long-duration chirps with finite slope $0 < \delta \leq df(t)/dt$ in frequency $f(t)$, suppressing signals with essentially constant frequencies. Butterfly filtering is realized by matched filtering against a bank of chirp templates, here of intermediate duration $\tau = 1$ s and covering of bandwidth of 350-2000 Hz in frequency. (Reprinted from (van Putten 2016).)

where $A_* = 3.52$. In this approximation, we have, consequently,

$$\Omega_B = \frac{B\epsilon'_B(f)}{\rho_c} \simeq 10^{-8} \left(\frac{k}{10\%} \right) \quad (95)$$

for a bandwidth $B \simeq 1000$ Hz in gravitational waves from SN Ib/c. Here, we consider a branching ratio k of SN Ib/c into broad line events that may successfully produce long gravitational wave bursts.

5. GPU-ACCELERATED SEARCHES FOR BROADBAND EXTENDED GRAVITATIONAL-WAVE EMISSION

Deep searches for BEGE from multi-phase central engines in core-collapse supernovae with durations (32), possibly extended to (33), can be pursued by *butterfly filtering*, to extract trajectories in the $(f(t), \dot{f}(t))$ -plane with finite slope $0 < \delta \leq df(t)/dt$ for some $\delta > 0$. These trajectories typify sources exhausting a finite reservoir in energy and angular momentum. From (magneto-)hydrodynamic sources such as accretion flows onto compact objects, phase coherence in gravitational wave emission is expected to be limited to intermediate time scales $\tau \ll T_{90}$, associated with possibly turbulent accretion flows.

Butterfly filtering is realized by matched filtering against a bank of chirp templates of duration τ , here $\tau = 1$ s, covering 350-2000 Hz permitted by LIGO S6 data down-sampled to 4096 Hz. In this frequency range, LIGO noise is essentially Gaussian over the finite bandwidth of a given chirp template. The output of correlations against such chirp templates is again Gaussian in the absence of any signal or anomaly in the detector output. This high frequency range fortuitously covers our outlook on BEGE discussed in the previous section. Butterfly filtering hereby attains essentially maximal sensitivity based on the theory of matched filtering (van Putten 2016). Butterfly filtering output is a *chirp-based* spectrogram, distinct from the more common Fourier-based spectrograms.

Illustrative for the power of butterfly filtering is the identification of a Kolmogorov spectrum in high frequency *BeppoSAX* data, extracted from a mean of 1.26 photons per 0.5 ms bin (Fig. 8). Realization of near-optimal sensitivity requires a large bank of chirp templates, that densely covers the two-dimensional parameter space inherent to butterfly filtering. In covering frequencies $O(10^3)$ Hz and chirps with $\Delta f = O(10^2)$ Hz, the theoretical minimum size of a bank will be on the order of $O(10^5)$ templates. The results of Fig. 8 derive from a bank of 8.64 million templates.

For LIGO, an effective gravitational wave strain noise amplitude is $h_n = \sqrt{f S_h(f)} = 3.6 \times 10^{-22}$ about 1000 Hz at advanced detector sensitivity (Cutler & Thorne 2002). Butterfly filtering by chirps of $\tau = 1$ s duration recovers (81) with a signal-to-noise ratio $S/N = (\pi r h_n)^{-1} \sqrt{2dE/5df}$ as an average over detector orientations, i.e.,

$$S/N \simeq 3.7 D_{100}^{-1} M_1 \left(\frac{\sqrt{f S_h[1000 \text{ Hz}]}}{3.6 \times 10^{-22}} \right)^{-1}. \quad (96)$$

This result obtains for a single gravitational wave detector. Detection in all three LIGO-Virgo detectors would imply an enhanced signal-to-noise ratio $\rho \simeq 6.4$, apart from additional significance gained from an associated supernova signature (e.g. (van Putten 2002)). Here, we use a dimensionless strain h amplitude, satisfying

$$h = \left(\frac{M}{D} \right) h_S \quad (97)$$

for a source of mass M at a distance D . For rotating systems, h_S effectively scales with the Newtonian tidal field of a mass-inhomogeneity. The experimental and data-analysis challenge is defined by the fact that, for stellar mass systems at astrophysical distances, M/D is exceptionally small, whereby h is, at best, on the order of $10^{-23} - 10^{-22}$ for the most extreme sources in the Local Universe.

While LIGO data in the shot-noise dominated frequency range 350-2000 Hz is largely Gaussian over intermediate bandwidths of chirps over $\tau = 1$ s, it features frequent spurious signals, commonly referred to as *glitches*. This necessitates going beyond single detector analysis, seeking *correlated detections* in both the H1 and L1 detectors. Furthermore, LIGO data sets are large. LIGO S6 alone covers well over one year of observations in 1 TByte of data. Deep searches in LIGO data by butterfly filtering similar to that in (8) requires acceleration on *Graphics Processor Units* (GPU). On about a dozen modern GPUs, heterogeneous GPU-CPU analysis enables butterfly filtering against banks of up to 16 million templates in size at over one million correlations per second, i.e., deep searches in all of LIGO S6 or better than real-time analysis of LIGO observation runs. Specifically, it enables blind all-sky searches without triggers from electromagnetic or neutrinos.

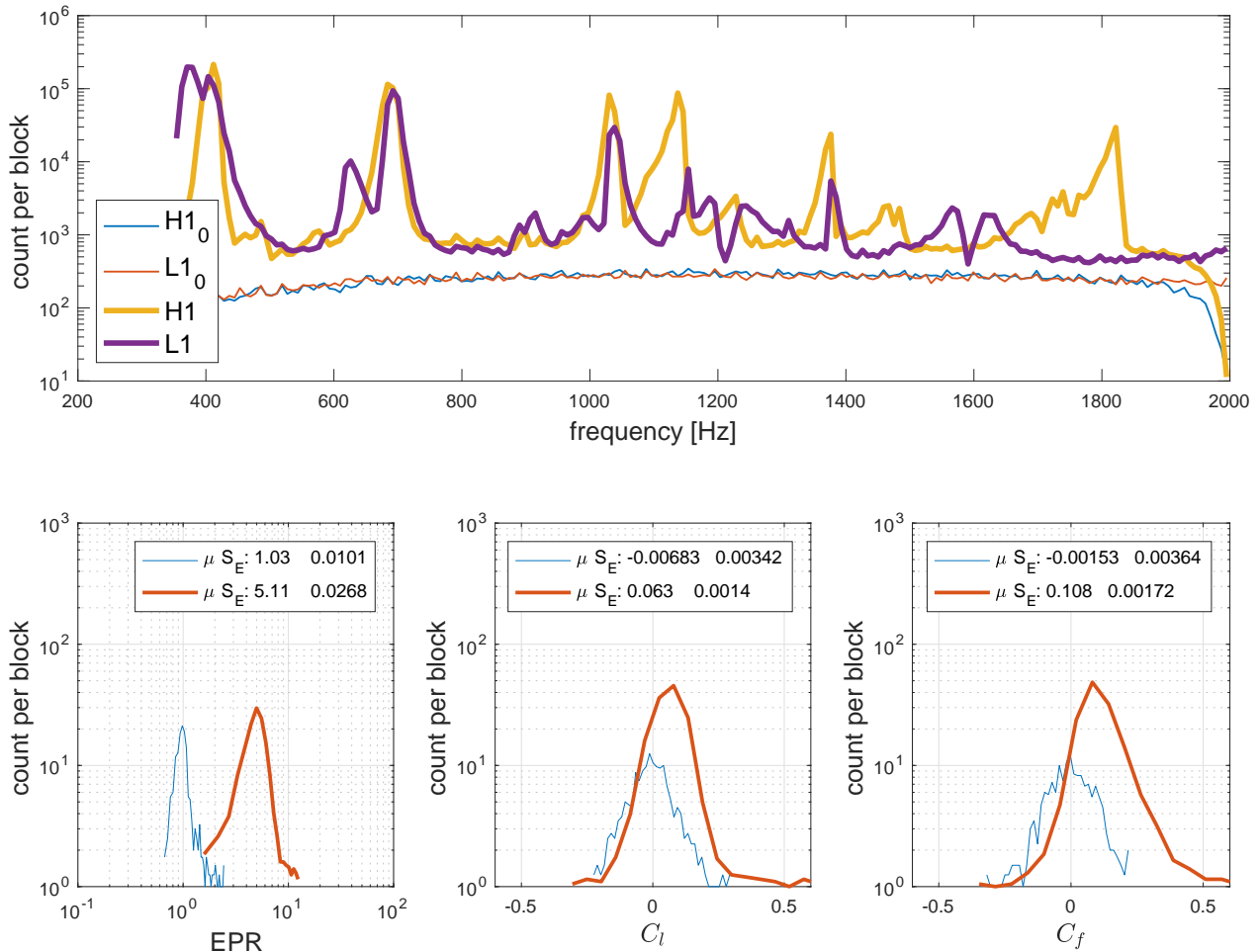


Figure 20. Pseudo-spectra of H1 and L1 in simultaneous hits ($\rho > 5.5\sigma$) in LIGO S6 butterfly filtering against a bank of 8M chirp templates, shown as an average over 20 blocks (182 hr of H1/L1 data) with control by $H1_0 \wedge L1_0$ following time randomization.

For H1L1-correlated searches, chirp-based spectrograms of H1 and L1 each can be combined to a new spectrogram of correlations C_l and C_f in H1L1 butterfly output ρ and, respectively, f , that we shall refer to as correlations in *loudness* and, respectively, *pitch*. H1L1 correlations in loudness and pitch are unambiguous, by the relatively small standard errors in the mean (below). Overall, they are of known and unknown origin. For instance, H1 and L1 are frequently subject to LIGO injections for calibration purposes. However, the observed correlations appear to be quite consistent with time, though strongly non-uniform over frequency. While a detailed analysis of this H1L1 correlations is beyond the scope of this discussion, the results given serve to show the challenges encountered in unraveling detections of astrophysical origin obtained by the present deep searches.

5.1. LIGO S6 correlations in loudness and pitch

In searching for astrophysical signals in H1L1 correlations, we recently applied GPU-accelerated butterfly filtering to LIGO S6 (van Putten 2017). In this approach, butterfly output to the CPU from the GPU is restricted to tails in matched filtering correlations ρ with standard deviation σ ,

satisfying

$$\rho > \kappa\sigma, \quad (98)$$

where we put $\kappa = 5.5$. Given our focus on signals with finite slope $df(t)/dt \geq \delta > 0$, we are at liberty to down select “hits” (98) at the same GPS time of the LIGO detectors, as any time-delay Δt in signal arrival time has an equivalent frequency shift $\Delta f \geq \delta\Delta t$.

Fig. 20 shows H1L1 correlations in simultaneous hits in butterfly filtering against a bank of 8 million chirp templates, along with control obtained by time randomization of H1 and L1 data. Somewhat unexpected, we observe a pronounced *excess probability ratio*

$$EPR = \frac{p_{12}}{p_1 p_2} = 5.11 \pm 0.0268 \quad (99)$$

H1L1 correlations, where p_i refer to the probability of hits (98) by each detector individually ($i = 1$ for H1, $i = 2$ for L1). The result is beyond $EPR=1$, as expected and measured by our control, defined by the same analysis following time randomization of H1 and L1. (Effectively the same control obtains following time randomization of either H1 or L1.) Going one step deeper, the results unambiguously show correlations C_l in loudness and C_f in pitch with mean values μ_l and, respectively, μ_f , satisfying

$$\text{loudness: } \mu_l = 0.063 \pm 0.0014, \quad \text{pitch: } \mu_f = 0.108 \pm 0.00172. \quad (100)$$

It should be mentioned that H1 and L1 are frequently given hardware injections, but over much less than 1% of of total measurement time. As such, injections are unlikely to account for (99-100).

Correlations (99) and, respectively, (100) obtained by butterfly filtering with a massive bank of 8 million templates seems to justify further analysis. This requiring novel algorithms, to search for evidence of signals of astrophysical origin in correlations that are highly dispersed over frequency and unsteady in time.

6. SUMMARY AND FUTURE PROSPECTS

While the central engine of GRBs remains to be identified, diverse evidence from electromagnetic observations (Table 3) points to an association with black holes featuring ultra-relativistic outflows marked by (5-7), that defy an explanation in terms of Newtonian processes from baryonic inner engines. In particular, extended emission in LGRBs and SGRBEEs points to rotating black holes described by the Kerr metric. While these events are somewhat rare, the parent population of supernovae of type Ib/c is far more numerous by about two orders of magnitude. The formation and evolution of accreting black holes in core-collapse events gives an outlook on multi-messenger emission over short and long timescales, the latter including the lifetime of black holes spin associated with relativistic frame dragging induced interactions with matter at the ISCO. Thus, rapidly rotating black holes may account for (6-7), that are otherwise challenging to explain by magnetic winds from rotating neutron stars. Specifically, we mention

- *Universality of soft extended emission* in *Swift*'s SGRBEE and LGRBs alike (Table 2), satisfying the same Amati relation (Fig. 5), whose durations can be identified with the lifetime of black hole spin (Fig. 13);
- *Large energy reservoir in angular momentum* (21), that can account for hyper-energetic events whose central engines defy the limitations of (proto)-neutron stars (Table 1);

Table 3. Observational evidence for LGRBs from rotating black holes. (Adapted from [van Putten \(2016\)](#).)

INSTRUMENT	OBSERVATION/DISCOVERY	RESULT	REF.
<i>Swift</i>	LGRBs with no SN, SGRBEE	Extended Emission to mergers	(1)
	Amati-relation	Universal to LGRBs and EEs to SGRBs	(1)
	X-ray afterglows SGRBs	SGRB 050509B	(2)
<i>HETE-II</i>	X-ray afterglows SGRBs	SGRB050709	(3)
<i>BeppoSAX</i>	X-ray afterglows LGRBs	GRB970228, common to LGRBs, SGRB(EE)s	(1,4)
	Broadband Kolmogorov spectrum	No signature (proto-)pulsars	(5)
BATSE	Bi-modal distribution durations.	short-hard and long-soft GRBs	(6)
	ms variability	Compact relativistic central engine	(7)
	Normalized light curves LGRBs	BH spin-down against ISCO	(8)
Optical	LGRB association to SNe Ib/c	Branching ratio < 1%	(9)
	Calorimetry, E_k SNe	$E_{rot} > E_c[NS]$ in some GRB-SNe	(10)

Note. (1) Revisited in [van Putten et al. \(2014b\)](#); (2) [Gehrels et al. \(2005\)](#); (3) [Villasenor et al. \(2005\)](#); [Fox et al. \(2005\)](#); [Hjörth et al. \(2005\)](#); (4) [Costa et al. \(1997\)](#); (5) [van Putten et al. \(2014b\)](#); (6) [Kouveliotou et al. \(1993\)](#); (7) [Sari & Piran \(1997\)](#); [Piran & Sari \(1997\)](#); [Kobayashi et al. \(1997\)](#), and [van Putten \(2000\)](#); [Nakar & Piran \(2002\)](#); (8) [van Putten \(2009, 2012a\)](#); [Nathanail et al. \(2015\)](#), see further [van Putten \(2008\)](#); [Shahmoradi & Nemiroff \(2015\)](#); (9) [van Putten \(2004\)](#); [Guetta & Della Valle \(2007\)](#); (10) in the model of [Bisnovatyi-Kogan \(1970\)](#), E_{rot} exceeds the maximal spin energy $E_c[NS]$ of a (proto-)neutron star in some hyper-energetic events ([van Putten et al. 2011b](#)).

- *Prominent intermittency* in GRB light curves with a positive correlation to luminosity ([Reichert et al. 2001](#)), consistent with intermittent feedback by rotating black holes ([van Putten 2015b](#));
- *Smooth broadband Kolmogorov spectra* in *BeppoSAX* light curves of LGRBs (Fig. 8) up to the kHz range with no bump at high frequency, i.e., any signature of proto-pulsars is strikingly absent (Fig. 7);
- *Slowly spinning remnants* common to LGRBs from core-collapse and SGRBEEs from mergers (Fig. 9) with $a/M \simeq 0.3$, that appears both in (2) and the plateau of the superluminous event SN2015L ([van Putten & Della Valle 2017](#)).

For non-axisymmetric accreting flows onto rotating black holes formed in core-collapse events, broadband extended gravitational-wave emission may derive from orbital angular momentum and (catalytic) conversion of spin of the black hole, losing angular momentum to matter at the ISCO. Long duration times scales derive from in fall of the stellar remnant envelope and, respectively, the lifetime of black hole spin. An overview of this broad outlook on gravitational radiation from core-collapse events is shown in Fig. 18 and summarized in Table 4. In particular, we mention

1. *Ascending chirps* from accretion flows with fragments or non-axisymmetric wave patterns, formed within a critical radius where cooling conspires with self-gravity or where angular mo-

momentum loss by gravitational radiation is dominant over angular momentum loss by viscous transport;

2. *Descending chirps* from ISCO waves induced by energetic feedback of the central black hole via an inner torus magnetosphere. Non-axisymmetric waves are expected from heating and enhanced magnetic pressure, balanced by cooling in gravitational radiation, MeV neutrino emission and magnetic winds. In this process, the ISCO expands as the black hole loses angular momentum;
3. *Broadband turbulence* appears to be prevalent in LGRBs, deep within about the ISCO of the central engine (van Putten 2001b, 2012a) and in the prompt gamma-ray emission process (Figs. 6 and 13).

These emissions may be preceded by QNM ringing and the random black hole kicks in black hole formation, during a surge in black hole mass prior to the formation of an accretion disk, possibly continued during further growth to a nearly extremal black hole leading up to an accompanying LGRB.

6.1. Deep searches by GPU-accelerated butterfly filtering

Probes of BEGE (Fig. 18) with complex time and frequency behavior due to non-axisymmetric mass motion and turbulence requires a broadband detection algorithm, seeking to capture phase coherence on intermediate time scales of chirps, that may be ascending and descending. To this end, we consider extracting chirp-based spectrograms by butterfly filtering. Banks of large size allow deep searches in noisy time-series, that successfully identified broadband Kolmogorov spectrum in LGRBs (Fig. 8) and broadband H1L1 correlations by a factor of 5.11 (Fig. 20). The latter poses a challenge, to identify signals of astrophysical origin in a background of detector correlations that is dispersed over a broad frequency range with unsteady behavior (in time).

Overall, we distinguish three types of searches:

1. *Source detection* by detecting excess hit counts of ascending and descending chirps below, respectively, above a few hundred Hz. In the frequency range of 350-2000 Hz, essentially maximal sensitivity is attained when the bank of templates is large, allowing for a distances up to about 100 Mpc for energetic CC-SNe and LGRBs for Advanced LIGO-Virgo. Source detection ignores time ordering in matches to individual chirps templates, however;
2. *Chirp detection* of long duration comprising a large number of hits. This is expected to reach a distance sensitivity of tens of Mpc for Advanced LIGO-Virgo.
3. *Stochastic background detection* from an astrophysical source population. In particular, Type Ib/c supernovae may collectively produce a bump at a few hundred Hz (93), derived from their cosmological distribution locked to the cosmic star formation rate.

6.2. Scientific objective and observational strategy

For upcoming searches by LIGO-Virgo and KAGRA, it appears advantageous to focus on the progenitor population of energetic CC-SNe rather than GRBs themselves, to circumvent the relatively limited event rates of GRBs and the challenge in finding them due to beaming. Supernovae are much more numerous and quite easy to find using modest sized robot telescopes. If a fraction of 1% or more

Table 4. Broadband extended gravitational-wave emission from accretion flows onto rotating black holes.

QUANTITY	SCALE	COMMENT	REF.
BH DISK-TORUS			
M	$10^1 M_\odot$		(Bailyn et al. 1998; Woosley & Bloom 2006)
E_{rot}^H	$1 M_\odot c^2$		(Kerr 1963)
f_{ISCO}	10^{2-3} Hz		Fig. 11
M_{acc}	$10^{-1} - 10^0 M_\odot$	$\dot{M}\tau$	(65)
M_T	$10^{-2} M$		(18)
LONG GW BURST			
efficiency	$< 50\%$		Fig. 12
E_{rad}	$< 1 M_\odot c^2$		Fig. 12
T	10^1 s	T_{90}, t_{ff}, T_{spin}	Figs. 11-12, (32)
L	$10^{-1} M_\odot c^2 \text{ s}^{-1}$		Fig. 12
ACCRETION			
Fragments			(Piro & Pfahl 2007)
$f_c < f < 2f_{ISCO}$	$10^0 - 10^3$ Hz		(48)
$h_{char}(f)$	$1.7 \times 10^{-22} (f/f_e)^{\frac{2}{3}}$	$f_c < f < f_e$	cf. (20)
$h_{char}(f)$	$1.7 \times 10^{-22} (f/f_e)^{-\frac{1}{6}}$	$f_e < f < 2f_{ISCO}$	(50)
Disk waves			(Levinson et al. 2015)
$f < 2f_{ISCO}$	$10^0 - 10^3$ Hz		
$h_{char}(f)$	$1.2 \times 10^{-21} (f/f_b)^{\frac{1}{6}}$	$f < f_b$	(71)
$h_{char}(f)$	$1.2 \times 10^{-21} (f/f_b)^{-\frac{1}{6}}$	$f_b < f < 2f_{ISCO}$	(71)
ISCO waves			(van Putten 2002; van Putten & Levinson 2003)
$f = 2f_{ISCO}$	10^{2-3} Hz		
$h_{char}(f)$	3.4×10^{-21}		(81),(van Putten 2001b)
DETECTION			
$D[\text{source}]$	10^2 Mpc	spectral bump	(96)
$D[\text{chirp}]$	10^1 Mpc	track in tf -plane	(van Putten et al. 2011a)
Ω_B	$10^{-9} - 10^{-8}$	stochastic	(94)
$f_{B,peak}$	10^2 Hz	spectral bump	(93)

is luminous in gravitational waves, they will be competitive with neutron star mergers as suitable targets of opportunity.

True calorimetry will be essential to identifying the true nature of the inner engine of energetic CC-SNe, that should include gravitational radiation following the identification of high density matter

- and possibly high-density mass motion - in the pivotal event SN1987A. A detailed probe may identify, for instance, different engines to narrow- and broad line events (Fig. 1), provide first principle constraints on total mass accretion (ascending chirps) and the total rotational energy of the central compact object (descending chirps). The latter offers a window to identification of Kerr black holes, including their initial state and evolution, as the most luminous objects in Nature (van Putten & Levinson 2002). For calorimetry, ignoring temporal evolution, the above mentioned source detection is sufficient.

Sensitivity of LIGO-Virgo and KAGRA detectors is limited by instrumental strain noise. They are broadband covering a window of tens of Hz to a few kHz, susceptible to seismic noise at low frequency, thermal noise at intermediate frequencies and shot noise at higher frequencies. Below a few hundred Hz, they are ideally suited to probe mergers of stellar mass compact objects. While these are amply highlighted in existing development programs preparing for upcoming gravitational wave searches, we here highlight a window on broadband extended emission from CC-SNe that extends to the high frequency bandwidth of sensitivity. Our outlook is guided by evidence for black holes in energetic events based on their association with LGRBs, aforementioned SN1987A and some general considerations of accretion flows onto rotating black holes.

In detecting nearby Type Ib/c supernovae in optical surveys, and the main challenges are sufficient completeness of the survey and cadence to resolve the supernova light curve (Heo et al. 2015). A narrow window of the time-of-onset to within one day will be crucial to minimizing computational effort in source detection by application of TSMF. The most nearby events may be captured by surveys focused on galaxies most prolific in core-collapse supernovae, e.g., M51 and M82, each featuring over one CC-SN per decade.

Acknowledgments. M.H.P.M. van Putten acknowledges support from the National Research Foundation of Korea and faculty research fund of Sejong University in 2012. A. Levinson acknowledges supported by a grant from the Israel Science Foundation no. 1277/13. The BeppoSAX mission was an effort of the Italian Space Agency ASI with the participation of The Netherlands Space Agency NIVR. M.H.P.M. van Putten acknowledges computational support in part by the National Science Foundation through TeraGrid (now XSEDE) resources provided by Purdue University under grant No. TG-DMS100033. Some calculations were performed at CAC/KIAS and KISTI. F. Frontera, C. Guidorzi and L. Amati acknowledge financial support from the Italian Ministry of Education, University, and Research through the PRIN-MIUR 2009 project on Gamma-Ray Bursts (Prot. 2009 ERC3HT). This work was partially supported by the National Research Foundation of Korea under grants 2015R1D1A1A01059793 and 2016R1A5A1013277 and made use of LIGO S6 data from the LIGO Open Science Center (losc.ligo.org), provided by the LIGO Laboratory and LIGO Scientific Collaboration. LIGO is funded by the U.S. National Science Foundation. Additional support is acknowledged from MEXT, JSPS Leading-edge Research Infrastructure Program, JSPS Grant-in-Aid for Specially Promoted Research 26000005, MEXT Grant-in-Aid for Scientific Research on In-

novative Areas 24103005, JSPS Core-to-Core Program, A. Advanced Research Networks, and the joint research program of the Institute for Cosmic Ray Research.

APPENDIX

APPENDIX A. GRAVITATIONAL RADIATION

The Einstein equations are a hyperbolic-elliptic system of equations for a four metric g_{ab} with signature $(-, +, +, +)$ in the line element

$$ds^2 = g_{ab} dx^a dx^b. \quad (1)$$

This can be made explicit following a foliation of space-time in Cauchy surfaces (Arnowitt et al. 1962) or in a Lorentz gauge on $SO(3,1)$ connections in the Riemann-Cartan formalism (van Putten 1996). The resulting gravitational wave motion is subject to elliptic constraints given by conservation of energy and momentum.

Hyperbolicity

The linearized equations of motion about Minkowski space-time reveal the two modes of transverse gravitational waves of spin two. Traditionally, the derivation is given in 3+1 in a special choice of coordinates, that exploits gauge covariance in the choice of coordinates. Here, we note a derivation utilizing the constraints of energy-momentum conservation.

To start, consider slicing of space-time into space-like hypersurfaces of constant coordinate time $t = x^0$. Let h_{ij} denote the three-metric intrinsic to these hypersurfaces, that are coordinated by the remaining x^i ($i = 1, 2, 3$). The line-element can be equivalently expressed as (e.g. (Thorne et al. 1986))

$$ds^2 = -\alpha^2 dt^2 + h_{ij} (dx^i + \beta^i dt) (dx^j + \beta^j dt), \quad (2)$$

where (α, β^i) denote the lapse function and, respectively, shift functions. In foliating space-time into three-dimensional hypersurfaces, the (α, β^i) are a gauge, and are not dynamical variables. The three-metric h_{ij} defines parallel transport of vectors in the hypersurfaces of constant coordinate time t and, as such, comes with a covariant three-derivative D_i and associated Christoffel symbols Γ_{ij}^k .

Following (2), the Ricci tensor ${}^{(4)}R$ of g_{ab} expands to ${}^{(3)}R$ of h_{ij} and quadratic terms of the extrinsic curvature tensor $K_{ij} = -1/(2\alpha)L_t h_{ij}$, where L_t denotes the Lie derivative of h_{ij} with respect to the coordinate time t . The Hilbert action for g_{ab} hereby reveals explicit contributions from “potential” and “kinetic” energies in

$$S = \frac{1}{16\pi} \int ({}^{(3)}R + K_{ij}K^{ij} - K^2) \alpha \sqrt{h} dx^3 dt. \quad (3)$$

Following (Arnowitt et al. 1962), variations with respect to the non-dynamical variables (α, β^i) obtain the conservation laws of energy and momentum, given by the constraints

$$R - K_{ij}K^{ij} + K^2 = 0, \quad D^i K_{ij} - D_j K = 0, \quad (4)$$

where $R = R_i^i$ denotes the trace of the Ricci tensor of h_{ij} . Variation with respect to h_{ij} gives the first-order evolution equation

$$L_t K_{ij} = (R_{ij} - D_i D_j) \alpha + (K K_{ij} - 2K_i^m K_{jm}) \alpha, \quad (5)$$

where $L_t K_{ij} = \partial_t K_{ij} - (K_i^m D_m \beta_j + K_j^m D_m \beta_i + \beta^m D_m K_{ij})$. Similar to the latter, we may expand $L_t h_{ij}$ to obtain the first-order evolution equation

$$\partial_t h_{ij} = D_i \beta_j + D_j \beta_i - 2\alpha K_{ij}. \quad (6)$$

Combined, (4-6) defines a constraint Hamiltonian system of equations for the dynamical variables (h_{ij}, K_{ij}) .

The existence of gravitational waves represents the hyperbolic structure of (4-6). This becomes explicit by analysis of harmonic perturbations in the curvature driven gauge (van Putten 2010; van Putten & Levinson 2012)

$$\partial_t \alpha = -K, \quad \beta^i = 0. \quad (7)$$

We next consider small perturbations about Minkowski space-time ($h_{ij} = \delta_{ij}, \alpha = 1, K_{ij} = 0$), where δ_{ij} denotes the Kronecker delta symbol, that is, $h_{ij} = \delta_{ij} + \delta h_{ij}$, $\alpha = 1 + \delta\alpha$ and $K_{ij} = \delta K_{ij}$. In the gauge (7), (5-6) imply

$$\partial_t^2 h_{ij} = -2(R_{ij} - D_i D_j \delta\alpha), \quad \partial_t^2 K = \Delta K, \quad (8)$$

where we used that ${}^{(3)}R$ is second order according to the Hamiltonian energy constraint in (4), Here, we recall the perturbative expansion (Wald 1984)

$$R_{ij} = -\frac{1}{2}\Delta\delta h_{ij} + \frac{1}{2}\partial_i\partial^e\delta\bar{h}_{ej} + \frac{1}{2}\partial_j\delta\bar{h}_{ej}, \quad (9)$$

where $\bar{h}_{ij} = \delta h_{ij} - \frac{1}{2}\delta_{ij}\delta h$, $\delta h = \delta^{ij}\delta h_{ij}$. A harmonic plane wave $\delta h_{ij} = \hat{h}_{ij}e^{-i\omega t}e^{ik_i x^i}$ (similarly for K_{ij}) of angular frequency ω with wave vector k_i can be applied to (5) and (7), giving $k_i \hat{K}_{ij} = k_j \hat{K}$, $-i\omega\hat{\alpha} = -\hat{K}$, $\delta\hat{h}_{ij} = -2i\omega^{-1}\hat{K}_{ij}$ and, for $\partial_i\partial^e\bar{h}_{ej}$,

$$k_i k^e \hat{h}_{ej} - \frac{1}{2}k_i k_j \delta\hat{h} = i\omega^{-1} \left(-2k_i k^e \hat{K}_{ej} + k_i k_j \hat{K} \right) = -i\omega^{-1} k_i k_j \hat{K}. \quad (10)$$

By (9), it follows that $\hat{R}_{ij} - \partial_i\partial_j\hat{\alpha} = \frac{1}{2}k^2\hat{h}_{ij} - i\omega^{-1}k_i k_j \hat{K} + i\omega^{-1}k_i k_j \hat{K}$, whereby the first evolution equation in (8) reduces to the dispersion relation

$$\omega^2 = k^2 \quad (11)$$

of propagation along light cones in a local Minkowski background space-time.

The Einstein equations, $G_{ab} = 16\pi T_{ab}$ describe the response of space-time curvature to a stress-energy tensor T_{ab} of matter and fields, where $G_{ab} = {}^{(4)}R_{ab} - \frac{1}{2}g_{ab}{}^{(4)}R$ is the Einstein tensor. Following (9) and (11), the covariant wave equation for perturbations $g_{ab} = \eta_{ab} + \delta g_{ab}$ in the four-metric on a fixed background space-time with metric η_{ab} is

$$\square_\eta \delta g_{ab} = -16\pi T_{ab}, \quad (12)$$

where \square denotes the d'Alembertian associated with η_{ab} . The coefficient -16π in (12) results from the factor $-\frac{1}{2}$ in (9).

Searches for contemporaneous emission in electromagnetic and gravitational from cosmological GRBs have been suggested to test for gravitons to be massless as described by (12). However, these tests only serve to identify differences in masses of gravitons and photons, as may be seen by expressing wave motion of both in terms of four vector fields. Let $\omega_{a\mu\nu}$ denote the Riemann-Cartan connection of four-dimensional space-time in the SO(3,1) tetrad formalism and A_a denote the vector potential of the electromagnetic field. In the Lorentz gauge to both (van Putten 1996), propagation in vacuum satisfies

$$\square\omega_{a\mu\nu} - R_a^c\omega_{c\mu\nu} - [\omega^c, \nabla_a\omega_c]_{\mu\nu} = 0, \quad \square A_a - R_a^c A_c = 0, \quad (13)$$

where \square denotes the d'Alembertian associated with the SO(3,1) gauge covariant derivative $\hat{\nabla}_a = \nabla_a + [\omega_a, \cdot]$. In the presence of a cosmological constant $\Lambda > 0$ (Riess et al. 1998; Perlmutter et al. 1999), $R_{ab} = \Lambda g_{ab}$, whereby (13) becomes

$$\square\omega_{a\mu\nu} - \Lambda\omega_{c\mu\nu} - [\omega^c, \nabla_a\omega_c]_{\mu\nu} = 0, \quad \square A_a - \Lambda A_c = 0, \quad (14)$$

showing gravitons and photons of the same effective mass $m = \sqrt{\Lambda} \simeq 10^{-29} \text{ cm}^{-1}$ in geometrical units, as defined by the dispersion relation of (14).

Luminosity in gravitational radiation

Consider the transverse traceless perturbations (Misner et al. 1973)

$$\delta h_{ij}^{TT} = \begin{pmatrix} h_+ & h_\times & 0 \\ h_\times & -h_+ & 0 \\ 0 & 0 & 0 \end{pmatrix} = h_+ e_{ij}^+ + h_\times e_{ij}^\times, \quad (15)$$

decomposed in the two linear polarization tensors e_{ij}^+ and e_{ij}^\times of gravitational waves in the (x, y) plane orthogonal to the direction of propagation along the z -axis. The perturbed line-element (1) now assumes the form

$$ds^2 = \eta_{ab} dx^a dx^b + h_+(dx^2 - dy^2) + 2h_\times dx dy. \quad (16)$$

With rotational symmetry over an angle π about the z -axis, gravitational waves are of spin-2 (Fierz et al. 1939). In the far field region away from a source region, the Hilbert action (3) reduces to the kinetic term $K_{ij}K^{ij}$, and hence by (6) to

$$S = \frac{1}{16\pi} \int \frac{1}{2} [(\partial_a h_+)^2 + (\partial_a h_\times)^2] dx^3 dt. \quad (17)$$

We can now read off the stress-energy tensor of gravitational wave motion:

$$t^{00} = t^{0z} = t^{zz} = \frac{1}{16\pi} \langle \dot{h}_+^2 + \dot{h}_\times^2 \rangle \quad (18)$$

The two polarization wave modes (15) and the associated gravitational wave stress-energy tensor (18) are characteristic properties of general relativity. Alternative theories may have additional degrees of freedom (Sathyaprakash & Schutz 2009).

For a source described by a stress-energy tensor T_{ab} , the gravitational wave emission results from the associated time harmonic perturbations in the tidal gravitational field. Following (12), we have in response to a distance source over a region V

$$\delta h_{ij}(r, t) = \frac{4}{r} \int_V T_{ij}(t - r, x^i) d^3x. \quad (19)$$

Explicit evaluation for a circular binary of point masses M_1 and M_2 , orbital frequency Ω and orbital separation a shows the quadrupole gravitational wave formula (Wald 1984; Thooft 2002)

$$L_{GW} = \frac{32}{5} \Omega^6 a^4 \mu^2 = \frac{32}{5} (\Omega \mu)^{\frac{10}{3}} \quad (20)$$

in units of $L_0 = c^5/G$, where $\mu = M_1^{\frac{3}{5}} M_2^{\frac{3}{5}} / (M_1 + M_2)^{\frac{1}{5}}$ denotes the chirp mass, c is the velocity of light and G is Newton's constant.

To see (20), we first recall the following identity for a mass distribution with velocity four-vector u^b (e.g. (Thooft 2002))

$$\int_V T^{ij} d^3x = \frac{1}{2} \partial_0^2 I_0^{ij} \quad (21)$$

between $\int_V T^{ij} d^3x = \int_V u^i u^j dm$, $dm = \rho d^3x$ and the moment of inertia tensor

$$I_0^{ij} = \int_V T^{00} x^i x^j d^3x \simeq \int_V x^i x^j dm, \quad (22)$$

where the latter refers to the non-relativistic limit $u^0 \simeq 1$. The identity (21) follows from the conservation of energy-momentum, $\nabla_a T^{ab} = 0$. About a flat space-time background, $\nabla_a \nabla_b T^{ab} = 0$ implies $\partial_0^2 T^{00} + 2\partial_0 \partial_i T^{0i} + \partial_i \partial_j T^{ij} = 0$, i.e., $\partial_0^2 T^{00} - \partial_i \partial_j T^{ij} = 0$ using $\partial_0 T^{00} + \partial_i T^{0i} = 0$. Integration by parts twice of $\partial_0^2 \int_V x^i x^j T^{00} d^3x = \int_V x^i x^j \partial_k \partial_l T^{kl}$ obtains (21).

Consequently, (19) gives for the *traceless* metric perturbations

$$h_{ij}^T(t, r) = \frac{2}{r} \frac{d^2 I_{ij}(t - r)}{dt^2}, \quad I^{jk} = I_0^{jk} - \frac{1}{3} \delta^{jk} \delta_{lm} I_0^{lm}. \quad (23)$$

By (17), we arrive at the gravitational wave luminosity

$$L_{GW} = \frac{dE_{GW}}{dt} = \frac{1}{5} \left\langle \frac{d^3 I_{jk}}{dt^3} \frac{d^3 I^{jk}}{dt^3} \right\rangle, \quad (24)$$

taking into account and reduction factor $2/5$ as only two of the five degrees of freedom in the traceless metric perturbation δh_{ij}^T are physical degrees of freedom representing outgoing gravitational radiation (Thooft 2002).

Radiation from multipole mass moments

Consider a ring having cross-sectional radius b and density ρ , rotating around a central object in the (x, y) plan at angular velocity Ω in a circular orbit of radius r . Let $m = \int_V \rho d^3x$ denotes the total mass of the ring, where the integration is over the ring's volume V . We restrict the analysis to

a thin ring, $b \ll r$, and compute I^{jk} to order $O(b^2/r^2)$. Let (x', y') denotes a Cartesian coordinate system rotating with the ring. One can always choose the axis such that

$$I_0^{x'x'} = \frac{1}{2}mr^2(1 + \xi), \quad I_0^{y'y'} = \frac{1}{2}mr^2(1 - \xi), \quad I_0^{x'y'} = 0. \quad (25)$$

to order $O(b^2/r^2)$. Here, ξ quantifies the mass quadrupole inhomogeneity, with $\xi = 0$ for an axisymmetric ring. For example, for a ring having a density $\rho = \rho_0 + \rho_2 \cos^2 \theta$ in cylindrical coordinates, with ρ_0 and ρ_2 being constants, one obtains $\xi = m_2/4m$, where $m = \int_V d^3x \rho$ is the total mass, and $m_2 = \int_V d^3x \rho_2$. Now, transforming to the non-rotating frame,

$$\begin{pmatrix} x \\ y \end{pmatrix} = \begin{pmatrix} x' \cos \Omega t & y' \sin \Omega t \\ -x' \sin \Omega t & +y' \cos \Omega t \end{pmatrix} \quad (26)$$

yields

$$\begin{aligned} I_0^{xx} &= I_0^{x'x'} \cos^2 \Omega t + I_0^{y'y'} \sin^2 \Omega t = \frac{1}{2}mr^2(1 + \xi \cos 2\Omega t), \\ I_0^{yy} &= I_0^{x'x'} \sin^2 \Omega t + I_0^{y'y'} \cos^2 \Omega t = \frac{1}{2}mr^2(1 - \xi \cos 2\Omega t), \\ I_0^{xy} &= \frac{1}{2}(I_0^{x'x'} - I_0^{y'y'}) \sin 2\Omega t = -\frac{1}{2}mr^2\xi \sin 2\Omega t. \end{aligned}$$

By employing (23) and (27) one has

$$\frac{d^3 I^{ij}}{dt^3} = 4\xi mr^2 \Omega^3 \begin{pmatrix} \sin \Omega t & \cos \Omega t \\ \cos \Omega t & -\sin \Omega t \end{pmatrix}. \quad (27)$$

Substituting into Equation (24) finally gives

$$L_{GW} = \frac{32}{5} \xi^2 m^2 r^4 \Omega^6. \quad (28)$$

The quadrupole formula for a circular binary of point masses is obtained upon taking $\xi = 1$, $m = \mu$ and $r = a$, here μ is the reduced mass and a is the binary separation.

In (28), the limit $\xi = 1$ obtains the canonical formula of quadrupole gravitational wave emission. A circular binary of masses M_i ($i = 1, 2$) with chirp mass $\mu = (M_1 M_2)^{5/3} (M_1 + M_2)^{-1/5}$. For a matched filtering detection method, the relevant quantity is the amplitude that takes into account the square root of the associated number of wave periods. In the frequency domain, the corresponding quantity is the *characteristic strain amplitude*, given by the square root of the energy per unit logarithmic frequency interval (Flanagan & Hughes 1998a),

$$h_{char}(f) = \frac{\sqrt{2}}{\pi D} \sqrt{\left| \frac{dE}{df} \right|}. \quad (29)$$

Consider a circular binary with small mass-ratio $\sigma = M_2/M_1 \ll 1$, so that $M = M_1 + M_2 \simeq M_2$. At an orbital separation a , it emits quadrupole gravitational radiation at a frequency $\pi M f = (M/a)^{2/3}$.

The total energy $E = -\frac{1}{2}\sigma M^2/a = -\frac{1}{2}M\sigma(M\pi f)^{\frac{2}{3}}$ hereby shrinks, whereby (cf. (Misner et al. 1973))

$$\frac{dE}{df} = -\frac{\pi\sigma M^2}{3(\pi Mf)^{\frac{1}{3}}} \quad (30)$$

and hence (cf. (Thorne 1992; Ju et al. 2000))

$$h_{char}(f) = 8.6 \times 10^{-22} \sigma^{\frac{1}{2}} M_1^{\frac{1}{3}} \left(\frac{D}{100 \text{ Mpc}}\right)^{-1} \left(\frac{f}{100 \text{ Hz}}\right)^{-\frac{1}{6}} \quad (31)$$

for a central mass $M = M_1 \times 10 M_\odot$. It shows that the low frequency emission at early in spiral is particularly important for detection.

In the presence of an ellipticity e , the luminosity in gravitational waves is greater than (28) by additional radiation at frequency harmonics $m > 2$ (Peters & Mathews 1963). The result can be expressed by an enhancement factor $F(e) \geq 1$. The time rate of change in orbital frequency satisfies

$$\dot{f}_{orb} = \frac{96}{5} (2\pi)^{\frac{8}{3}} f_{orb}^{\frac{11}{3}} F(e), \quad F(e) = \frac{1 + \frac{73}{24}e^2 + \frac{37}{96}e^4}{(1 - e^2)^{\frac{7}{2}}}. \quad (32)$$

Given an initial ellipticity e_0 , the orbital separation $a = a(t)$ hereby satisfies

$$a(t) = a_0 \left(1 - \frac{t}{\tau_0}\right)^{\frac{1}{4}}, \quad \tau_0 = \frac{5a_0^4}{256M_1M_2(M_1 + M_2)} f(e_0), \quad (33)$$

where $f(e_0) \leq 1$ ($e_0 \geq 0$) obtains as an integral over $0 \leq e \leq e_0$ (see, e.g., (Postnov & Yungelson 2006) for a detailed expression).

It should be mentioned that (10-11) is derived for sources about a Minskowski background space-time. In an applying to the multipole mass-moments of a strongly magnetized torus about the ISCO of a rotating black hole (Bromberg et al. 2006), the radiation is emitted in a strongly curved space-time. It requires extending (10) by an additional grey body factor, that represents suppression of radiation at low l for a given l_{lm} . The grey body factor derives from scattering of relatively low frequency gravitational waves in the curved space-time around black holes, that results in partial absorption by the black hole. However, in a suspended accretion state which balances heating by input from the black hole and cooling in gravitational radiation (van Putten 2012a), l_{lm} is self-regulated such that L_{lm} in (10) times such grey body factor balances with the energetic input from the black hole. Emissions from l_{lm} beyond the ISCO are relatively less affected by space-time curvature. At large distances away from the black hole, the grey body factor is effectively one. A detailed derivation of the grey body factor is beyond the scope of this review.

APPENDIX B. RELATIVISTIC FRAME DRAGGING

The Kerr metric in Boyer-Lindquist coordinates (t, r, θ, ϕ) explicitly brings about the Killing vectors $k^b = (\partial_t)^b$ and $m^b = (\partial_\phi)^b$ of time slices of constant coordinate time t . It gives an exact solution of frame dragging in terms of the angular velocity ω of particles of zero-angular momentum. In Boyer-Lindquist coordinates (t, r, θ, ϕ) of the Kerr metric (Thorne et al. 1986), the world line of zero-angular momentum observers (ZAMOs, (Thorne et al. 1986) are orthogonal to slices of constant

time-at-infinity. The angular velocity $\omega = d\phi/dt$ decays with the cube of the distance to the black hole at large distances.

By frame dragging, the ISCO of corotating orbits shrinks to the event horizon from $6M$ around a non-rotating Schwarzschild black hole. This appears in X-ray spectroscopy of MCG 6-30-15 (Iwasawa 1996). These results are time variable over a time scale of a year, that may reflect intermittency in the inner radius of the disk (Fabian et al. 1995) or, alternatively, in circumnuclear clouds intermittently absorbing disk emissions.

The complete gravitational field induced by the angular momentum and mass of a rotating black hole is described by the Riemann tensor. For completeness, we here include a brief summary of earlier derivations on the associated energetic interactions (van Putten 2005a, 2012a).

Gravitational spin-orbit energy

Consider the tetrad 1-forms

$$e_{(0)} = \alpha dt, \quad e_{(1)} = \frac{\Sigma}{\rho}(d\phi - \omega dt) \sin \theta, \quad e_{(2)} = \frac{\rho}{\sqrt{\Delta}} dr, \quad e_{(3)} = \rho d\theta, \quad (34)$$

where $\alpha = \rho \Sigma^{-1} \sqrt{\Delta}$ is the redshift factor, $\Sigma^2 = (r^2 + a^2)^2 - a^2 \Delta \sin^2 \theta$, $\rho = r^2 + a^2 \cos^2 \theta$, $\Delta = r^2 - 2Mr + a^2$ and $\omega = 2aMr \Sigma^{-2}$ is the angular velocity of frame dragging. The Riemann tensor has the following non-zero components (Chandrasekhar 1983)

$$\begin{aligned} R_{0123} &= A, & R_{1230} &= AC, & R_{1302} &= AD \\ -R_{3002} &= R_{1213} = -3aA\sqrt{\Delta}\Sigma^{-2}(r^2 + a^2) \sin \theta \\ -R_{1220} &= R_{1330} = -3aB\sqrt{\Delta}\Sigma^{-2}(r^2 + a^2) \sin \theta \\ -R_{1010} &= R_{2323} = B = R_{0202} + R_{0303} \\ -R_{1313} &= R_{0202} = BD, & -R_{1212} &= R_{0303} = -BC, \end{aligned} \quad (35)$$

where

$$\begin{aligned} A &= aM\rho^{-6}(3r^2 - a^2 \cos^2 \theta), & B &= Mr\rho^{-6}(r^2 - 3a^2 \cos^2 \theta), \\ C &= \Sigma^{-2}[(r^2 + a^2)^2 + 2a^2 \Delta \sin^2 \theta], & D &= \Sigma^{-2}[2(r^2 + a^2)2 + a^2 \Delta \sin^2 \theta]. \end{aligned} \quad (36)$$

About the black hole spin axis ($\theta = 0$), $2A = -\partial_r \omega = 2aM\rho^{-6}(3r^2 - a^2)$, $C = 1$, $D = 2$, J induced components appear in the first three of (35). Integrating the Papapetrou force on a test particle with velocity four-vector u^b satisfies (Papapetrou 1951)

$$F_2 = \frac{1}{2} \epsilon_{abef} R_{cd}^{ef} J_p^a u^b u^d = J_p R_{3120} = J_p AD = -\partial_2 \omega J_p \quad (37)$$

gives

$$E = \int_r^\infty F_2 ds. \quad (38)$$

Alternatively, consider the angular velocity $\Omega = u^\phi/u^t$. The normalization $-1 = u^c u_c = [g_{tt} + g_{\phi\phi} \Omega(\Omega - 2\omega)] (u^t)^2$ gives two roots

$$\Omega_\pm = \omega \pm \sqrt{\omega^2 - (g_{tt} + (u^t)^{-2})/g_{\phi\phi}}. \quad (39)$$

Two particles with the same angular momentum in absolute value,

$$J_{p,\pm} = g_{\phi\phi}u^t(\Omega_{\pm} + \omega) = g_{\phi\phi}u^t\sqrt{\omega^2 - (g_{tt} + (u^t)^{-2})/g_{\phi\phi}} = \pm J_p \quad (40)$$

hereby have (with the same u^t) the total energies $E_{\pm} = (u^t)^{-1} + \Omega_{\pm}J_{\pm}$. One-half the difference satisfies

$$E = \frac{1}{2}(E_+ - E_-) = \omega J_p. \quad (41)$$

As a gravitational interaction, the curvature-spin coupling (41) acts universally on angular momentum, whether mechanical or electromagnetic in origin.

The result of (38) combined with canonical pair-creation processes will be a possibly force-free outflow along open magnetic field lines along the black hole spin axis, such as envisioned in (Blandford & Znajek 1977). Intermittent inner engines hereby produce outgoing Alfvén fronts, that communicate the raw Faraday induced potential within the inner engine (roughly, on the event horizon of the black hole) out to large distance. The result may thus produce a linear accelerator ahead of the Alfvén front in regions of relatively low opacity, facilitating the production of UHECRs (van Putten 2009).

The structure of force-free outflows is a limit of ideal MHD (Globus & Levinson 2014), which neglects inertia (and hence Reynolds stresses) in addition to being free of dissipation of the electromagnetic field. Originally, this limit was motivated to model extragalactic outflows, e.g., (Fanaroff & Riley 1974), but increasingly this limit appears to be relevant also to extreme sources such as GRBs (e.g. (Lyutikov & Blandford 2003; Lyutikov et al. 2003)).

Let $p_B = B^2/8\pi$ and $e_B = B^2/8\pi$ denote the magnetic pressure and energy density. In a magnetic flux tube of radius R , the dissipationless limit implies adiabatic compression: $p_B(2\pi R dR) = d(\pi e_B R^2)$, i.e., the magnetic flux $\Phi = \pi B R^2$ is *frozen* into the fluid. In contrast, a torsional perturbation mediating angular momentum outflow creates an *Alfvén wave* with velocity (Lichnerowich 1967)

$$v_A = \frac{B}{\sqrt{4\pi\rho + B^2}}, \quad (42)$$

where ρ denotes the fluid density as seen in the comoving frame. The Alfvén wave is purely rotational, leaving density (and magnetic flux) invariant. It should be mentioned that (42) is unique to MHD in U(1). It does not generalize to colored MHD (van Putten 1994).

Neglecting inertia, the Alfvén velocity reaches the velocity of light. Neglecting Reynolds stresses,

$$F_{ab}j^b = 0, \quad (43)$$

which reduces the number of degrees of freedom in the electromagnetic field to two. For an electric current $j^b = \rho_e v^b$ associated with a charge density ρ_e with four-velocity v^b , (43) implies $v^i \partial_i A_\phi = 0$ and $v^i \partial_i A_0 = 0$ for a time-independent tube $A_\phi = \text{const.}$ along the polar axis $\theta = 0$. The electric potential hereby satisfies $A_0 = A_0(A_\phi)$, and the electric field $\partial_i A_0 = A'_0 \partial_i A_\phi$, in the Boyer-Lindquist frame of reference, is normal to the flux surfaces. Force-free flux surfaces are equipotential surfaces ((Golreich & Julien 1969; Blandford & Znajek 1977; Thorne et al. 1986)).

Alfvén surfaces in force-free outflows from Intermittent inner engines can thus transmit Faraday induced potentials outwards. They can produce linear accelerators upstream at large distances from the source, providing a suitable condition for the creation of UHCRs from ionic contaminants by, e.g., UV-irradiation from a surrounding torus in AGN.

Alfvén waves in a torus magnetosphere

Consider the electromagnetic two-tensor F_{ab} (Lichnerowich 1967)

$$\mathbf{F} = \mathbf{u} \wedge \mathbf{e} + *\mathbf{u} \wedge \mathbf{h} \quad (44)$$

in the four-vector representation (u^b, e^b, h^b) associated with a time like unit tangent u^b , $u^c u_c = -1$, of ZAMOs. Following (Bardeen et al. 1972; Thorne et al. 1986), we have the one-form $\mathbf{u} = -\alpha dt$ with redshift α . Then $\mathbf{u} = \alpha^{-1}(\mathbf{k} + \omega \mathbf{m})$ is linear combination of the Killing vectors, satisfying $\nabla_c u^c = 0$. ZAMOs measure an electric field e^b and a magnetic field h^b , $e^b = u_c F^{ac}$ and $h^b = u_c *F^{cb}$, each with three degrees of freedom given $u^c e_c = u^c h_c = 0$. The same ZAMOs observe $\mathbf{e} = (0, E^i)$ and $\mathbf{h} = (0, B^i)$, where $i = 1, 2, 3$ refers to the coordinates of the surfaces of constant t . The star $*$ denotes the Hodge dual, satisfying $*^2 = -1$ in four dimensions.

Faraday's equation

$$\nabla_a *F^{ab} = 0 \quad (45)$$

can be expanded by considering $\nabla_a(u^a h^b - u^b h^a) = L_u h^b + (\nabla_c u^c)h^b - (\nabla_c h^c)u^b$, where $L_u h^b = (u^c \nabla_c)h^b - (h^c \nabla_c)u^b$ denotes the Lie-derivative of h^b with respect to u^b . Projected onto surfaces of constant t (orthogonal to u^b), we have

$$(L_u \mathbf{h})_{\perp} = \alpha^{-1} (\partial_t \mathbf{B} + L_{\omega} \mathbf{B}) \quad (46)$$

evaluated in the frame of ZAMOs, where L_{ω} is the Lie-derivative with respect to $\omega^i \equiv \omega m^i$ (m^i is not a unit three-vector). Next, $\nabla_a = D_a - u_a(u^c \nabla_c)$ and $(*\mathbf{u} \wedge \mathbf{h})_{abcd} = \epsilon_{abcd} u^c e^d$. With acceleration $(u^c \nabla_c)u_b = \alpha^{-1} \nabla_b \alpha$, consider $\nabla^b(\epsilon_{abcd} u^c e^d) = \epsilon_{abcd} (D^b u^c) e^d - \epsilon_{abcd} u^b a^c e^d + \epsilon_{abcd} u^c \nabla^b e^d$. Projection of the right hand side onto the space like coordinates $i = (r, \theta, \phi)$ normal to u^b satisfies

$$\epsilon_{ibcd} (D^b u^c) e^d + \tilde{\epsilon}_{ijk} a^j e^k + \tilde{\epsilon}_{ijk} \nabla^j e^k = \epsilon_{ibcd} (D^b u^c) e^d + \alpha^{-1} \tilde{\epsilon}_{ijk} \nabla^j (\alpha e^k), \quad (47)$$

where $\epsilon_{aijk} u^a = \tilde{\epsilon}_{ijk} = \sqrt{h} \Delta_{ijk}$ with $\sqrt{-g} = \alpha \sqrt{h}$ over the space like volume element \sqrt{h} , where Δ_{ijk} , $\Delta_{123} = 1$. The first term on the right hand side vanishes, since $D_b u_c$ is spacelike: $u^b (D_b u_c) = 0$ by construction and $u^c D_b u_c = 0$ by $u^2 = -1$. Consequently, Faraday's law includes an additional term (derived alternatively in (Thorne et al. 1986) and references therein)

$$\tilde{\nabla} \times \alpha \mathbf{E} = -\partial_t \mathbf{B} + 4\pi J_m, \quad (48)$$

where $\tilde{\nabla}_i = D_i$ and

$$J_m = -\frac{1}{4\pi} L_{\omega} \mathbf{B}. \quad (49)$$

J_m appears analogously to a current of virtual magnetic monopoles.

Applied to a torus magnetosphere, (49) satisfies

$$\omega_i J_m^i \simeq \frac{1}{8\pi} \mathbf{B} \cdot \tilde{\nabla}(\omega_i \omega^i) > 0, \quad \omega_i \omega^i = 4 \frac{z^2 \sin^2 \lambda}{(z^2 + \sin^2 \lambda)^3} \left(\theta = \frac{\pi}{2} \right), \quad (50)$$

where the inequality refers to a poloidally ingoing magnetic field.

By (50), frame dragging induced poloidal current loops in the inner torus magnetosphere. The resulting poloidal Alfvén waves produces Maxwell stresses by which rotating black holes lose angular momentum to surrounding matter. The black hole hereby spins down, which should have an imprint on any light curve derived from high energy emissions derived from (38), while surrounding matter is brought into a state of forced turbulence by competing torques acting on the inner and outer faces (van Putten 1999), possibly related to forced turbulence in Taylor-Couette flows (Stefani et al. 2009).

The Alfvén waves effectively transport angular momentum out an onto the torus, provided they are not canceled by Reynolds stresses from a baryon-rich torus wind back into the black hole. In this event, the inner face of the torus will be spun up, whereby it assumes a state of super-Keplerian motion. The resulting differential rotation can induce non-axisymmetric wave instabilities (Appendix C). The associated surface gravity suppresses baryon-rich outflows from the inner face of the torus. A detailed description of this suppression of Reynolds stresses falls outside the scope of the present discussion, however.

REFERENCES

- Aasi, J., Abbott, B.P., Abbott, T., et al., 2014, Phys. Rev. D, 89, 122004
- Abbott, B., and the LIGO/GEO collaboration, 2004, Nucl. Instrum. Meth. Phys. Research A, 517, 154
- Abbott, B.P., Abbott, R., Abbott, T.D., et al., arXiv:1511.04398v1
- Abramovici, A., Althouse, W.E., Drever, R.W.P., et al., 1992, Science, 256, 325
- Acernese, F. et al. (Virgo Collaboration), 2006, Class. Quantum Grav., 23, S635
- Acernese, F. et al. (Virgo Collaboration), 2007, Class. Quantum Grav., 24, S381
- Amati, L., Piro, L., & Antonelli, L.A., et al., 1998, Nucl. Phys. B., 69, 656
- Amati, L., et al., 2002, A&A, 390, 81
- Amati, L., et al., 2006, MNRAS, 372, 233
- Amati, L., et al., 2007, A&A, 463, 913
- Amati, L., et al., 2008, MNRAS, 391, 577
- Amati, L., Frontera, F., Guidorzi, C., A&A, 2009, 508, 173
- Amati, L., et al., 2010, JKPS, 56, 1603
- Ando, S., Baret, B., Bartos, I., et al., 2013, Rev. Mod. Phys., 85, 2013
- Anninos, P., Hobill, D., Seidel, E., Smarr, L., & Suen, W.M., 1993, Phys. Rev. Lett. 71, 2851
- Antonelli, L. A., et al., 2009, A&A, 507, L45
- Arnowitz, R., Deser, R., & Misner, C.W., 1962, in Gravitation: An Introduction to Current Research, ed. L. Witten (New York: Wiley), p. 227
- Bailyn, C.D., Jain, R.K., Coppi, P., & Orosz, J.A., 1998, ApJ, 499, 367
- Balbus, S.A., & Hawley, J.F., 1991, ApJ, 376, 214
- Baiotti, L., Giacomazzo, B., and Rezzolla, L., 2008, Phys. Rev. D, 78, 084033
- Band, D., Matteson, J., Ford, L., et al., 1993, ApJ, 413
- Barbon, R., Buondí, V., Cappellaro, E., & Turatto, M., A&A Suppl. Ser., 139, 531
- Bardeen, J. M. 1970, Nature, 226, 64
- Bardeen, J.M., Press, W.H., & Teukolsky, S.A., 1972, Phys. Rev. D, 178, 347
- Barnes, J. & Kasen, D., 2013, ApJ, 775, 18
- Barkat, Z., Rakavy, G. & Sack, N., 1967, Phys. Rev. Lett. 18, 379
- <http://www.batse.msfc.nasa.gov/batse/>
- Barthelmy, S.D., et al., 2005, Nature, 438, 994

- Barthelmy, S.D., et al., 2007, Proc. Roy. Soc. London A, 365, 1281
- Bekenstein, J. 1973, ApJ, 183, 657
- Beloborodov, A. M., Stern, B. E., & Svensson, R. 1998, ApJ, 508, L25
- Beloborodov, A. M., Stern, B. E., & Svensson, R. 2000, ApJ, 535, 158
- Beloborodov, A. 2013, ApJ, 764, 157
- AAS Meeting #225, #328.04
- Berger, E., & Soderberg, A.M., 2005, GCN Circ. 4384
- Berger, E., 2005b, GCN Circ. 3801
- Berger, E., et al., 2005c, Nature, 438, 15
- Berger, E., 2006, in Gamma-ray bursts in the Swift era, 16th Maryland Astroph. Conf., AIP Conf. Proc., 836, 33; arXiv:astro-ph/0602004v1
- Berger, E., et al., 2006, GCN Circ. 5965
- Berger, E., et al., 2007a, ApJ, 660, 496
- Berger, E., et al., 2007b, ApJ, 664, 1000
- Berger, E., et al., 2007c, GCN Circ. 7151
- Berger, E., et al., 2007d, GCN circ. 5995
- Berger, E., et al., 2007e, GCN circ. 7154
- Bernardini, M.G., et al., 2011, A&A, 526, A27
- Bernuzzi, S., Dietrich, T., & Nagar, A., 2015, 115, 091101
- Bernuzzi, S., Radice, D., Ott, C.D., et al., 2015, arXiv:1512.06397
- Bethe, H.A., Brown, G.E., Lee, C.-H., eds., 2003, *Formation and Evolution of Black Holes in the Galaxy* (Springer-Verlag)
- Bildsten, L., Townsley, D.M., Deloye, C.J., & Nelemans, G., 2006, ApJ, 640, 466
- Biretta, J.A., Zhou, F. and Owen, F.N., 1995, ApJ, 447, 582
- Bisnovatyi-Kogan, G.S., & Kazhdan, Ya.M., 1966, Astron. Zh. 43, 761; 1967, Sov. Astron. 10, 604
- Bisnovatyi-Kogan, G. S., 1970, Astron. Zh., 47, 813
- Bisnovatyi-Kogan, G.S., & Ruzmaikin, A.A., 1976, Ap. Space. Sci. 42, 401
- Bisnovatyi-Kogan, G.S., & Lovelace, R.V.E., 2007, ApJ, 667, L167
- Blandford, R.D., & Znajek, R.L., 1977, Mon. Not. R. Astron. Soc. 179, 433
- Bloom, J.S., et al., 2005, arXiv:astro-ph/0505480v2
- Bloom, J.S., et al., 2006, ApJ, 638, 354
- Bloom, J.S., et al., 2007, ApJ, 654, 878
- Bogovalov, S. V. 1995, Astronomy Letters, 21, 565
- Bondi, H., 1952, MNRAS, 112, 195
- Bromberg, O., Levinson, A., & van Putten, M.H.P.M., 2006, NewA, 619, 627
- Bromberg, O., & Levinson, A., 2007, ApJ, 671, 678
- Bromberg, O., et al. 2011a, ApJ, 740, 100
- Bromberg,), et al. 2011b, ApJ, 733, 85
- Bromberg,), et al., 2012, ApJ, 749, 110
- Bromberg, O., Nakar, E., Piran, T., & Sari, R., 2013, ApJ, 764, 179
- Bromberg, O., Granot, J., Lyubarski, Y., & Piran, T., 2014, MNRAS, 443, 1532
- Budnik, R. et al. 2010, ApJ, 725, 63
- Bufano, F., Benetti, S., Sollerman, J., Pian, E., & Cupani, G. 2011, Astron. Nachr., 332, 262
- Burgay, M., et al., 2003, Nature, 426, 531
- Burrows, A., & Lattimer, J.M., 1987, ApJ, 318, L63
- Burrows, A., Dessart, L., Livne, E., Ott, C.D., & Murphy, J., 2007, ApJ, 664, 416
- Calafut, V., & Wiita, P., 2014 , arXiv:1407.3687
- Cano, Z., de Ugarte Postigo, A., Pozanenko, A., et al., 2014, A&A; arXiv:1405.3114.
- Cappellaro, E., Evans, R., & Turatto, M., 1999, A&A, 351, 459
- Caito, L., et al., 2010, A&A, 521, 80
- Caito, L., Bernardini, M.G., Bianco, C.L., Dainotti, M.G., Guida, R., Ruffini, R., et al., 2010, A&A, 498, 501
- Campana, S., Mangano, V., Blustin, A. J., et al. 2006, Nature, 442, 1008
- Carter, B., 1968, Phys. Rev., 174, 1559
- Cenko, S.B., et al., 2006, GCN Circ. 5946
- Cenko, S.B., et al., 2008, arxiv:0802.0874v1
- Cenko, S. B., Frail, D. A., Harrison, F. A., et al. 2010, ApJ, 711, 641
- Chandra, P., Cenko, S. B., Frail, D. A., et al. 2008, ApJ, 683, 924
- Chardonnet, P. et al., 2010, ApJ Supp., 325, 153
- Chen, W-X, & Beloborodov, A., 2007, ApJ, 657, 383
- Chornock, R., Berger, E., Levesque, E. M., et al. 2010, arXiv:1004.2262
- Chandrasekhar, S., 1983, *The Mathematical Theory of Black Holes* (New York: Oxford University Press)
- Chincarini, G., Mao, J., Margutti, R., et al. 2010, MNRAS, 406, 2113
- Chiueh, T, Li, Z-Y. & Begelman, M. C, 1991, ApJ, 377, 462

- Ciufolini, I., & Pavlis, E.C., 2004, *Nature*, 431, 958.
- Ciufolini, I., 2007, *Nature* 449, 41
- Ciufolini, I., Paolozzi, A., Pavlis, E.C., et al., 2009, *Space Sci Rev.*, 148, 71
- Cobb, B.E., et al., 2006a, *GCN Circ.* 5282
- Cobb, B. E., Bailyn, C. D., van Dokkum, P. G., & Natarajan, P. 2006b, *ApJ*, 645, L116
- Cohen, J.M., Tiomno, J., & Wald, R.M., 1973, *Phys. Rev. D.* 7, 998
- Colgate, S. A. 1968, *Canadian J. Phys.*, 46, S476
- Colgate, S. A. 1970, *Acta Physica Academiae Scientiarum Hungaricae*, 29, Suppl. 1, 353
- Coughlin, M., Meyers, P., Kandhasamy, S., et al., 2015, *Phys. Rev. D*, 92, 43007
- Colgate, S. A. 1974, *ApJ*, 187, 333
- Contopoulos, J., 1995, *ApJ*, 450, 616
- Costa, E., et al., 1997, *Nature*, 387, 878
- Couch, S.M., Pooley, D., Wheeler, J.G., & Milosavljević, M., 2011, *ApJ*, 727, 104
- Coward, D.M., et al., 2012, *MNRAS*, 425, 2668
- Coward, D.M., et al., 2013, *MNRAS*, 422, 2141
- Crider, A. Liang, E. P., Smith, I. A. et al. 1997, *ApJL*, 479, L39
- Cucchiara, A., et al., 2006, *GCN Circ.* 5470
- Cucchiara, A., et al., 2013, *ApJ*, 777, 94
- Cutler, C., & Thorne, K.S., 2002, in *Proc. GR16*, Durban, South Afrika
- Dichiara, S., Guidorzi, C., Amati, L. A., & Frontera, F. 2013a, *MNRAS*, 431, 3608
- Dichiara, S., Guidorzi, C., Frontera, F., & Amati, L. A. 2013b, *ApJ*, 777, 132
- Della Valle, M., et al., 2003, *A&A*, 406, L33
- Della Valle, M., et al., 2006, *Nature*, 444, 1050
- Detweiler, S., & Lindblom, L., 1981, *ApJ*, 250, 739
- de Ugarte Postigo, A., et al., 2006, *GCN circ.* 5951
- de Ugarte Postigo, A., Goldoni, P., Milvang-Jensen, B., et al. 2011, *GCN*, 11579
- Dessart, L., Burrows, A., Livne, E., & Ott, C.D., 2008, *ApJ*, 673, L43
- Dokuchaev, V.I., 1986. *Sov. Phys. JETP* 65, 1079
- Dong, D., Shappee, B.J., Prieto, J.L., et al., 2015, *Science*, 351, 6270
- Drenkhahn, G., & Spruit, H.C., 2002, *A&A*, 391, 1141
- Drout, M.R., Soderberg, A.M., Gal-Yam, A., et al., 2011, *ApJ*, 741, 97
- Duez, M. D., Shapiro, S. L., & Yo, H.-J. 2004, *Phys. Rev. D*, 69, 104016
- Echeverria F., 1988, *Phys. Rev. D*, 40, 3194
- Eichler, D., Livio, M., Piran, T., & Schramm, D. 1989, *Nature*, 340,126
- Eichler, D. 1994, *ApJS*, 90, 877
- Eichler, D. & Levinson, A. 2000, *ApJ*, 529, 146
- Eichler, D., Guetta, D., & Manis, H., 2009, 690, L61
- Eichler, D., 2011, *ApJ*, 730, 41
- Epstein, R., Ph.D. Thesis, (Stanford University, Stanford, 1976)
- Espaillet, C., Patterson, J., Warner, B., & Woudt, P., 2005, *PASP*, 117, 189
- Everitt, C.W.F., et al., 2011, *Phys. Rev. Lett.* 106, 221101
- Fabian, A.C., et al., 1995, *MNRAS*, 277, L11
- Fanaroff, B.L., & Riley, J.M., 1974, *MNRAS*, 167, 31P
- Faulkner, J., 1971, *ApJ*, 170, L99
- Faulkner, J., Flannery, B.P., Warner, B., 1972, *ApJ*, 175, L79
- Ferrero, P., et al., 2007, *ApJ*, 134, 2118
- Fierz, M., & Pauli, W., 1939, *Proc. R. Soc. Lond.*, A173, 211
- Filippenko, A.V., 1997, *ARA&A*, 35, 309
- Fishbone, L.G., *ApJ.*, 175, L155
- Flanagan, E.E., & Hughes, S.A., 1998a, *Phys. Rev. D*, 57, 4535
- Flanagan, E.E., & Hughes, S.A., 1998b, *Phys. Rev. D*, 57, 4566
- Friedrichs, K.O. & Lax P.D., 1971, *Proc. Natl. Acad. Sc. USA*, 68, 1686
- Friedrichs, K.O., 1974, *Commun. Pure Appl. Math.*, 28, 749
- Frolov, V., & Novikov, I.D., 1998, *Black Hole Physics: Basic Concepts and New Developments* (Kluwer Academic Publishers)
- Fong, W., et al., 2010, *ApJ*, 708, 9
- Font, J.A., & Papadoupoulos, P., 2001, in *Proc. Spanish Rel. Meeting*, eds. J.F. Pascual-Sánchez, L. Floría, A San Migual & F. Vicente (World Scientific), pp. 311
- Fox, D.B., et al., 2006, *Nature*, 437, 845
- Frail, D.A., et al., 2001, *ApJ*, 567, L41
- Frontera, F., et al., 2001, *ApJ*, 550, 47
- Frontera, F., Amati, L., Farinelli, R., et al., 2013, *ApJ*, 779, 175
- Frederiks, D., 2013, *GCN Circ.* 14772
- Fruchter, A.S., et al., 2006, *Nature*, 441, 463
- Fryer, C. L., Holz, D.E., & Hughes, S. A., 2002, *ApJ*, 565, 430

- Fryer, C.L., & New, K.C.B., 2011, *Living Rev. Relativity*, 1
- Fryer, C.L., Rueda, J.A., & Ruffini, R., 2014, *ApJ*, 793, L36
- Fynbo, J.P.U., et al., 2006, *Nature*, 444, 1047
- Galama, T.J., Vreeswijk, P.M., van Paradijs, J., et al. 1998, *Nature*, 395, 670
- Gammie, C. F., 2001, *ApJ*, 553, 174
- Gal-Yam, A., et al., 2006, *Nature*, 444, 1053
- Gal-Yam, A., Mazzali, P., Ofek, E. O., et al. 2009, *Nature*, 462, 624
- Garrison, R., Shelton, I., Madore, B., Cassatella, A., Wamsteker, W., Sanz, L., Gry, C., 1987, *IAUC* 4330, 1
- Gehrels, N., et al., 2005, *Nature*, 437, 851
- Gehrels, N., Ramirez-Ruiz, E., & Fox, D.B., 2009, *ARAA*. 47, 567
- Gezari, S. 2008, *ApJ*, 683, L131
- Ghirlanda, G., Ghisellini, G., & Firmani, C., 2006, *New J. Phys.*, 8, 123
- Ghirlanda, G., Ghisellini, G., Salvaterra, R., et al., 2013, *MNRAS*, 428, 123
- Giannios, D. & Spruit, H. 2007, *A&A*, 469, 1
- Giannios, D. 2012, *MNRAS*, 422, 3092
- Gibbons, G.W., 1972, *Commun. Math. Phys.* 27, 87
- Gilmozzi, R., Cassatella, A., Clavel, J., et al., 1987, *Nature*, 328, 318
- Globus, N., & Levinson, A., 2014, *ApJ*, 796, 26
- Goldreich, P., & Lynden-Bell, D., 1965, *MNRAS*, 130, 125
- Goldreich, P., & Julian, W.H., 1969, *ApJ*, 157, 869
- Golenetskii, S., et al., 2005, *GCN Circ.* 4394
- Golenetskii, S., et al., 2006, *GCN Circ.* 5748
- Gompertz, B.P., et al., 2014, *MNRAS*, 438, 240
- Gossan, S.E., Putton, P., Stuver, A., et al., 2015, *arXiv:1511.02836v1*
- Graham, J.F., et al., 2007, *GCN Circ.* 6836
- Graham, J.F., et al., 2009, *ApJ*, 698, 1620
- Granot, J., Komissarov, S.S., & Spitkovsky, A., 2011, *MNRAS*, 411, 1323
- Granot, J., 2012, *MNRAS*, 421, 2442
- Greiner, J., Cuby, J.G., & McCaughrean, M.J., 2001, *Nature*, 414, 522
- Grieco, V., Matteucci, F., Meynet, G., Longo, F., Della Valle, M., Salvaterra, R., 2012, *MNRAS*, 423, 3049
- Griv, E., 2011, *ApJ*, 733, 43
- Gupta, A.C., & van Putten, M.H.P.M., 2012, *in Astron. Soc. India Conf. Ser.*, 5, p123
- Nicuesa Guelbenzu, A., et al. 2012, *A&A*, 538, L7
- Guetta, D., & Piran, T., 2005, *A&A*, 435, 421
- Guetta, D., & Della Valle, M., 2007, *ApJ*, 657, L73
- Guetta, D., Pian, E., & Taxman, E., 2011, *A&A*, 435, 421
- Guidorzi, C., Margutti, M., Amati, L. A., et al. 2012, *MNRAS*, 422, 1785
- Hadley, K.Z., & Fernandez, P., 2014, *Astrophys. Space Sci.*, 353, 191
- Heo, J.-E., Yoon, S., Lee, D.-S., et al. 2015, *NewA*, 42, 24
- Herald, D., McNaught, R.H., Morel, M., et al., 1987, *IAUC* 4317, 1
- Hawley, J.F., & Balbus, S.A., 1991, *ApJ*, 376, 223
- Heyvaerts, J. & Norman, C. 1989, *ApJ*, 347, 1055
- Hjörth, J., Sollerman, J., Moller, P., et al. 2003, *Nature*, 423, 847
- Hjörth, J., Watson, D., Fynbo, J. P. U., et al. 2005, *Natur*, 437, 859
- Hjörth, J., & Bloom, J.S., 2011, *in Gamma-Ray Bursts*, eds. C. Kouveliotou, R. A. M. J. Wijers, S. E. Woosley (Cambridge University Press)
- Höfflich, P., Wheeler, J.C., & Wang, L., 1999, *ApJ*, 521, 179
- Höfflich, P., & Schaefer, B.E., 2009, *ApJ*, 705, 483
- Inayoshi, K., Hirai, R., Kinugawa, T., & Hotokezaka, K., 2017, *MNRAS*, 468, 5020
- Iwasawa, K., Fabian, A.C., & Reynolds, C.S., et al., 1996, *MNRAS*, 282, 672
- Jakobsson, P., Fynbo, J. P. U., *arXiv:0704.1421*
- Ju, L., Blair, D.G., & Zhao, C., 2000, *Rep. Prog. Phys.*, 63, 1317
- Kalogera, V., 2017, *Nat. Astron.*, 1, 0088
- KAGRA Project (NAOJ), <http://gwcenter.icrr.u-tokyo.ac.jp/en/>
- Kasen, D., & Bildsten, L., 2010, *ApJ*, 717, 245
- Kasen, D., Badnell, N. R. & Barnes, J., 2013, *ApJ*, 774, 25
- Katz, B., Budnik, R., & Waxman, E. 2010, *ApJ*, 716, 781
- Kelly, P.L., Kirshner, R.P., & Pahre, M., 2008, *ApJ*, 687, 1201
- Keren, S., & Levinson, A., 2014, *ApJ*, 789, 128
- Kerr, R.P., 1963, *Phys. Rev. Lett.*, 11, 237
- King, A.R., & Pringle, J.E., 2006, *MNRAS*, 373, L90
- Kinugawa T., Inayoshi K., Hotokezaka K., Nakauchi D., Nakamura T., 2014, *MNRAS*, 442, 2963

- Kirshner, R.P., Sonneborn, G., Grenshaw, D.M., Nassiopoulos, G.E., 1987, ApJ, 320, 602
- Klebesadel, R., Strong I. and Olson R., 1973, ApJ, 182, L85
- Kiuchi, K., et al., 2011, Phys. Rev. Lett., 106, 251102
- Kobayashi, S., & Meszaros, P. 2003, ApJ, 589, 861
- Kobayashi, S., Piran, T., & Sari, R., 1997, ApJ, 490, 92
- Kocevski, D., et al., 2010, MNRAS, 404, 963
- Kokkotas, K.D., & Schmidt, B.G., 1999, Living Rev. Relativity, 2, <http://www.livingreviews.org/lrr-1999-2>
- Komissarov, S.S., 2012, MNRAS, 422, 326
- Kotake, K., Sato, K., & Takahashi, K., 2006, Rep. Prog. Phys., 69, 971
- Kouveliotou, C., et al., 1993, ApJ, 413, L101
- Kunkel, W., Madore, B., Shelton, I., et al., 1987, IAUC 4316, 1
- Kulkarni, S. R., et al., 1998, Nature, 395, 663
- Kulkarni, S.R., Zwicky Transient Factory Proposal, priv. commun.
- Kumar, P., Narayan, R., & Johnson, J. L., 2008a, Science, 321, 376
- Kumar, P., Narayan, R., & Johnson, J. L., 2008b, MNRAS, 388, 1729
- Kyutoku, K., 2013, *The Black Hole-Neutron Star Binary Merger in General Relativity* (Springer-Verlag)
- Lattimer, J.M., & Schramm, D.N., 1974, ApJ, 192, L145
- Lattimer, J.M., & Schramm, D.N., 1976, ApJ, 210, 549
- Lazzati, D. Morsony, B. & Begelman, M. 2009, ApJ, 700, L47
- Lazzati, D., Morsony, B.J., Blackwell, C.H., & Begelman, M., 2012, ApJ, 750, 68
- Lee, W.H., & Kluzniak, 1998, ApJ, 494, L53
- Lee, W.H., & Kluzniak, 1999, ApJ, 526, 178
- Lei, W.H., Wang, D.X., Zou, Y.C., & Zhang, L., 2008, ChJAA, 8, 405
- Leung, P.T., Liu, Y.T., Suen, W.-M., Tam, C.Y., & Young, K., 1997, Phys. Rev. Lett., 78, 2894
- Levan, A.J., Tanvir, N.R., Starling, R.L.C., et al., 2014, ApJ, 781, 13
- Levinson, A., & Eichler, D., 1993, ApJ, 418, 386
- Levinson, A., & Van Putten, M., 1997, ApJ, 488, 69
- Levinson, A., et al., 2002, ApJ, 576, 923
- Levinson, A. & Bromberg, O. 2008, Phys. Rev. Lett., 100, 131101
- Levinson, A., 2010, ApJ, 720, 1490
- Levinson, A. 2012, ApJ, 756, 174
- Levinson, A., & Begelman, M. C., 2013, ApJ, 764, 148
- Levinson, A., & Glubus, N., 2013, ApJ, 770, 159
- Levinson, A., van Putten, M.H.P.M., & Pick, G., 2015, ApJ, to appear
- Li, W., Leaman, J., Chornock, R., et al. 2011a, MNRAS, 412, 1441
- Li, W., Chornock, R., Leaman, J., et al. 2011b, MNRAS, 412, 1473
- Lichnerowicz A., 1967, Relativistic hydrodynamics and magneto-hydrodynamics (W.A. Benjamin Inc., New York)
- LIGO Virgo Collaboration, 2016, Phy. Rev. Lett., 116, 241102
- Lipunov, V.M., 1983, Ap&SS, 97, 121
- Lipunova, G.V., Gorbovskey, E.S., Bogomazov, A.I., & Liponov, V.M., 2009, MNRAS, 397, 1695
- Lovelace, R.V.E., & Romanova, M.M., 2014, Fluid Dyn. Res., 46, 041401
- Lubow, S.H., Papaloizou, J.C.B., & Pringle, J.E., 1994, MNRAS, 267, 235
- Lyne, A.G., Burgay, M., Kramer, M., Possenti, A., et al., 2004, Science, 303, 1153
- Lyutikov, M., & Blandford, R., 2003, arXiv:0312347
- Lyutikov, M., Pariev, V.I., & Blandford, R., 2003, ApJ, 597, 998
- Lyubarsky, Y. 2009, ApJ, 698, 1570
- Lyubarsky, Y. 2010, ApJ, 725, L234
- Lyutikov M., 2011, MNRAS, 411, 422
- HEASARC, <http://swift.gsfc.nasa.gov/archive/grbtable/>
- Macchetto, F., Marconi, A., Axon, D.J., Capetti, A., Sparks, W., & Crane, P., ApJ, 489, 579
- MacFadyen A. I., & Woosley S. E., 1999, ApJ, 524, 262
- Maeda, K., et al. 2002, ApJ, 565, 405
- Maeda, K., et al., 2008, Science, 319, 1220
- Malesani, D., Tagliaferri, G., Chincarini, G., et al. 2004, ApJ, 609, L5
- Mangano V., et al., 2007, A&A, 470, 105
- Maselli, A., et al., 2013, Science, 343, 48
- Masetti, N., Palazzi, E., Pian, E., et al. 2006, GCN, 4803, 1

- Matheson, T., Garnavich, P. M., Stanek, K. Z., et al. 2003, *ApJ*, 599, 394
- Mattei, J., Johnson, G.E., Rosino, L., Rafanelli, P., Kirshner, R., 1979. *IAU Circ.* 3348, 1
- Maurer, J. I., Mazzali, P. A., Deng, J., et al. 2010, *MNRAS*, 402, 161
- Mazzali, P.A., et al., 2005, *Science*, 308, 1284
- Mazzali, P.A., Valenti, S., Della Valle, S., et al., 2008, *Science*, 321, 1185
- McKinney, J.C., 2005, *ApJ*, 630, L5
- McKinney, J. C. & Uzdensky, D. A. 2012, *MNRAS*, 419, 573
- Mejia, A.C., et al., 2005, *ApJ*, 619, 1098
- Melandri, A., et al., 2013, *GCN Circ.* 14673
- Mészáros, P., & Rees, M.J., 1993, *ApJ* 405, 278
- Mészáros, P.M., and Waxman, E., 2001, *Phys. Rev. Lett.*, 87, 171102
- Metzger, M., Djorgovski, S.G., Kulkarni, S.R., et al., 1997 *Nature*, 387, 879
- Metzger, D.B., et al., 2011, *Mon. Not. R. Astron. Soc.* 413, 2031
- Mirabel, I.F., & Rodriguez, L.F., 1994, *Nature*, 371, 46
- Misner, C.W., Thorne, K.S., & Wheeler, J.A., 1973, *Gravitation* (San Francisco: W.H. Freeman and Company)
- Modjaz, M., Stanek, K. Z., Garnavich, P. M., et al. 2006, *ApJ*, 645, L21
- Modjaz, M., et al., 2014, *AJ*, 147, 99M
- Moretti, A., et al., 2006, *GCN-Report-9.1*, gcns.gsfc.nasa.gov/reports/report_9_1.pdf
- Mirabal, N., Halpern, J. H., An, D., Thorstensen, J. R., & Terndrup, D. M. 2006, *ApJ*, 643, L99
- Morsony, B. Lazzati, D. & Begelman, M. C. 2010, *ApJ*, 723, 267
- Nagar, A., Zanotti, O., Font, J.A., & Rezzolla, L., 2007, *Phys. Rev. D*, 2007, 75, 044016
- Nakar, E., & Piran, T., 2002, *MNRAS*, 330, 920
- Nakar, E., & Sari, R., 2010, *ApJ*, 725, 904
- Nakar, E., & Sari, R., 2012, *ApJ*, 747, 88
- Narayan, R., Piran, T., & Kumar, P. 2001, *ApJ*, 557, 949
- Nathanail, A., Strantzalis, A., & Contopoulos, I. 2015, *MNRAS*, 455, 4479
- Nelemans, G., 2005, *in* *The Astrophysics of Cataclysmic Variables and Related Objects*, eds. J.-M. Hameury & J.-P. Lasota, *ASP Conf. Ser.*, 330
- Nice, D.J., Splaver, E.M., & Stairs, I.H., 2004, *in* *Rasio, F.A., and Stairs, I.H., eds., "Binary Radio Pulsars, Meeting at the Aspen Center for Physics," ASP Conf. Ser.*, 328, 371
- Nicholl, M., et al., 2013, *Nature*, 502, 346
- Nisenson, P., & Papaliosios, C., 1999, *ApJ*, 518, L29
- Norris, J.P., et al., 2010, *ApJ*, 717, 411
- Novikov, I.D., 1975, *Astron. Zh.* 52, 657; 1976, *Sov. Astron.* 19, 398
- Ofek, E.O., et al., 2007, *ApJ*, 662, 1129
- Ott, C.D., 2009, *Class. Quant. Grav.*, 2009, 26, 063001
- Paczynski, B.P., 1967, *Acta. Astron.*, 17, 287
- Paczynski, B.P., 1991, *Acta. Astron.*, 41, 257
- Paczynski, B.P., 1998, *ApJ*, 494, L45
- Page, K.L., et al., 2006, *ApJ*, 637, L13
- Papaliosios, C., Krasovska, M., Koechlin, L., Nisenson, P., & Standley, C., 1989, *Nature*, 338, 565
- Papaloizou, J.C.B., & Pringle, J.E., 1984, *MNRAS*, 208, 721
- Papapetrou, A., 1951, *Proc. Roy. Soc.*, 209, 248
- Pastorello, A., et al., 2007, *Nature*, 449, 1
- Patnaude, D.J., Loeb, A., & Jones, C., 2011, *NewA*, 16, 187
- Pearson, T.J., Unwin, S.C., Cohen, M.H., Linfield, R.P., Readhead, A.C.S., Seielstad G.A., Simon, R.S. & Walker, R.C., 1981, *Nature*, 290, 365
- Peer, A. Meszaros, P. & Rees, M. 2006, *ApJ*, 642, 995
- Perley, D.A., et al., 2009, *ApJ*, 696, 1871
- Perley, D.A., et al., 2010, *GCN circ.* 11464
- Perley, D.A., 2013, *GCN circ.* 15319
- Perlmutter, S., et al., 1999, *ApJ*, 517, 565
- Peters, P.C., & Mathews, J., 1963, *Phys. Rev.*, 131, 435
- Phinney, E.S., 2001, *astro-ph/0108028*
- Piran, T., 1999, 314, 575
- Piran, T., 2004, *RvMP*, 76, 1143
- Piran, T., & Sari, R., 1997, *arXiv:9702093*
- Pian, E., Mazzali, P. A., Masetti, N., et al. 2006, *Nature*, 442, 1011
- Pirani, F.A.E., 1956, *Act. Phys. Pol.*, XV, 389
- Pirani, F.A.E., 1957, *Phys. Rev.* 105, 1089
- Pirani, F.A.E., 2009, *Gen Relativ Gravit*, 41, 1215
- Piro, A.L., & Pfahl, E., 2007, *ApJ*, 658, 1173
- Popham, R., Woosley, S.E., & Fryer, C., 1999, *ApJ*, 518, 356
- Porciani, C., & Madau, P., 2001, *ApJ*, 548, 522

- Portegies Zwart, S.F., & Yungelson, L.R., 1998, *A&A*, 332, 173
- Postnov, K.A., & Yungelson, L.R., 2006, *Living Rev. Relativity*, 9, 6
(<http://www.livingreviews.org/lrr-2006-6>)
- Preece, R. D. et al. 1998, *ApJL*, 506, L23
- Prestegard, T., & Thrane, E., 2009,
<https://dcc.ligo.org/public/0093/L1200204/001/burstedgalle.pdf>
- Pringle, J.E., 1981, *ARAA*, 19, 137
- Prochaska, J.X., et al., 2005, *GCN circ.* 3700
- Prochaska, J.X., et al., 2006, *ApJ*, 642, 989
- Punturo, M., 2003, *Virgo Internal Note* VIR-NOT-PER-1390-51(8)
- Quimby, R.M., et al., 2009, 2011, *Nature*, 474, 487
- Raab, F.J. (for the LIGO Scientific Collaboration), 2006, *J. Phys. Conf. Ser.*, 39, 25
- Rau, A., et al., 2009, *GCN Circ.* 9353
- Raskin, C., et al., 2008, *ApJ*, 689, 358
- Rees, M. J., Ruffini, R., & Wheeler, J. A. 1974, *Black Holes, Gravitational Waves and Cosmology: An Introduction to Current Research* (New York: Gordon & Breach), Ch.7
- Rees, M.J. & Mészáros, P., 1992, *MNRAS*, 258, P41
- Rees, M.J., & Meszaros, P., 1994, *ApJ*, 430, L93
- Reichert D. E., Lamb D. Q., Fenimore E. E., Ramirez-Ruiz E., Cline T. L., & Hurley K., 2001, *ApJ*, 552, 57
- Rice, W.K.M., Lodato, G., & Armitage, P.J., 2005, *MNRAS*, 364, L56
- Riess, A., et al., 1998, *ApJ*, 116, 1009
- Rosswog, S., 2007, *MNRAS*, 376, 48
- Romanova, M.M., & Lovelace, R.V.E., 1992, *A&A*, 262, 26
- Röver, C. Bizouard, M.-A., Christensen, N., Dimmelmeier, H., Heng, I.-S., & Meyer, R., 2009, *Phys. Rev. D*, 80, 102004
- Ryde, F., 2004, *ApJ*, 614, 827
- Ryde, F., 2005, *ApJ*, 625, L95
- Ryde, F. & Peer, A. 2009, 702, 1211
- Ruffini, R., & Wilson, J.R., 1975, *Phys. Rev. D*, 12, 2959
- Sari, R., & Piran, T., 1997, *ApJ*, 485, 270
- Sari, R., Piran, T., & Narayan, R., 1998, *ApJ*, L17
- Sathyaprakash, B.S., & Schutz, B.F., 2009, *Liv. Rev. Relativity*, 12, 2
- Scolnic, D., Riess, A., Huber, M., et al., 2011, *AAS*, #218, 127.09
- Shahmoradi, A., & Nemiroff, R. J. 2015, *MNRAS*, 451, 126
- Shakura, N.I., & Sunyaev, R.A., 1973, *Astron. Astrophys.*, 24, 337.
- Shapiro, S.L., Teukolsky, S.A., 1983, *Black Holes, White Dwarfs and Neutron Stars*. Wiley, New York
- Shibata, M., Kyutoku, K., Yamamo, T., & Taniguchi, K., 2009, *Phys. Rev. D*, 79, 044030
- Sialla, K., Boër, M., & Gendre, B., 2014, *MNRAS*, 437, 649
- Sigg, D., 1998, in *Proc. TASI*, Boulder Colorado
- Smak, J. 1967, *Acta Astron.*, 17, 255
- Sollerman, J., Jaunsen, A. O., Fynbo, J. P. U., et al. 2006, *A&A*, 454, 503
- Somiya, K., (for the KAGRA Collaboration), 2012, *Class. Quantum Grav.*, 29, 124007
- Soderberg, A. M., Berger, E., S. Page, K.L., et al. 2008, *Nature*, 453, 469
- http://swift.gsfc.nasa.gov/analysis/threads/bat_threads.htm
- Stanek, K. Z., Matheson, T., Garnavich, P. M., et al. 2003, *ApJ*, 591, L17
- Stefani, F., Gerbeth, G., Gundrum, T., et al., *Phys. Rev. E*, 2009, 80, 066303
- Sutton, P.J., Jones, G., Chatterji, S., et al., 2010, *N. J. Phys.*, 12, 053034
- Svirski, G, Nakar, E, & Sari, R. 2012, *ApJ*, 759, 108
- Szilágyi, B., Blackman, J., Buonanno, A., et al., 2015, *Phys. Rev. Lett.*, 115, 031102
- Tagger, M., Henriksen, R.N., Sygnet, J.F., & Pellat, R., 1990, *ApJ* 353, 654
- Tagger, M., & Pellat, R., 1999, *A&A*, 349, 1003
- Tagger, M., 2001, *A&A*, 380, 750
- Tagger, M., & Varnière, P., 2006, *ApJ*, 642, 1457
- Tagger, M., & Melia, F., 2006, *ApJ*, 636, L33
- Tanaka, M., & Hotokezaka, K., 2013, *ApJ*, 775, 113
- Tanvir, N.R., Chapman, R., Levan, A.J., & Priddey, R.S., 2005, *Nature*, 438, 991
- Tanvir, N.R., Levan, A.J., Fruchter, A.S., et al., 2013, *Nature*, 500, 547
- Taubenberger, S., et al., 2009, *MNRAS*, 397, 677
- Taylor, J.H., & Weisberg, J.M., 1989, *ApJ*, 345, 434
- Taylor, J.H., 1994, *Rev. Mod. Phys.*, 66, 711
- Thompson, C., 1994, *Mon. Not. R. Astron. Soc.* 270, 480
- Thompson, C, Mészáros, P., & Rees, M.J., 2007, *ApJ*, 666, 1012
- Thorne, K.S., 1974, *ApJ*, 191, 507

- Thorne, K.S., 1992, *in* *Advances in General Relativity*, eds. A Janis and J Porter (Boston: Birkhauser)
- Thomson, R.C., Mackay, C.D. & Wright, A.E., 1993, *Nature*, 365, 133
- Thone, C.C., et al., 2008, *ApJ*, 676, 1151
- Thorne, K.S., 1980, *Rev. Mod. Phys.*, 52, 299
- Thorne, K.S., Price, R.H., & McDonald, D.H., 1986, *Black Holes: The Membrane Paradigm* (New Haven, CT: Yale University Press)
- Thorne, K.S., 1988, *in* *Near Zero: New Frontiers of Physics*, eds. J.D. Fairbank, B.S. Deaver, Jr., C.W.F. Everitt and P.F. Michelson (W.H. Feeman and Company, New York), Ch. VI.2
- Thorne, K.S., 1992, *in* *Recent Advances in General Relativity*, eds. A Janis and J Porter (Boston: Birkhauser)
- Thorsett, S.E., & Chakrabarty, D., 1999, *ApJ*, 512, 288
- 't Hooft, G., 2002, *Introduction to General Relativity* (Princeton, NJ: Rinton Press)
- Thrane, E., & Coughlin, M., 2013, *Phys. Rev. D* 88, 083010
- Thrane, E., & Coughlin, M., 2014, *Phys. Rev. D* 89, 063012
- Thuan, T.X., & Ostiker, J.P., 1974, *ApJ*, 191, L105
- Toomre, A., 1964, *ApJ*, 139, 1217
- Trautman, A., 2009, *Gen Relativ Gravit*, 41, 1195
- Turtle, A.J., et al., 1987, *Nature*, 327, 38
- Ukwatta, T., et al., 2010, *GCN circ.* 10976
- Usov, V., 1994, *MNRAS*, 267, 1035
- van Paradijs, J., et al., 1997, *Nature*, 386, 686
- van Putten, M.H.P.M., 1991, *Commun. Math. Phys.*, 141, 63; *ibid.* 1993, *J. Math. Phys.*, 43, 6195
- van Putten, M.H.P.M., 1993, *J. Comput. Phys.*, 105, 339; *ibid.*, 1994, *IJBC*, 4, 57; *ibid.* 1994, *SIAM J. Numer. Anal.*, 32, 1504
- van Putten, M.H.P.M., 1994, *Phys. Rev. D.*, 50, 6640
- van Putten, M.H.P.M., & Eardley, D.M., 1996, *Phys. Rev. D*, 53, 3056
- van Putten, M.H.P.M., 1999, *Science*, 284, 115
- van Putten, M.H.P.M., 2000, *Phys. Rev. Lett.*, 84, 3752
- van Putten, M.H.P.M., & Ostriker, E., 2001, *ApJ*, 552, L31
- van Putten, M.H.P.M., 2001a, *Phys. Rep.*, 354, 1
- van Putten, M.H.P.M., 2001b, *Phys. Rev. Lett.*, 87, 091101
- van Putten, M.H.P.M., 2002, *ApJ*, 575, L71
- van Putten, M.H.P.M., & Levinson, 2002, *Science*, 294, 1837
- van Putten, M.H.P.M., 2003, *ApJ*, 583, 374
- van Putten, M.H.P.M., & Levinson, A., 2003, *ApJ*, 584, 937
- van Putten, M.H.P.M., 2004, *ApJ Lett*, 611, L81
- van Putten, M.H.P.M., Lee, H.K., Lee, C.H., & Kim, H., 2004, *Phys. Rev. D*, 2004, 69, 104026
- van Putten, M.H.P.M., 2005a, *Nuov. Cim. C*, 28, 597; *ibid.*, 2008, *ApJ*, 685, L63
- van Putten, M.H.P.M., 2005b, *Gravitational radiation, Luminous Black Holes and Gamma-Ray Burst Supernovae* (Cambridge: Cambridge University Press)
- van Putten, M.H.P.M., 2008, *ApJ*, 684, L91
- van Putten, M.H.P.M., 2008, *ApJ*, 685, L63
- van Putten, M.H.P.M., & Gupta, A.C., 2009, *MNRAS*, 394, 2238
- van Putten, M.H.P.M., 2009, *MNRAS*, 396, L81
- van Putten, M.H.P.M., 2010, *Class. Quant. Grav.*, 27, 075011
- van Putten, M.H.P.M., Kanda, N., Tagoshi, H., Tatsumi, D., Masa-Katsu, F., & Della Valle, M., 2011a, *Phys. Rev. D* 83, 044046
- van Putten, M.H.P.M., Della Valle, M., & Levinson, A., 2011b, *A&A*, 535, L6
- van Putten, M.H.P.M., 2012a, *Prog. Theor. Phys.*, 127, 331
- van Putten, M.H.P.M., 2012b, *Phys. Rev. D*, 2012, 85, 064046
- van Putten, M.H.P.M., & Levinson, A., 2012, *Relativistic Astrophysics of the Transient Universe* (Cambridge: Cambridge University Press)
- van Putten, M.H.P.M., Guidorzi, C., & Frontera, P., 2014a, *ApJ*, 786, 146
- van Putten, M.H.P.M., Gyeong-Min, Lee, Della Valle, M., Amati, L., & Levinson, A., 2014b, *MNRASL*, 444, L58
- van Putten, M.H.P.M., Lee, G.M., Della Valle, M., Amati, L., & Levinson, A., 2014, *MNRASL*, 444, L58
- van Putten, M.H.P.M., 2015b, *MNRAS*, 447, L113
- van Putten, M.H.P.M., 2015c, *ApJ*, 810, 7
- van Putten, M.H.P.M., 2016, *ApJ*, 819, 169
- van Putten, M.H.P.M., & Della Valle, 2017, *MNRAS*, 464, 3219

- van Putten, M.H.P.M., 2017, PTEP, to appear; arXiv:1708.01609
- Villasenor, J. S., Lamb, D. Q., Ricker, G. R., et al. 2005, *Natur*, 437, 855
- Verbunt, F., 1997, *Class. Quantum Grav.* 14, 1417
- Vurm, I. Lyubarsky, Y. & Piran, T. 2013, *ApJ*, 764, 143
- Wald, R.M., 1974. *Phys. Rev. D.* 10, 1680
- Wald, R.M., 1984, *General Relativity* (Chicago: University of Chicago Press)
- Walsh, J.L., Barth, A.J., Ho, L.C., & Sarzi, M., 2013, *ApJ*, 770, 86
- Wanderman, D., & Piran, T., *MNRAS*, 2010, 406, 1944
- Weaver, T. A. 1976, *ApJS*, 32, 233
- Weisberg, J.M., Nice, D.J., & Taylor, J.H., 2010, *ApJ*, 722, 1030
- Woosley, S.L., 1993, *ApJ*, 405, 273
- Woosley, S.E., & Bloom, J.S., 2006, *Ann.Rev.Astron.Astrophys.*, 44, 507
- Woosley, S.E., 2010, *ApJ*, 719, L204
- Woudt, P.A., & Warner, B., *in Proc. IAU JD5*, “White Dwarfs: Galactic and Cosmological Probes,” eds. Ed Sion, Stephane Vennes and Harry Shipman; astro-ph/0310494v1
- Xu, D., et al., 2009, *ApJ*, 696, 971
- Zalamea, I., & Beloborodov, A., 2011, *MNRAS*, 410, 2302
- Zhang, B., 2006, *Nature*, 444, 1010
- Zhang, B., Zhang, B.-B., Liang, E.-W., Gehrels, N., Burrows, D.N., & Mészáros, P., 2007, *ApJ*, 655, L25
- Zhang, B., & Yahn, H., 2011, *ApJ*, 726, 90
- Zrake, J, & MacFadyen A.I., 2013, *ApJ*, 763, L12